NANYANG TECHNOLOGICAL UNIVERSITY
SINGAPORE

BACTERIAL CELLULOSE: FROM CULTURING TO THE DEVELOPMENT OF FUNCTIONAL MATERIALS

SUNDARAVADANAM VISHNU VADANAN

SCHOOL OF CHEMICAL AND BIOMEDICAL ENGINEERING

2020

Bacterial Cellulose:
From Culturing to the Development of Functional Materials

Sundaravadanam Vishnu Vadanan

School of Chemical and Biomedical Engineering (SCBE)

A thesis submitted to the Nanyang Technological University

in partial fulfilment of the requirement for the degree of

Doctor of Philosophy

2020

Statement of Originality

I hereby certify that the work embodied in this thesis is the result of original research, is free of plagiarised materials, and has not been submitted for a higher degree to any other University or Institution.

21-08-2020

. . . . . .

Date

. . . . . .

Sundaravadanam Vishnu Vadanan

Supervisor Declaration Statement

I have reviewed the content and presentation style of this thesis and declare it is free of plagiarism and of sufficient grammatical clarity to be examined. To the best of my knowledge, the research and writing are those of the candidate except as acknowledged in the Author Attribution Statement. I confirm that the investigations were conducted in accord with the ethics policies and integrity standards of Nanyang Technological University and that the research data are presented honestly and without prejudice.

21-08-2020

. . . . . .

Date

. . . . . .

Assoc. Professor Sierin Lim

Authorship Attribution Statement

This thesis contains material from 1 paper published in the following peer-reviewed journal(s) where I was the first and/or corresponding author.

Chapter 1 is published as **S.V. Vadanan**, A. Basu, S. Lim; A novel platform for evaluating the environmental impacts on bacterial cellulose production. **Scientific Reports**, 8 (1) (2018), p. 5780, DOI: 10.1038/s41598-018-23701-y.

The contributions of the co-authors are as follows:

1. Assoc. Prof Sierin Lim provided the initial project direction and edited the manuscript drafts.
2. I conducted most of the experiments, characterizations and wrote part of the manuscript.
3. Dr. Anindya Basu helped in the project planning, guidance, initial characterizations and writing the manuscript.

21-08-2020

. . . . . .

Date

. . . . . .

Sundaravadanam Vishnu Vadanan

Acknowledgements

I would like to extend my heart felt gratitude to everyone who has helped and played a crucial role during the 4 years of my PhD. Without these people, I would not be submitting my dissertation.

First and foremost, I wish to express my sincere gratitude to my PhD supervisor, Associate Professor Sierin Lim, for her constant motivation and timely guidance. Her enthusiasm, vision and encouragement inspired me to give my best effort in my research work.

My sincere gratitude to my mentor and friend Dr. Rupali Reddy Pasula, for encouraging and guiding me throughout with her profound knowledge and expertise. I would also sincerely wish to thank my previous Research fellow in the lab, Dr. Anindya Basu, who played a crucial role in the initial shaping of my experimental skills and projects. It was his timely interventions and advices that gave me a head start to my work. I also express my gratitude to all my group members and colleagues; whose help was instrumental in my doctoral thesis work. I would like to thank Ambili Anoop, Dr. Mridul Sarker, Dr. Shu Hui Hiew, Dr. Shahrouz Amini, Dr. Pham Thao, Dr. Usha Rani, Dr. Sathyamoorthy Bhaskar, Samyukta Ravishankar, Juhi Singh, Dr. Min Yan Teh, Ehsan Bin Mahsoor and Habib Mohammed.

I would also like to thank SCBE and Ministry of Education, Singapore for giving me an opportunity to pursue my doctoral degree and funding my research project.

Heartfelt thanks to my friends (Bonds, Chets and Subs) and roommates (Ank and Ankita) for their immense and wholehearted moral support and encouragement. And finally, I present this dissertation to my family, Appa, Ma, Pasu, JP Uncle, Jeeja aunty,

Jincy chechi, for their unflinching support and motivation. This is equally your success and accomplishment, as much as mine.

Lastly, my wife Jeeva, who's been a constant pillar of support and motivation. Thank you for being there through the good and bad times and being the most understanding!

Table of Contents

Summary

Cellulose is the most abundant biopolymer found in the biosphere with plant as the major source. It is a representative of microbial exopolysaccharides. Bacterial cellulose (BC) is produced in much lesser extent but it is chemically pure. The absence of hemicellulose and lignin distinguishes it from plant cellulose. BC is a product of primary metabolism and serves as protective envelope. The presence of ultrafine reticulated structure resulted in BC having unique material properties, making it suitable for diverse applications. However, wider applications of this exopolysaccharide is limited due to the inadequate understanding of the bacteria and large scale production of the polymer.

The goal of this project is to develop tools to understand the biology of the bacteria and optimization of the culture conditions for enhanced BC production. We also, attempt to understand the assembly of cellulose fibres and the role of cellulose synthase enzyme in the process of cellulose production. With basic understanding of the bacteria and the self-assembly of cellulose nanofibers, it lead to the development of new BC-based functional materials for biomedical applications through sustainable approaches.

We designed a surface growth platform to understand the chemotactic behaviour of the bacteria and the impact of cellulose production. The platform is based on surface growth pattern of the organism and it allows us to confirm that cellulose fibrils produced by the bacteria play a pivotal role towards their chemotaxis. The platform efficiently determines the impacts of different growth conditions on cellulose production and is translatable to static culture conditions. The analytical platform provides a means for fundamental biological studies of bacteria chemotaxis as well as systematic approach towards rational design and development of scalable bioprocessing strategies for industrial production of bacterial cellulose.

Upon identification of the highest cellulose producing bacteria, the process of formation and assembly of cellulose chains was investigated. The substrate specificity of cellulase synthase enzyme was explored for the process of exopolysaccharide production. With preliminary idea regarding the process of polymerization and

crystallization, new tunable functional materials can be designed to control the biodegradability of BC based composites. There is also, a clear indication that the substituted glucose substrates were not modified post polymerization and assembly of cellulose chains.

BC was combined with different classes of materials, conductive polymers, and amyloid fusion proteins through sustainable methods. A top-down strategy was employed to design BC-PEDOT:PSS conductive aerogels with high conductivity values (0.7 Scm^{-1}), as substrates for flexible electronics. Bioinspired bottom-up strategy employed to design BC-based magnetic membranes, functionalized with magnetite nucleating peptide domains (m6A peptide), for improved wound healing applications. Through this strategy, high saturation magnetization of 40 $emug^{-1}$ was obtained for BC-m6A membranes, four times higher than normal *ex situ* BC doping. The BC-m6A membrane displayed exceptional wound healing capabilities in the presence of the magnetic field and improved wound healing by 61%.

Our simple design strategy and optimization adopted for obtaining a hybrid functional material for use in the development of biomedical devices, is unquestionably low-cost, facile, and highly efficient approach. The hybrid functional materials developed display potential in biomedical applications.

Chapter 1

Introduction

1.1 Background

In the last few decades, there is increasing awareness to develop materials of biological source[1]. By tradition, synthetic polymers were used in a wide range of applications from packaging to automobile bodies, from clothing to food additives and medicine. Thus, polymers superseded the use of other common materials such as wood, glass and ceramics[2]. Some of the commonly used synthetic polymers are polypropylene, polyethylene, polystyrene and poly vinyl chloride, which possess various favourable properties such as chemical inertness, light weight, durability and low production cost[2-5]. Despite their positive properties, these polymers cause significant environmental issues due to chemical stability, toxic by-products, low surface area-to-volume ratio and high molecular weight enabling them to remain impervious to degradation by microbes and persist in the environment long after disposal[6,7]. To avoid increased environmental issues, there is a need to explore a new class of materials that consume less energy and can be manufactured from renewable sources. An ideal situation would be to produce sustainable materials for various applications, and they can be broken down after use, only to be reused or reabsorbed for future purpose[8,9].

Natural polymers or biopolymers have recently gained popularity since they are produced from natural sources such as plants or animals and are biodegradable in nature. Biopolymers are polymeric macromolecules produced either by biological systems or chemically synthesized from biological resources such as sugars, natural fats and amino acids[10,11]. These classes of biopolymers include proteins and peptides[12,13], polysaccharides (starch, cellulose, chitin)[14-16] and nucleic acids such as DNA and RNA[17,18], polyphenols, polyphosphates and polyhydroxyalkanoates[19-21].

Researchers have been able to synthesize proteins that mimic the biominerals found in bones and shells[22]. DNA is being explored as an assembly unit for

nanostructural materials and for its electrical properties[23]. Polysaccharides, after polypeptides are the most varied and complex group of natural polymers since various bonds can be formed at different positions of the monomer sugar units. Some of the applications being adhesives, packaging materials, clothing, filter membranes and food products[24,25]. Other biopolymers such as polyphenols and polyhydroxyalkanoates find applications as structural materials and biodegradable thermoplastics respectively[20,21,26].

Utilization of biopolymers as biomaterials has greatly influenced the advancement of various applications[27]. With increasing demand, there is a desire to ensure biopolymers such as starch and cellulose do not compete with the food chain. The exploitation of such polymeric materials is being investigated, since most of the cultivable land is required to grow food crops and not to substitute plastics[28,29]. Therefore, other possibilities for natural materials should be pursued and bacterially derived polymers prove to be a promising option[30-32].

In recent years, discoveries related to bacterial polymer synthesis has led to the production of tailor-made polymers for biomedical and industrial applications[33]. Better understanding of the regulatory processes and molecular mechanisms concerned with the biosynthesis of polymers enables one to engineer the bacteria for efficient production of the biopolymer and to produce modified versions of the biopolymer with unique material properties for niche applications[34]. Microorganisms can produce both intracellular and extracellular biopolymers such as polysaccharides, polyamides and polyesters. These microbial polysaccharides can be associated with cell surface as capsular polysaccharide (K30 antigen and glycogen) or loosely connected with the cell surface as exopolysaccharides (hyaluronic acid, xanthan, cellulose and alginate)[34,35].

Exopolysaccharides (EPS) vary based on the backbone structure, monomer composition and molecular mass. The yield of these exopolysaccharides depend on certain physicochemical parameters such as temperature, pH, composition of medium and incubation time[36,37]. Based on monomer repeating units EPS can be divided into heteropolysaccharides (xanthan and dextran) and homopolysaccharides (curdlan and cellulose)[38]. BC is a homopolysaccharide consisting of β-(1-4)-glucans as a repeating unit. It is synthesized by gram negative bacteria *Acetobacter, Rhizobium, Sarcina* and *Agrobacterium*[39].

Bacterial cellulose has displayed exceptional potential as an effective biopolymer in diverse fields such as food, textiles, biomedical and bioremediation. The structural features of plant cellulose are inferior compared to BC[40,41]. However, the commercial application is hindered due to scalability and limited molecular understanding regarding the process of BC formation[42,43]. Consequently, more emphasis will be laid on this biopolymer, its optimum production, biologics of the bacteria, structural investigation of exopolysaccharide, and development of various functional materials through different sustainable strategies will be explored.

1.2 Hypothesis

The overall aim of this work revolves around developing novel BC based functional materials for various skin-based applications. To achieve this goal, first, we need to understand the biology of the bacteria and secure BC production. Second, have control over the structural properties of the exopolysaccharide. Third, greener and sustainable strategies to design BC based functional materials. We hypothesize that identification of highest cellulose-producing bacterial strain and the structural investigation of the produced exopolysaccharide is paramount to the systematic development of BC based functional materials.

1.3 Research Objectives

The conventional method requires 7-14 days to determine cellulose production yield and optimization of culture conditions. We propose to develop analytical and screening platforms to understand the bacteria better, optimization of its growth conditions and to improve detection time.

During cellulose biogenesis, cellulose synthase enzyme is unique to the whole process of BC production. The exceptional structure and properties of bacterial cellulose result from the extrusion of precursor polymeric molecules and their assembly outside the bacterial cells. We intend to investigate the specificity and flexibility of the cellulose synthase complex and study their structural effects.

With control over BC production and structural properties of the biopolymer, there is a need to utilize this biomaterial in a sustainable approach for skin-based applications. Therefore, the third problem is focussed on developing renewable strategies for the utilization of BC as a matrix, to develop BC based functional materials through environmentally friendly strategies.

1.4 Specific Objectives

To test the proposed hypothesis, the dissertation had the following specific objectives :

1. Develop a novel analytical platform that can be used for studying the biology and optimizing growth conditions of cellulose producing bacteria. The platform will be based on surface growth pattern of bacteria. It will evaluate the importance of cellulose production for bacterial chemotaxis and assess the impact of environmental factors on cellulose production.

2. Investigation of substrate specificity of cellulose synthase complex, various substituted glucose analogues will be introduced and its effect on the process of BC polymerization and crystallization will be studied. Structural morphology of the various cellulose pellicles will be analyzed to check for changes in the fiber growth and network arrangement. The effects of the process of crystallization will be analyzed through X-ray diffraction.

3. Design of bacterial cellulose-poly(3,4-ethylenedioxythiophene) polystyrene sulfonate (PEDOT:PSS) conductive aerogels as substrates for flexible electronics. A variation of dispersion casting (top-down approach) will be used in developing BC-polymer aerogels through acoustic cavitation. The conducting polymer, PEDOT:PSS will be used in this study due to its high conducting nature and biocompatibility. Structural morphology of the BC based hybrid materials will be analyzed. Confirmation of the chemical incorporation of PEDOT:PSS into BC matrix will be verified through IR spectroscopy. Evaluation of the sheet resistance of the BC-polymer aerogels.

4. Synthesis of magnetic bacterial cellulose membranes inspired by novel bioengineering approach. A bioengineered *E.coli* bacteria containing amyloid protein CsgA will be used to functionalize cellulose films. Short peptide domains, m6A, will be genetically tagged to amyloid protein for nanoparticle templating. Magnetite nanoparticles (Fe_3O_4) will be synthesized *in situ* in the presence of functionalized cellulose membranes. The role of magnetic membranes in wound healing will be studied.

Chapter 2

Literature Review

2.1 Introduction to cellulose

Polysaccharides are the most common biopolymers on earth, consisting of cellulose, starch, glycogen, and chitin. These macromolecules are made up of long chains of repeating monomer units with a general formula $(C_6H_{10}O_5)_n$. The repeating unit is characteristically the monosaccharide glucose molecule bound together by glycosidic bonds[44]. These polymers can form a linear chain as in cellulose or a highly branched system as found in glycogen. They are classified into two categories based on the functions, structural polysaccharide (cellulose and chitin) and storage polysaccharide (glycogen and starch)[45,46]. Biopolymers offer a promising future due to their biocompatibility, biodegradability, and renewability. Cellulose is the most abundant and widespread biopolymer in nature that can be produced in the biosphere[45,46].

French chemist, Anselme Payen discovered cellulose in the year 1838 which was first isolated from plant tissues. It represents 33% of the earth's biosphere with an annual production of 1.5×10^{12} tons[47]. Characteristic structure of cellulose obtained from plants is shown in Figure 2.1, it can be extracted from cotton, plant fibres and wood. Plant cellulose exists as a composite, it is physically and chemically bound together consisting of polymers lignin along with carbohydrates cellulose and hemicellulose. Lignin represents a matrix in plant matter bringing cellulose fibres together to form a resin system. Hemicellulose behaves as an interfacial compatibilizer in the resin system, with cellulose being the reinforcement material[48]. The degree of polymerization for plant cellulose can vary between 10000 in nature to 15000 in native cotton. Although, cellulose forms a significant portion of plant matter, its mechanical properties such as stiffness and strength are inferior to pure cellulose[49,50]. Plant cellulose can be effectively purified through certain chemical and mechanical pre-treatments to obtain a pure form.

Only certain species of bacteria can produce pure form of cellulose, and *Acetobacter xylinum* bacteria can yield bacterial cellulose in industrial amounts[40].

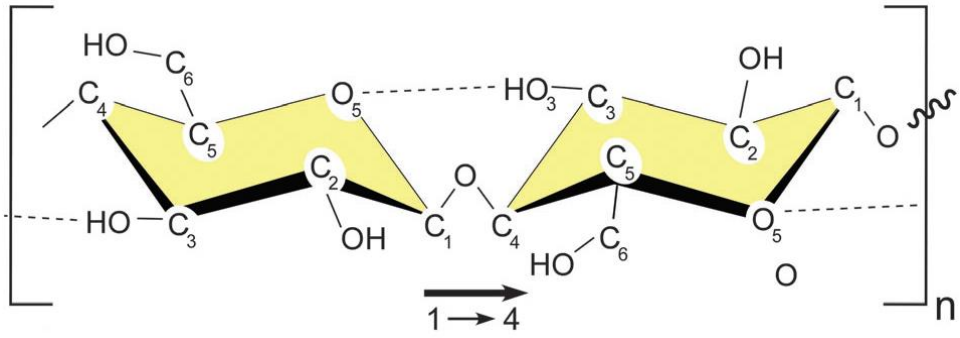

Figure 2.1 Chemical structure of cellulose with β- 1,4 glycosidic bonds, reproduced with permission from 46, ©1972, Royal Society of Chemistry.

2.2 Bacterial Cellulose

Cellulose can be effectively obtained through two strategies, either top-down approach where it is extracted from plants and subjected to high shear stress to form smaller size cellulose suspensions, or bottom-up approach where its synthesized by bacteria[45]. Bacterial cellulose was discovered by A.J. Brown in 1886 while he was working with *Bacterium aceti* grown in nutrient culture media which composed of 1 %(w/v) acetic acid in the form of ordinary vinegar and red wine that was diluted to half its bulk with water. After a few days of incubation, a translucent jelly-like mass was noticed on the surface of the nutrient solution[51]. This gelatinous membrane covers the entire surface of the medium and has the capability to grow to a thickness of about 25 mm if favourable conditions exist. Brown described the membrane to be tough especially if one attempts to tear it across the growth plane[52]. In 1947, Hestrin *et al*. used *Acetobacter xylinum* as a model bacterium to prove that the resting and lyophilized bacteria produce cellulose in the presence of oxygen and glucose[53,54].

Later research confirms the chemical composition of bacterial cellulose and plant cellulose are same, but BC displays superior physical properties. Cellulose produced by various bacteria include gram-positive bacteria such as *Sarcina ventriculi* and gram-negative bacteria such as *Acetobacter*, *Achromobacter*, *Pseudomonas*,

Rhizobium, *Salmonella* and *Azotobacter*. *Gluconacetobacter xylinum*, *Gluconacetobacter hansenii* and *Gluconacetobacter pasteurianus* are the most effective producers of cellulose[32,55].

In nature, bacteria synthesize cellulose as extracellular polysaccharides, which form a protective envelope around the cells. Microbial cellulose which is chemically pure, contains no lignin and hemicellulose as shown in Figure 2.2. It is predominantly left-hand twisted with individual nanofibers ranging from 25-100nm in diameter and several microns in length. BC produced is the "gold-standard" for nanocellulose since one of the dimensions are in the nanometer range and is synthesized in a controlled manner by bacteria[39,52].

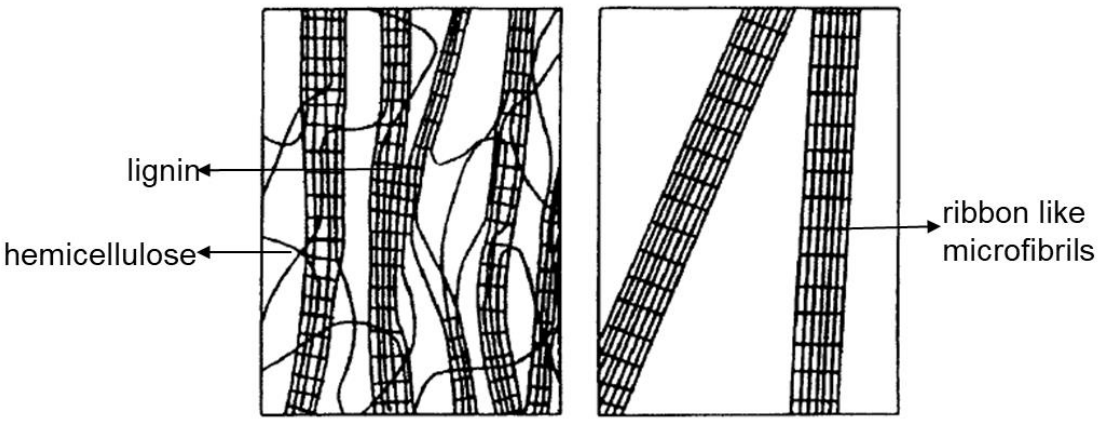

Figure 2.2 Plant cellulose vs. bacterial cellulose. The absence of lignin and hemicellulose indicated in bacterial cellulose, reproduced with permission from 49, © 2000, Springer Nature.

BC has high water holding capacity and great tensile strength due to ultrafine network architecture and high degree of polymerization (no. of glucan monomers connected to form a polyglucan chain)[56]. It can be grown to any shape due to its high moldability during synthesis and can be produced from a variety of substrates. Moreover, the BC produced is highly crystalline when compared to plant cellulose. It is vastly porous since the microfibrils formed are considerably smaller than those in plant cellulose[49,55]. Some of the common physical properties of plant and bacterial cellulose is listed in Table 2.1.

Table 2.1 Physical properties of plant cellulose and bacterial cellulose, reproduced with permission from 57, © 2007, Elsevier.

Properties	Plant cellulose	Bacterial cellulose
Fibre width	1.4-4 x 10^{-2} mm	70-80 nm
Crystallinity	56-65%	70-90%
Degree of polymerization	10000-14000	2000-8000
Young's modulus	5.5-12.6 GPa	15-30 GPa
Water content	60%	98.5%

2.3 Gluconacetobacter species

Gluconacetobacter xylinum is an aerobic bacterium which synthesizes cellulose. It was discovered as a non-pathogenic mesophile by Brown. He suggested calling this microorganism *Bacterium xylinum* because of its ability to produce cellulose[51]. However, since it is an acetic acid producing bacteria, it was renamed as *Acetobacter xylinum.* Presently, the bacterium is termed *Gluconacetobacter xylinus* that belongs to the genus *Gluconacetobacter* and is one of the 29 genera of the *Acetobacteraceae* family[57]. They are gram-negative rod-shaped bacteria, occurring as pairs, chains, individuals or small clusters in the form of colonies[58]. In nature, it is usually found on rotting fallen fruits and commonly found in soil, sometimes in symbiosis with plants such as coffee and sugarcane. An overview of the different BC producing species is presented in Table 2.2[39,59]. Due to its unique ability to produce cellulose in large quantities, *Gluconacetobacter xylinum* has been primarily considered as a model organism for the biosynthesis of cellulose by researchers.

Table 2.2 Different bacterial genera of cellulose producers and their biological roles, reproduced with permission from 39, © 2008, Taylor & Francis.

Genus	Cellulose structure	Biological role
Acetobacter	Extracellular pellicle	To hold in aerobic environment
Rhizobium	Short extracellular fibrils	Attachment to plant tissue
Agrobacterium	Short extracellular fibrils	Attachment to plant tissue
Pseudomonas	No distinct fibrils	Flocculation in wastewater
Aerobacter	Extracellular Fibrils	Flocculation in wastewater
Achromobacter	Ribbons	Flocculation in wastewater
Sarcina	Amorphous	Unknown

Three different cellulose producing strains were used in this work for various investigative experiments. *Gluconacetobacter hansenii* (ATCC 53582) was isolated from sugarcane exudates and is typically 8-10 µm in length and 1-3 µm in width making them the longest of the three strains as observed in Figure 2.3[60]. *Gluconacetobacter xylinum* (ATCC 700178) was isolated from plant-derived foodstuff, 5-7 µm in length and 2-4 µm in width (Figure 2.3)[61]. *Komagataeibacter rhaeticus* (iGEM strain) was isolated from Kombucha tea and is similar in size to *Gluconacetobacter xylinum* strain (Figure 2.3)[62].

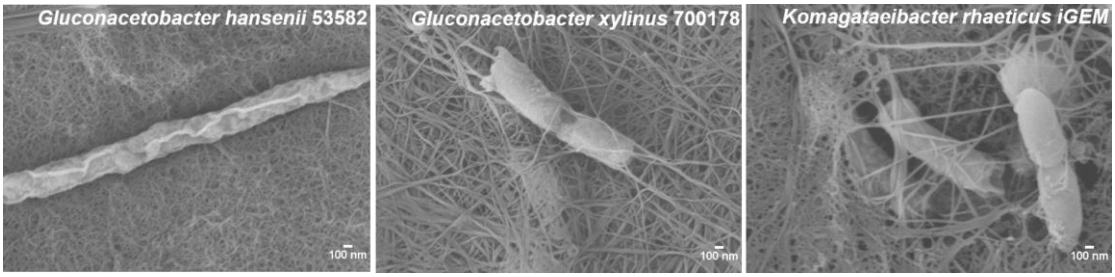

Figure 2.3 Electron micrograph displaying various cellulose producing strains used in this work (*Scale bar: 100 nm*)[63].

G. xylinum characteristically produces two types of cellulose, cellulose I ribbon like polymer and cellulose II the thermodynamically stable amorphous polymer. The differences in assembly of the two types are shown in Figure 2.4. Close to 200,000 glucose molecules can be polymerized per second by a single *G. xylinum* cell into β-1,4-

glucan chains[46]. These chains are secreted through pores, which are arranged along the longitudinal axis of the cell. Enzyme cellulose synthase is present at the pores which facilitates in extruding the chains to the surrounding medium. These chains fuse together to form microfibrils with 40-60 nm width, that are the in the form of ribbon like bundles. Microfibrils form the floating cellulose matrix produced by the aerobe which is thought to grow where there is higher oxygen concentration[64,65].

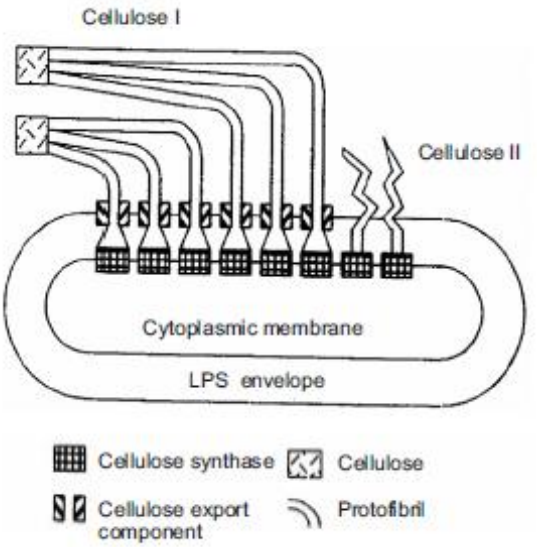

Figure 2.4 Schematic representation of the assembly of cellulose chains extruded by bacteria, reproduced with permission from 49, © 2000, Springer Nature.

G. xylinum is non-motile in nature but moves forward due to the extrusion of cellulose bundles at a rate of 2 µm/min. Sub-elementary fibril/nanofibril of 1.5 nm width are extruded out of the 3.5 nm pore width of the terminal complex present along the bacterial wall as shown in Figure 2.5. These nanofibrils aggregate to form 3-4 nm nanofibers due to the crystallization of the glucan chains. Later the nanofibers combine to form 40-60 nm wide microfibrils. The enzymes responsible for biosynthesis are associated with the cell either through the inner or outer membranes. The process of polymerization and assembling of cellulose microfibril bundles is still unclear[39,66].

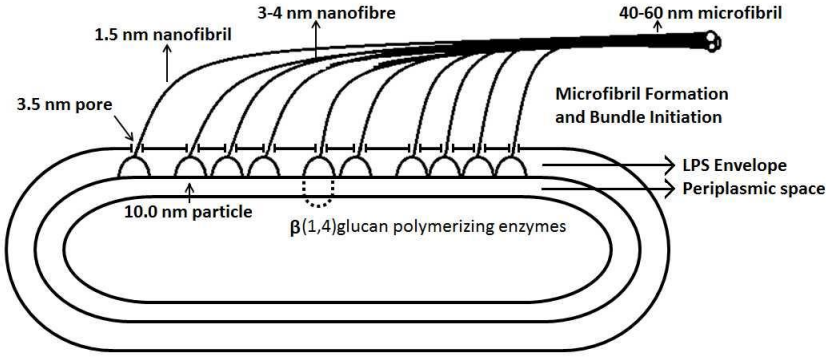

Figure 2.5. Possible model of glucan chain assembly at the bacterial cell wall. The figure is adapted and redrawn from [39], © 2008, Taylor & Francis.

However, there are still discussions regarding the benefits for the bacteria in cellulose production. A few probable hypotheses suggest that it produces cellulose to remain on the surface of the medium near highest oxygen concentration. To protect against external environment conditions such as ultraviolet light and heavy metal ions thereby, aiding in nutrient diffusion. In addition, it may also aid in the retention of moisture and prevent natural substrates from drying while the bacterium is growing on the substrates[67,68].

2.4 Bacterial cellulose biosynthesis pathway

Biosynthesis of cellulose is a highly regulated multi-step process comprising of individual enzymes and complex catalytic proteins whose structures have not been defined clearly. *G. xylinum* either follows the Krebs cycle coupled with gluconeogenesis or pentose phosphate cycle. It converts the various carbon compounds such as glycerol, hexoses, fructose, pyruvate, and dicarboxylic acids into cellulose with about 50% efficiency. Pyruvate and dicarboxylic acids enter the Krebs cycle. Due to oxaloacetate decarboxylation to pyruvate, it undergoes conversion to hexoses through gluconeogenesis and forms glycerol, dihydroxyacetone and other intermediates of the pentose phosphate cycle[69,70].

Biosynthesis of cellulose involves four fundamental enzyme-mediated steps. It starts with transformation of glucose to UDP-glucose via glucose-6-phosphate and glucose-1-phosphate and finally the enzyme cellulose synthase (CS) adds UDP-glucose to the chain and forms a growing polymer as shown in Figure 2.6. CS is very important

in the synthesis process. The enzymes involved in the biosynthesis process are glucokinase (GK), phosphoglucose isomerase (PGI), UDPG-phosphorylase (UGP) and phosphoglucomutase (PGM). Uridine diphophoglucose (UDPGlc) is a very important intermediate product that is formed by converting a carbon source through a series of enzymatic steps. The UDPGlc formed is converted to cellulose by CS which is present on the cytoplasmic membrane, and the cellulose product will be obtained extracellularly[53,71].

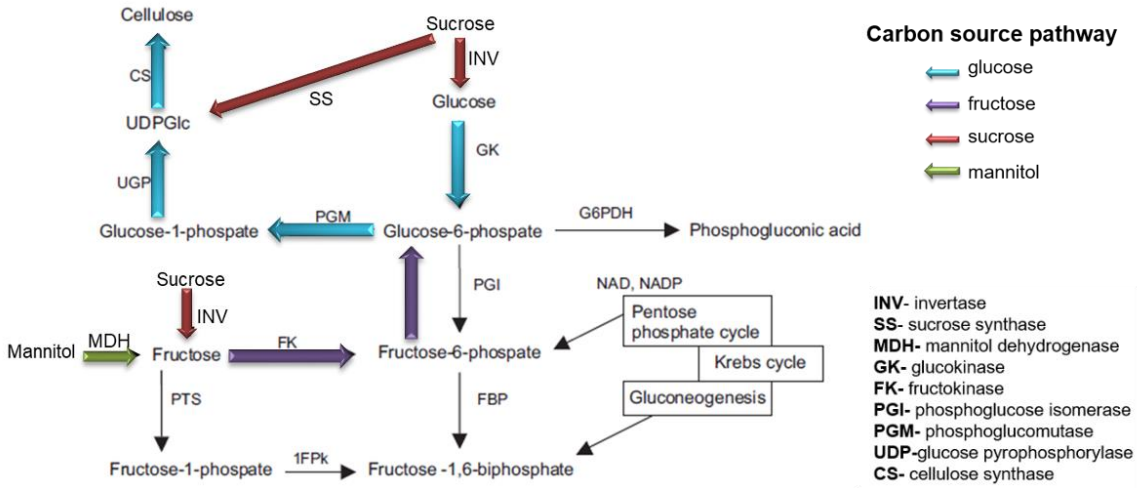

Figure 2.6 Cellulose biosynthesis pathway of Gluconacetobacter xylinus E25 grown on different carbon sources[55].

UDPGlc is a direct cellulose precursor in many organisms as observed in the pathway. UGPase is believed to play a vital role in the biosynthesis of cellulose since it is 100 times further active in cellulose producers than in noncellulose producers. Disaccharides such as maltose and sucrose need to hydrolyze to form monosaccharides, glucose and fructose to produce cellulose. Though the pathways related to UDPGlc is well established, the molecular mechanisms related to the polymerization of the glucan molecules into long and unbranched cellulose chains are not well-defined. The molecule cyclic diguanylic acid (c-di-GMP) plays an important role in the production of cellulose. It activates the membrane enzyme, cellulose synthase. In the absence of c-di-GMP, cellulose synthase remains inactive or the cellulose producing activity is reduced. The balance between bound and free c-di-GMP is maintained through intracellular potassium concentration[69,72].

2.5 Bacterial cellulose growth conditions

One major problem encountered is its low productivity and high production costs associated with its synthesis, especially if the production requires to scale up to meet industrial demands. Various groups have studied the different media composition and cultivation conditions for *Gluconacetobacter* strains and different species, to obtain the most optimum growth conditions for maximum yield[73].

2.5.1 Bioprocess methods

Currently cellulose is produced through three different methods, static culture system, agitating cultures, and reactors.

In static culture system, cellulose is produced at the air/liquid interface by *G. xylinum* as shown in Figure 2.7. It is the most simple and basic method of cellulose production. Production can be interrupted if the medium is mixed or agitated. The set-up is incubated for 5-20 days with cellulose gradually occupying the whole container. BC production is directly proportional to the area of air/water interface if the depth is less than 4.5 cm[74]. It is imperative that oxygen diffuses down and the nutrients move up to the cells[75-77].

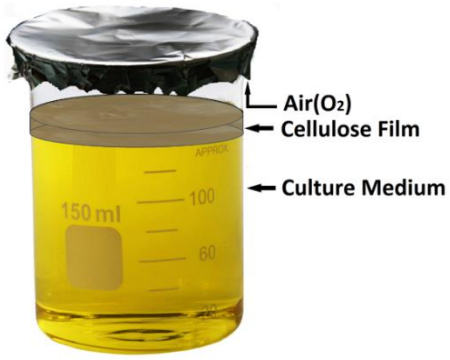

Figure 2.7 Cellulose growing at air-water interface in a static culture.

Agitating cultures reduce cultivation time. Chemical structure of BC produced is similar between shaking and static conditions. Although, the growth rate of bacteria increases its yield, is comparatively lower than static system. This is because while shaking there is mutation of the cellulose producing cells to non-cellulose producers. In addition, shaking culture broth tends to increase in viscosity due to the accumulation of

BC leading to inhomogeneity of the culture[78-80]. To improve the yield of BC, bioreactors were designed[52].

Bioreactors tend to increase the doubling time of *G. xylinum* compared to static conditions. In a stirred tank reactor, medium homogeneity is maintained due to the vigorous agitation of the impellers but increases shear stress on cells. Due to vigorous movements, higher power required for mixing[81,82]. Airlift reactors solved the problem of stirred tank reactors by reducing the shear stress and it requires lower power supply. It increases the BC production and cell concentration due to enriched supply of air/O_2 from bottom[83,84]. Cellulose produced from the above-mentioned reactors have inferior mechanical properties thereby, limiting its applications. Also, due to the adhesion of BC to the shaft in both agitation and airlift reactors make it challenging to remove the BC product[52,85]. Rotating disk reactors was designed to produce cellulose with superior mechanical properties. It consists of a tube-shaped inlet for inoculum transfer and several rotating disks attached to a rotating shaft. The reactor was designed in a manner with half the area of the disks was submerged in the culture and the other half was in contact with the atmosphere. With this design, BC will attach to the disks maintaining its mechanical properties[86,87].

2.5.2 Base media

Hestrin-Schramm (HS) medium was one of the most commonly used medium for initial research work related to bacterial cellulose[75]. Later, several modifications were applied to this medium to increase bacterial cellulose production by Yamanaka *et al.*[88], Zhou *et al.*[89] and Son *et al*[90]. A brief overview of the different medium compositions is summarized in Table 2.3.

Table 2.3 Composition of different media used for bacterial cellulose production (concentration in percent w/v)[88-90].

Components		Medium			
		HS	**Yamanaka**	**Zhou**	**Son**
Carbon source	Glucose	2	5	4	1.5
Nitrogen source	Yeast extract	0.5			
	Peptone	0.5	0.5		
	Corn steep liquor (CSL)			2	2
Phosphates	KH_2PO_4		0.3	0.2	0.3
	Na_2HPO_4	0.27			
	$Na_2HPO_4.12H_2O$		0.005	0.04	0.3
Sulphates	$MgSO_4.7H_2O$				
	$FeSO_4.7H_2O$				0.0005
	$(NH_4)_2SO_4$		0.5	0.4	0.2
Organic acid	Citric acid	0.115			
Others	H_3BO_3				0.0003
	Nicotinamide				0.00005

2.5.3 Carbon sources

Carbon source is one of the most influential factors affecting bacterial cellulose production. Different types of carbohydrates such as monosaccharides[91], disaccharides[92], oligosaccharides[93] and various organic acids[94], alcohols[95], sugar alcohols[53,96] have been investigated to scale up bacterial cellulose production. Carbon sources such as glucose, fructose, lactose, sucrose, galactose, xylose, starch, mannitol and arabitol were used to study bacterial cellulose production. Discussed below are some of the research work with respect to effect of carbon source on various strains for cellulose production[97].

Mikkelsen *et al*. explored the effect of production by *G. xylinus* ATCC 53524 on six different carbon sources, glucose, galactose, fructose, sucrose, mannitol and glycerol[98]. They identified sucrose as the best substrate followed by glycerol, mannitol, glucose and fructose with galactose being the least favourable source. Pourramezan *et al*. studied the culture environment for production by Acetobacter sp.4B-2 and identified sucrose as the best substrate followed by glucose, xylose and lactose[99]. Ishihara *et al*. identified glucose, mannitol and sucrose as ideal substrates for production by *A. xylinus* NCIM 2526 and used xylose as a source for *A. xylinus* IFO 15606[100]. Coban and Biyik studied the effect of production by *A. lovaniensis* HBB5 on different nitrogen and carbon sources[101]. The combination of yeast extract in HS and glucose produced the highest yield. Nyugen *et al*. used *G.xylinus* strain isolated from kombucha tea with mannitol to produce highest yield[102]. Basu *et* al. found carbon sources used for bacterial growth significantly impacts the interplay between process variables (i.e., factors responsible for BC production) and desired outcomes (i.e., BC yield) through Design of Experiments (DOE) strategy[103].

It is evident from the above works that different types of strains prefer different carbon sources for cellulose production. Optimization of the right type of medium and carbon source for a strain is of utmost importance to achieve maximum yields.

2.5.4 Bioprocess parameters for production

G. xylinus growth and cellulose production is primarily dependant on certain environmental factors, namely, temperature[104,105], pH[79,106,107], dissolved oxygen[69,108] and stirrer speed in bioreactors[86,109]. These microorganisms respond quickly to changes in the bioprocess parameters in various aspects such as induction and repression of protein synthesis and morphological variations in the cells[55,70].

The optimum working temperature range for the bacteria is between 26°C- 30°C. Son *et al*. investigated the effect of temperature from 20°C - 40°C on the production by *Acetobacter* sp. A9 and reported that 30°C was found to be the optimum temperature[110]. While lowering the temperature to 25°C did not significantly affect the yield of BC when compared to 30°C but increasing the temperature to 35°C did affects its yield[39,55].

The optimum pH range for bacterial growth and cellulose production is between 4-7. Wide ranges of pH were investigated with BC production being the maximum at pH 6.5[110]. pH values generally tend to drop as the incubation period increases due to the production of secondary metabolites such as gluconic acid and lactic acid during carbon and nitrogen consumption. Hence, maintaining the optimum pH range is vital for maximum yield[111,112].

Dissolved oxygen in the cultures is an important component for cellulose yield, quality of the membrane produced and cell metabolism. Low DO values can impede cell growth leading to low cellulose production. Whilst, high DO values can result in high gluconic acid concentration which in turn can affect cell viability resulting in low yield of BC[79,113,114].

2.6 Assembly of bacterial cellulose chains

When considering cellulose biogenesis, main emphasis is on cellulose synthase enzyme which is unique to the whole process of cellulose production[115]. Although, it was once considered polymerization occurs outside the cell through the covalent packing of the short chain precursors secreted by the cell, but later research confirmed polymerization is a membrane associated process. The exceptional structure and properties of BC result from the extrusion of glucan chains and their assembly outside the bacterial cells[69,116]. Cellulose precursor polymeric molecules produced inside the cells are extruded out through the terminal complexes present on the membrane of the cell to form protofibrils of 2-4 nm diameter, later these fibrils join to form ribbon shaped microfibrils of approximately 80x4 nm[49].

Presence of 50-80 pore-like terminal complexes along the longitudinal axis of the cell envelope are confirmed through electron micrographs[117,118]. The terminal complexes are lipopolysaccharide layers responsible for extruding individual β-1,4 glucan chains, the complexes are spatially arranged for assembly of cellulose fibrils which is a common feature observed in both lower and higher organisms[117]. The process of polymerization and crystallization of cellulose chains is generally defined as cell directed, since it occurs in the extracellular region, beginning with mutual orientation

and association of glucan chains, followed by aggregation, the microfibrils and ribbon bundles are all governed by the initial pattern of extrusion sites[119].

Stronger aeration or presence of molecules that cannot enter the cell from outside but can interfere with the hydrogen bonds between β-1,4 glucan chains such as Congo red, calcofluor white, fluorescent brightener and carboxy methyl cellulose (CMC) can significantly affect the process of crystallization[120-122]. Thermodynamically stable cellulose II structure is formed instead of the cellulose I ribbon like polymer[123]. Kinetically, disruption of the process of crystallization leads to increased incorporation of glucose molecules into the glucan chains. The surprising effect on polymerization has led to the conclusion that polymerization and crystallization are tightly coupled processes of cellulose biogenesis. In the sense, crystallization is a rate limiting step of cellulose biogenesis[69,124]. Kinetically, disruption of microfibril assembly is manifested by an enhancement of the overall rate of incorporation of glucose into insoluble polyglucan chains. The use of cellulose-binding agents alter microfibril assembly at different phases has been the principal experimental method for characterization of the microfibril and ribbon assembly process in *A. xylinum*[69]. For example, Congo Red, Carboxymethyl cellulose, Calcofluor, bind to 1.5-nm cellulose aggregates, interfering with the early-stage appearance of crystalline 3.5-nm microfibrils, a higher level of assembly in which large bundles of crystalline microfibrils fasciate to form the final, twisted-ribbon product is prevented[121,124]. On the basis of such observations, microfibril assembly is postulated to occur in a stepwise, hierarchical fashion. This process is usually described as cell directed because, although it occurs in the extracellular space, the mutual orientation and association of glucan chains, aggregates, microfibrils, bundles, and ribbon are apparently governed by the original pattern of extrusion sites[120,121,124].

2.7 Structural and mechanical properties of bacterial cellulose

The linear structure and presence of hydroxyl groups in cellulose chains gives rise to strong intramolecular and intermolecular hydrogen bonds leading to a highly crystalline structure as observed in Figure 2.8[125]. Cellulose in general can exist in

multiple forms. Cellulose I polymorph consists of two crystalline forms, namely, cellulose Iα and cellulose Iβ based on hydrogen bonding and orientations of the crystals.

Cellulose Iα is primarily made up of triclinic unit cells and cellulose Iβ is made up of monoclinic unit cells[126]. The ratio between the two crystalline forms of cellulose I polymorph can vary based on various species of organisms. Bacterial cellulose is rich in cellulose Iα crystals and higher plants such as cotton and wood are dominated by cellulose Iβ. Mercerization (alkaline NaOH treatment) and regeneration on cellulose I structure can transform the polymorph to a thermodynamically more stable cellulose II structure[68,127].

Cellulose I chains are arranged in parallel direction with all the non-reducing ends on one side and reducing ends to the other whereas, in cellulose II chains there is an antiparallel arrangement. Other polymorphs of cellulose are III_I, III_{II}, IV_I and IV_{II} based on different hydrogen-bonding links and molecular alignments. Cellulose I polymorph possesses a higher elastic modulus than cellulose II structure [68,127,128].

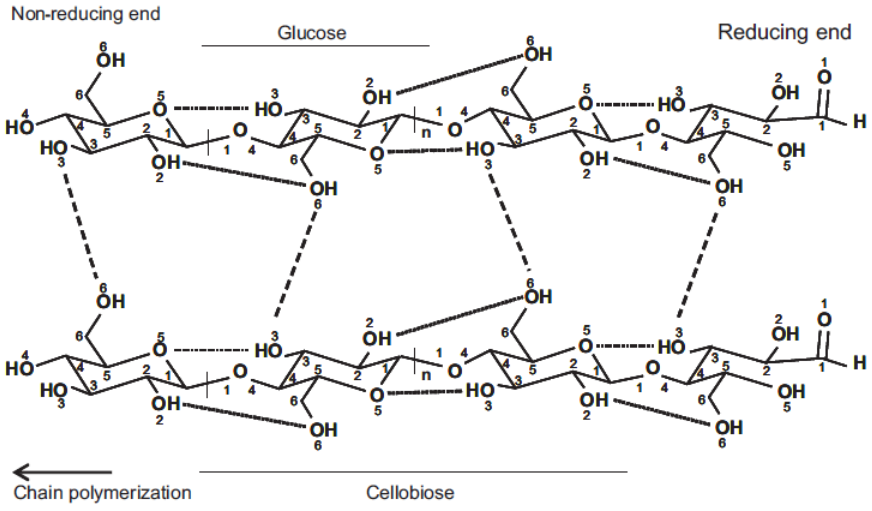

Figure 2.8 Structure and the inter- and intra-chain hydrogen bonding network in bacterial cellulose. Dashed lines: inter-chain hydrogen bonding. Dotted lines: intra-chain from [129], © 2007, Brazilian Journal of Plant Physiology

G. xylinus synthesizes cellulose in the form of a highly swollen gel with high crystallinity, superior mechanical strength and high-water absorption capacity. The

water retention ability of bacterial cellulose is greater than plant cellulose due to the presence of pores and tunnels within the wet pellicle, creating a large surface area[14,130]. The BC pellicle is very tough especially when an attempt is made to tear it across the plane of growth. The Young's modulus value obtained for the pellicles sample is around 10 GPa, due to the presence of hydrogen bond network within the polyglucan chains and between the adjacently arranged glucan chains[131,132]. This helps in increasing its mechanical strength and offers stability to the structure (Table 2.1).

Two crystalline forms, Iα and Iβ in bacterial cellulose can be distinguished either by X-ray diffraction or Raman spectroscopy. The characteristic XRD diffractogram for bacterial cellulose has three main peaks at 14.5°, 16.8° and 22.7° with crystal planes (1-10), (110) and (200) respectively corresponding to the two unit cells[133,134].

2.8 Applications of bacterial cellulose

BC exhibits certain properties like high density, high water binding capacity, high crystallinity, high purity, higher surface area and good shape as compared to the native cellulose. Due to these properties, it finds applications in areas including paper, textile, pharmaceutical, food, waste treatment and refinery (Figure 2.9)[135,136].

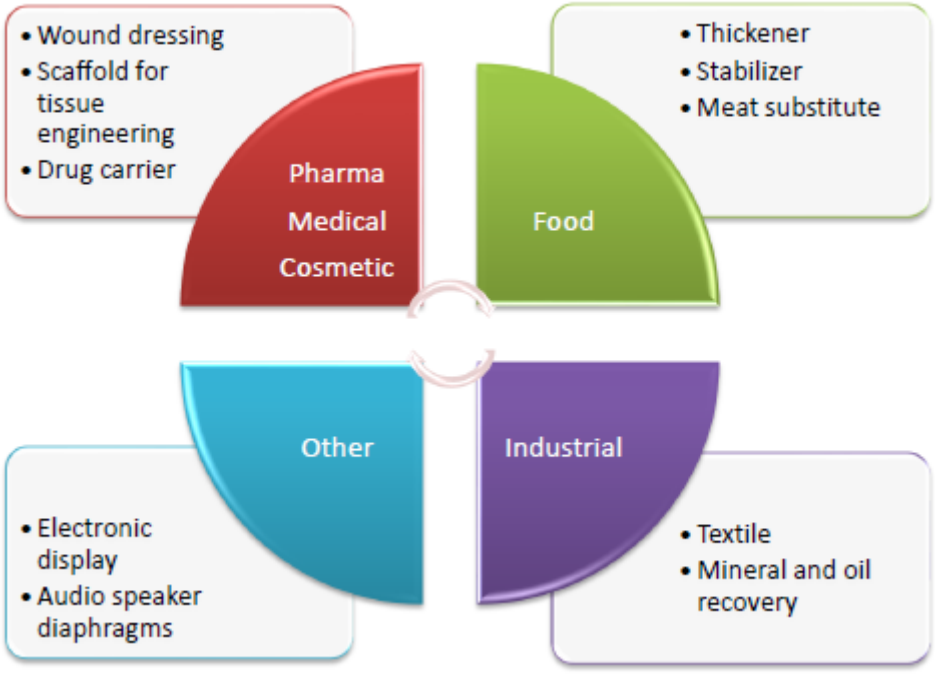

Figure 2.9 Different applications of bacterial cellulose in diverse fields.

Food applications

Compared to traditional dietary fibres, BC possesses high level of purity, thereby, categorized as "generally recognized as safe"(GRAS)[137]. This classification was formally accepted by United States FDA in 1992[138]. BC was first used in the Philippines as transparent jelly-like food in Nata de coco. It is a popular snack in Philippines and other countries. Owing to its indigestibility and gel-like properties, it is used as a food base[74]. In Japan, it was introduced into diet drinks. *Acetobacter* was allowed to grow along with yeast in sugar and tea extract, commonly known as manchurian tea or kombucha for improvement of health[138,139]. BC along with sucrose and CMC improves dispersion of dairy products and is also a perfect low-calorie additive and stabilizer[140].

Pharmaceutical and medical applications

BC has numerous applications in the field of biomedical engineering. In the early 1980s, Johnson & Johnson initiated attempts to commercialize the use of BC for treatment of wounds. Other commercially currently available wound products belong to

Brazilian company Biofill Produtos Biotecnologicos and an US based corporation, Xylos[141]. BC can be used as a scaffold for tissue engineered blood vessels (TEBV). It is an interesting approach that is being considered for treating problems associated with vascular diseases by delivering small vascular grafts[142]. It is also used as a drug delivery agent due to its highly porous microstructure where medicines can be introduced into the body along with bacterial cellulose[143,144]. BC provides good cell adhesion as a substrate through chemical modification or incorporation of element and aids in bone regeneration[145]. It can be applied as a wound dressing due to its high-water retention, mechanical property, and good biocompatibility[146,147]. BC has ability to be used as a substitute in veterinary and cosmetic treatments as well[32].

Industrial applications

The superior mechanical properties of BC microfibrils enables it to be employed for industrial scale applications. Ajinomoto Corporation and Mitsubishi Paper Mills in Japan have been designing various BC-based paper products. BC incorporated with gold nanoparticles or carbon nanotubes exhibits good electrical conductivity and can be used as electronic paper[68,148]. In the presence of an electronic dye, BC can change colour based on the voltage applied. This technology is the foundation for electronic books, flexible electronics, transforming wallpapers and dynamic papers[149].

Other applications

It can be incorporated along with organic compounds to design flexible electronic circuits to be used in skin-based applications[50,150]. BC is utilized as filtration material in percolating impurities and as a dialysis membrane to help in diffusion and osmosis respectively[151-153]. Sony, Japan utilized BC membranes to manufacture acoustic films[154]. BC is a promising candidate for food packaging containers to avoid contamination and damage[155,156].

2.9 Strategies to develop bacterial cellulose-based hybrid materials

The distinct properties of BC have encouraged efforts to apply it in various commercial brands. It has shown exceptional ability as both a matrix and reinforcement

material during the design of various composites. This creates a need to develop composites that is composed of BC and other materials[157].

BC composites can be synthesized through various strategies and the composites obtained have additional properties relative to bare BC. They are synthesized using a wide range of materials ranging from nanoparticles to polymers, metal/metal oxides to solid particles to cater to various applications. In general, there are three basic approaches to synthesize composites, namely, *in situ* method, *ex situ* method and dispersion and casting method[42].

2.9.1 *In situ* method of development of BC composites

In situ method utilizes the addition of reinforcement material during the synthesis of BC membranes, it becomes part of the fibre structure. BC fibres tend to become denser with incubation period and produces a network shaped structure that traps all the particles added to the BC culture media during synthesis. A schematic diagram describing the synthesis of BC composites through *in situ* method is shown in Figure 2.10. Some of the studies related to *in situ* method of BC composite synthesis are discussed.

Yan *et al*. added multi walled carbon nanotubes (MWCNT) to BC media during synthesis and incubated for 14 days[78]. Morphological analysis confirmed CNT's were trapped in between the BC fibres. Ruka *et al*. added various concentrations of water insoluble poly-3-butyrate to BC media. This affected BC yield and the morphology and crystallinity of BC[158]. Saibuatong and Phisalaphong incorporated aloe-vera into BC media and produced BC-aloe vera films resulting in superior physico-mechanical properties[159]. Graphene oxide (GO) was directly introduced into the bacterial culture. BC and GO displayed good interaction and biocompatibility as carriers for drug delivery[160]. Conductive BC composites were developed by adding conductive polymers directly into the culture medium[161-163]. Similarly, metal oxides and metal nanoparticles were impregnated into BC[164].

The challenges associated with this method is that the particles remain suspended in media for a short span of time and later settle down at the bottom. In static

culture, BC is produced at the air-media interface, it floats on the surface of the media. After precipitation in the media, the particles fail to get entrapped in between the cellulose fibres. Agitated culture system seemed to have overcome this problem through continuous agitation, the particles are suspended in media and prevented from settling. However, BC produced through this technique cannot be used in biomedical applications where the composite is required to be in gel or sheet form[1,157].

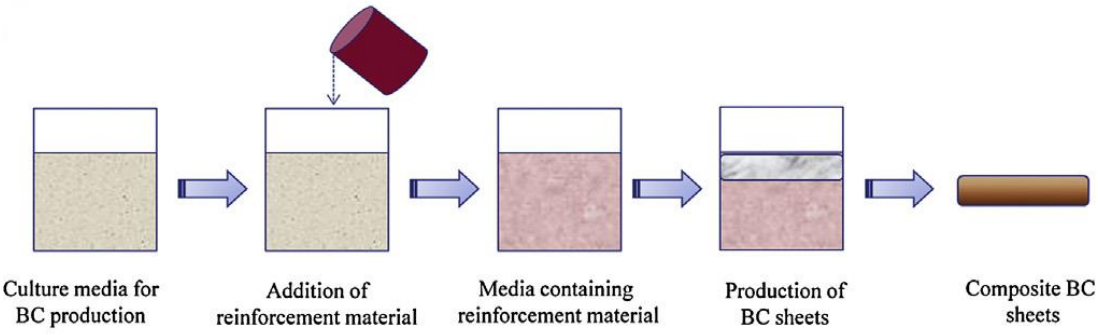

Figure 2.10 Schematic representation of BC composites synthesized through an in situ synthetic approach, reproduced with permission from 42, © 2013, Elsevier.

2.9.2 *Ex situ* method of development of BC composites

The issues faced with *in situ* method can be solved by impregnating nanoparticle or polymer solutions into the produced BC membranes. The interaction between the matrix and reinforcement materials can be either physical sorption or through hydrogen bonding. In physical absorption, particles can easily penetrate and get entrapped inside the porous BC structure whereas, hydrogen bonding results from the presence of OH moieties on polyglucan chains with the penetrating reinforcement materials (Figure 2.11). This approach is simpler and straight forward when compared to *in situ* method. The structure of BC is not compromised in any way to accommodate the reinforcement material.

Ul-Islam *et al*. developed BC-chitosan (Ch) composites through hydrogen bonding between the O-H and N-H groups of the respective materials[165]. Similarly, BC was combined with collagen[166], hydroxyapatite (HA)[167,168], hyaluronic acid[169,170] to produce BC composites with superior mechanical properties than bare BC for various biomedical applications. To improve the antimicrobial properties of BC, Yang *et al*.

incorporated silver nanoparticles (Ag NPs) into BC membranes through a green route without utilization of any harmful chemicals[171]. BC strips were immersed in silver nitrate solution and then heated gradually to enable hydrothermal production of Ag NPs. The particles later deposited in the porous BC matrix enabling good antimicrobial activity. Through similar strategy metal oxide [172-175], metal nanoparticles[176-180], carbon nanotubes (CNT)[181,182] and montmorillonite (MMT)[183,184] were introduced into porous BC matrix as show in Figure 2.11. BC was further combined with polymers such as polyaniline (PANI)[185-187], polylysine (PL)[188,189], poly(3-hydroxybutyrate) (P3HB)[190,191], Polypropylene (PP)[192,193], poly(3,4-ethylenedioxythiophene) polystyrene sulfonate (PEDOT:PSS)[194,195], polyvinyl alcohol (PVA)[196] for biomedical, packaging and flexible electronics applications.

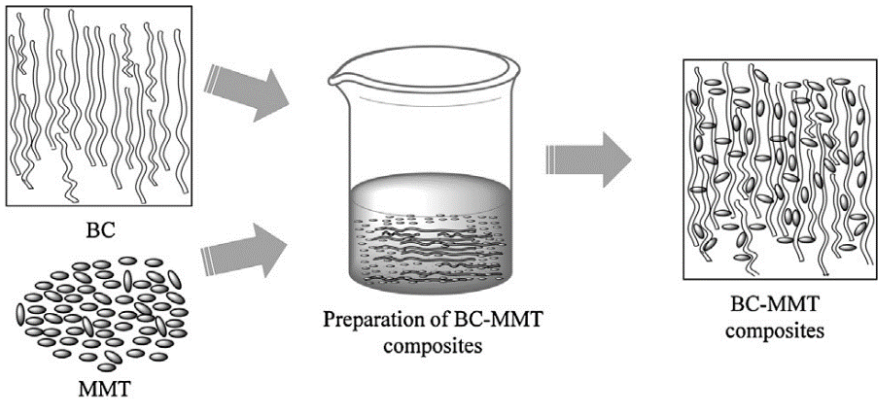

Figure 2.11. Schematic representation of BC composites synthesized through an ex situ synthetic approach reproduced with permission from 42, © 2013, Elsevier.

The primary hurdles associated with this approach are the size and nature of the reinforcement material. Larger particles cannot penetrate the BC pores, leaving only nano- or submicron particles possible to impregnate the matrix. Hydrophobic materials cannot interact with the highly hydrophilic BC structure[1]. Furthermore, the network arrangement of the BC fibrils is not uniform leading to non-homogeneous distribution of the reinforcement material in the matrix. New methods need to be explored and developed to tackle the above stated problems[1,42].

2.9.3 Dispersion and casting method for the development of BC composites

This method employs solutions of dissolved BC to synthesize a broad range of BC composites with various materials. Likewise, the composition of BC matrix and reinforcement materials can be easily controlled and there is homogeneous distribution and mixing of the both the materials. A general schematic of this method is shown in Figure 2.12. Strong inter and intra molecular H-bonds and high crystallinity of BC structure pose a challenge in solubilising BC completely[197,198]. Some research work has been done in this field to solubilise BC completely and further modify.

Few classes of compounds possess the ability to solubilise BC, namely, ionic liquids, N-methyl morpholine N-oxide (NMMO), TEMPO, NaOH, LiOH, Urea and thiourea[199-203]. Dissolved BC can be used to synthesize various types of BC films, nanofibers, microfibers, nanocrystals, and other composite materials. Gao *et al*. synthesized regenerated BC films after BC dissolution in NMMO and reported that these films possess superior mechanical and thermal properties[204]. The successful dissolution of BC and regeneration of films has developed great interest in this method for composite preparation.

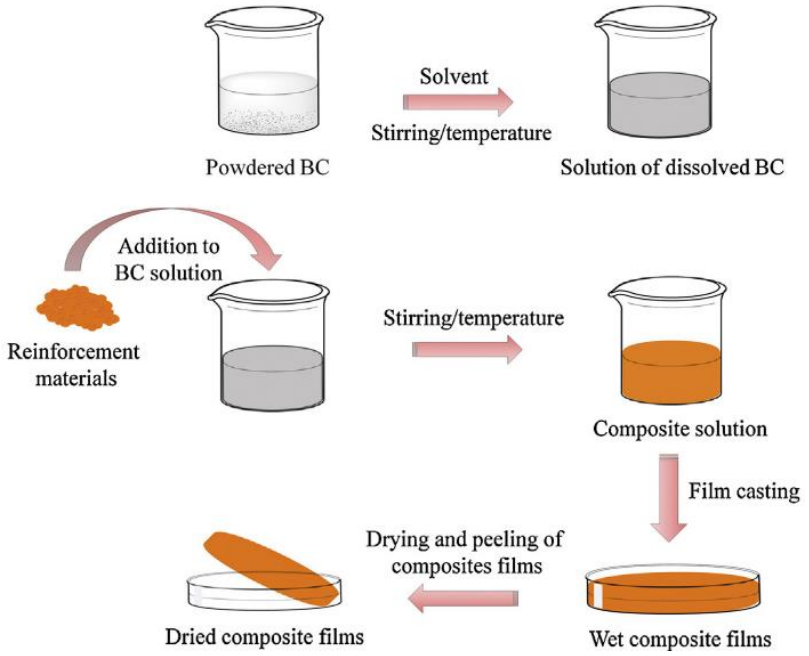

Figure 2.12. Schematic representation of BC composites synthesized from dissolved BC solutions reproduced with permission from 42, © 2013, Elsevier.

This approach has not been intensely utilized to produce BC composites but a wide range of inorganic materials such as clay, NPs and metals haven been investigated to produce polymer composites[2]. Composites synthesized through this method displayed better interaction between BC and the reinforcement material[199,205]. The drawback associated with this method involves the use of various strong solvents to solubilise BC. This leads to serious environmental problems with the disposal of solvents. The structural integrity of pristine BC is lost due to harsh chemical treatments[42].

2.9.4 Bioinspired approach

Bioinspired design employs biological principles to develop new solutions in fields that conventionally had fewer connections with biology[206,207]. A predominant goal of this strategy is to design biological systems for various applications. The functional materials are developed through a sustainable approach without the use of any harsh chemicals or mechanical treatments[208]. The live functional membranes incorporate both living systems with inorganic compounds to design materials with various functionalities. These "living materials" combine the advantages of live cells, which respond to their environment, produce complex biological molecules, and span multiple length scales, with the benefits of non-living materials, which add functions such as conducting electricity, emitting light and possessing magnetism[206,209].

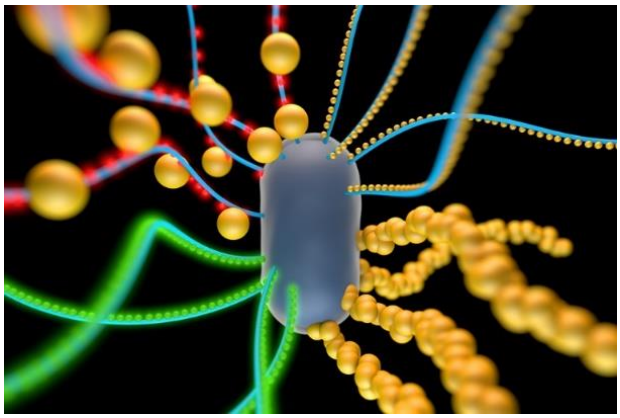

Figure 2.13. Bacterial cells engineered to impart tunable functional properties to hybrid materials[206].

Efforts have been focussed towards making live functional materials using bacterial cellulose. Co-cultivation of recombinant *bacterial* strains with *Gluconacetobacter* was explored as a possible strategy. Kaplan *et al,* developed a living membrane system based on the entrapment of recombinant *E. coli* bacteria in the cellulose matrix. The *E. coli* bacteria were genetically tagged with various fluorescent protein genes for stimulus detection and signaling. The living responsive membrane can sense and amplify the fluorescence signal based on environmental stimulus[208]. Similarly, Catchmark *et al,* developed a novel fermentation strategy to functionalize cellulose membranes. The co-cultivation strategy was adopted to produce cellulose films with enhanced mechanical properties. The BC films were produced by *G. hansenii* and *E. coli* was responsible for reinforcing BC with the production of exopolysaccharides (EPS) with high mechanical strength[210]. These strategies are based on the bottom-up approach, the bacterial cells are responsible for the development of functional membranes with desired material properties (Figure 2.13). It overcomes the limitations of the previous abovementioned strategies employed to develop BC composites. This approach opens a new sustainable route for imparting a wide variety of functionalities to BC based materials[209,211].

Chapter 3

A Novel Platform for Evaluating the Environmental Impacts on Bacterial Cellulose Production

Bacterial cellulose (BC) is a biocompatible material with versatile applications. However, its large-scale production is challenged by the limited biological knowledge of the bacteria. The advent of synthetic biology has led the way to the development of BC producing microbes as a novel chassis. Hence, investigation on optimal growth conditions for BC production and understanding of the fundamental biological processes are imperative. In this study, we report a novel analytical platform that can be used for studying the biology and optimizing growth conditions of cellulose producing bacteria. The platform is based on surface growth pattern of the organism and allows us to confirm that cellulose fibrils produced by the bacteria play a pivotal role towards their chemotaxis. The platform efficiently determines the impacts of different growth conditions on cellulose production and is translatable to static culture conditions. The analytical platform provides a means for fundamental biological studies of bacteria chemotaxis as well as systematic approach towards rational design and development of scalable bioprocessing strategies for industrial production of bacterial cellulose.

3.1 Introduction

With increasing demands for novel materials with diversified applications, BC has been gaining attention within the scientific community over the past decades[212,213]. With the advent of synthetic biology, BC producing microbes are being developed as a novel chassis[62]. For this purpose, investigations on optimal growth conditions, impacts of carbon sources on the BC production, and understanding of the fundamental biological processes are paramount.

Under cellulose producing conditions, it is difficult to monitor the bacterial growth rates, thereby making it extremely challenging to test the associated cellulose productivities under varied conditions. To further understand the cellulose production, bacteria such as *Gluconacetobacter xylinus*, which spontaneously convert glucose into its polymeric form, cellulose, has become the model organism in this field[214]. A systematic platform for screening of optimal cellulose producing conditions is particularly beneficial in circumventing practical difficulties associated with culturing of the bacteria by providing answers to some of these biological questions: Does the bacteria have preference towards carbon source and environmental conditions for growth or cellulose production? Can the bacteria perform chemotaxis and exhibit behaviour of common flagellate bacteria?

Leveraging on the preference of BC-producing bacteria to grow on substrate-surfaces[70], owing to its aerobic nature, we hypothesize that surface growth models will shed deeper insights regarding its biology[215]. Surface growth of chemotactic bacteria has been previously studied by several groups with Keller-Segel type as the widely accepted model[216,217]. In such experimental setup, a small drop of bacterial inoculum is added on top of a soft-agar medium surface at the centre of a petri-dish/plate and the bacteria can grow. shows the expected growth pattern. As the carbon source at the site of inoculation is consumed, the bacteria tend to form a concentric ring of actively growing cells which propagates in all directions simultaneously while leaving behind dead or dying cells[218,219]. Aligned to the same set-up, we establish the first analytical platform for monitoring BC producing bacteria surface growth under different culture conditions.

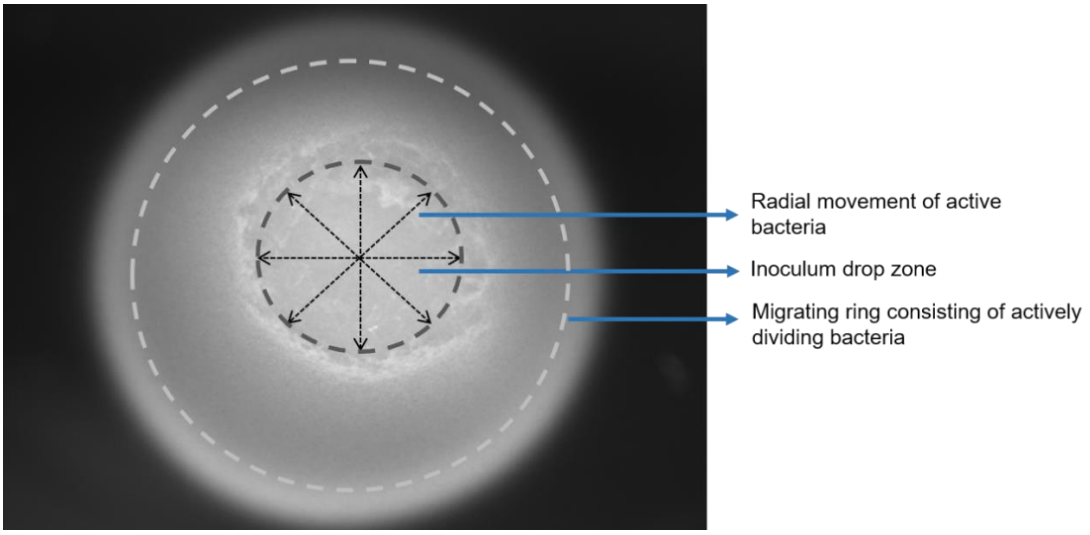

Figure 3.1 The expected growth pattern of a chemotactic bacteria on a soft agar swim plate set-up. The bacteria within the inoculum, when added to the central part of the plate, consume all carbohydrates at the region and form a ring of actively growing cells at the periphery. The chemotactic ring moves in all directions in search of fresh carbon source leaving behind dead or dying cells.

3.2 Materials and methods

3.2.1 Culture method and organisms

Three cellulose producing strains were considered for this study, *Gluconacetobacter hansenii* ATCC 53582, *Gluconacetobacter xylinus* ATCC 700178 and *Komagataeibacter rhaeticus* iGEM (a kind gift from Prof. Tom Ellis, Imperial College, London) were grown in Hestrin-Schramm (HS) medium. Carbon sources such as glucose, sucrose, fructose, and mannitol were substituted into the culture medium according to the experimental study design. A pre-inoculum was prepared in petri-plates in HS media with 2 %(w/v) of the desired sugar and allowed to grow for at least 2–3 days under static conditions at 26 °C. The BC pellicles formed were removed and the cell suspensions present in the dish were used as inoculum for the experimental studies.

3.2.2 Chemicals

Cells were cultured in a standard Hestrin and Schramm (HS) medium containing (w/v): 0.5% peptone, 0.5% yeast extract, 0.27% of sodium phosphate dibasic (Na_2HPO_4) and 0.12% of citric acid monohydrate[75]. Carbon sources such as D-glucose, D-fructose,

D-mannitol, sucrose was used (all ≥99.5% purity). Cellulase (obtained from *Trichoderma reesei,* ATCC 26921) was used for disruption of cellulose fibres . All chemicals were purchased from Sigma Aldrich, unless specified otherwise.

3.2.3 Swim plate experiments

The inoculum (OD600 = 0.005 to 0.01) at 10 µl was carefully dropped at the centre of each well of six-well or twelve-well culture plates containing HS-agar medium in the presence or absence of cellulase (obtained from *Trichoderma reesei*, ATCC 26921). Agar concentration within the HS medium was maintained at 0.15% since higher agar concentrations lead to increased viscous drag thereby limiting bacterial movement. Lower agar concentrations were attempted but were rendered difficult to handle in addition to minimal improvement to the experimental set-up. The culture suspensions were incubated in a well-humidified incubator under static conditions at 26 °C. The growth pattern of the surface pellicles was monitored using a light microscope with a 5x objective lens. The diameter of the pellicles, determined as the largest end-to-end distance with the help of a ruler, was used to compare the bacterial growth conditions. Each of the three independent experiment was conducted in triplicates and the data obtained were represented as mean ± standard error.

3.2.4 Morphology observations

Field emission scanning electron microscopy. The pellicles formed on the surface of the agar plates were carefully scooped out and washed with phosphate buffered saline (PBS, 1x). The samples were kept on glass coverslips and dried using graded concentration series of ethanol prior to visualization under a Field Emission Scanning Electron Microscope (JSM-6700F, JEOL, Japan) using standard protocols.

Confocal microscopy. Pellicles formed on the swim plates were carefully scooped out from the surface and washed at least thrice in PBS. The samples were then stained with the Baclight LIVE/DEAD assay kit (Life Technologies) as described elsewhere[220], along with minor modifications. Briefly, equimolar quantities of the dyes: Syto9 and Propidium iodide, were mixed and diluted ten times in 1% NaCl solution. The washed pellicles were added into the dye solution and allowed to incubate for 10

minutes in the dark. The pellicles were then immediately visualised under a confocal microscope.

3.2.5 Static culture experiments

Static cultures simulating bioreactor conditions for cellulose production were used for growing the desired strains under various conditions at 26 °C. Culture volumes ranging from 2 ml to 150 ml were grown in vessels of varied dimensions: starting from 12-well culture plates to 135 mm petri-dishes. Glucose or sucrose at media-concentrations ranging from 2% to 8% were used as the carbon source for *G. hansenii*, while *G. xylinus* and *K. rhaeticus* were grown in the presence of 2% to 4% glucose or mannitol. The bacterial cellulose pellicles obtained were treated in 0.5 M NaOH at 100 °C for 10 minutes to eliminate the entrapped cells and washed with deionized water until the pH was neutral. The pellicles were subsequently freeze dried and weighted using a high precision balance. The yield was defined as the mass of the dried cellulose pellicle obtained per mL of culture. Carbon utilization efficiency was defined as the ratio of pellicle diameter for the preferred carbon source to the pellicle diameter of cellulose obtained from glucose as the carbon source. All experiments were done in triplicates and the data obtained were represented as mean ± standard error.

3.3 Results and discussion

3.3.1 *Gluconacetobacter* exhibit chemotaxis

Upon incubation under a given condition, all strains produced visible BC pellicles within one day of incubation. At the initial phase, the pellicles resembled the shape and size of the inoculum droplet and subsequently grew into a concentric circle away from the drop zone as shown in Figure 3.2 (top panel). To examine their morphologies, the pellicles were carefully scooped out of the soft agar surface and visualised under a Field Emission Scanning Electron Microscope (FESEM). It was evident that for all the cases that the pellicles were being formed by fibres generated by our target organisms (Figure 2.3).

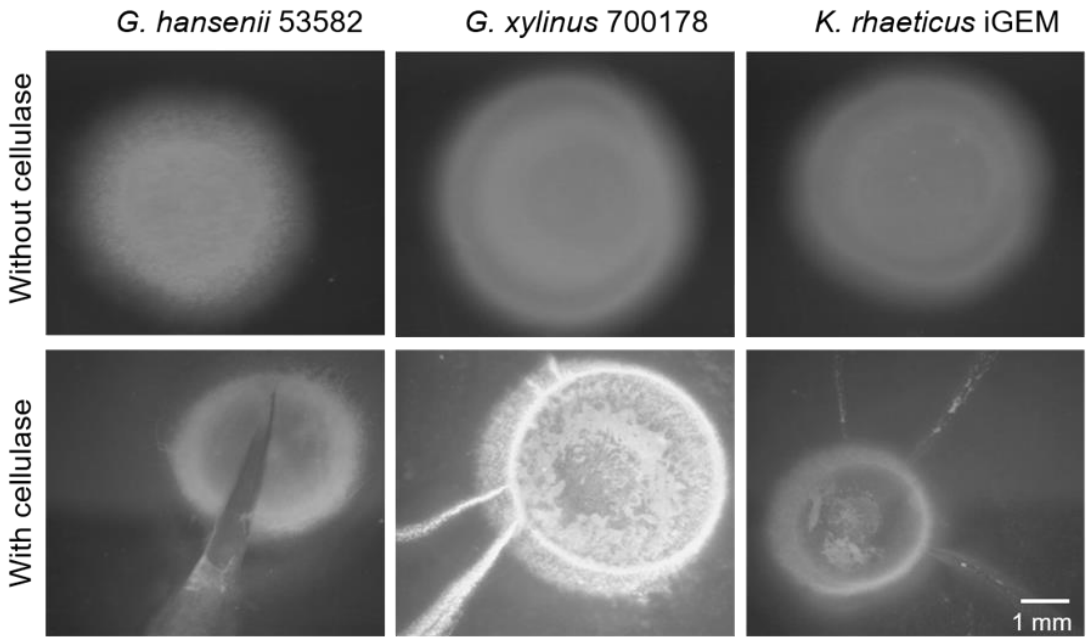

Figure 3.2 Swim plate experiments conducted for different cellulose producing bacterial strains in the absence (top panel) and the presence (bottom panel) of cellulase. The cultures were grown on soft agar in a humidified incubator. (*Scale bar: 1 mm*)

Based on the previously discussed Keller-Segel surface growth model of bacteria, we expected that the increase in the bacterial population at the site of inoculation would lead to depletion of nutrients with time. Under such conditions bacterial strains, capable of exhibiting chemotaxis, started moving towards the adjacent regions of higher nutrient concentration leaving behind the dead or dying cells[217,221]. To test this hypothesis on our strains, the pellicles were stained with a mixture of propidium iodide and Syto9 to determine the live/dead bacterial population distribution. Both dyes intercalate with DNA. Propidium iodide penetrates only dead bacterial cells resulting in red fluorescence while Syto9 stains live bacteria green[220,222-224].

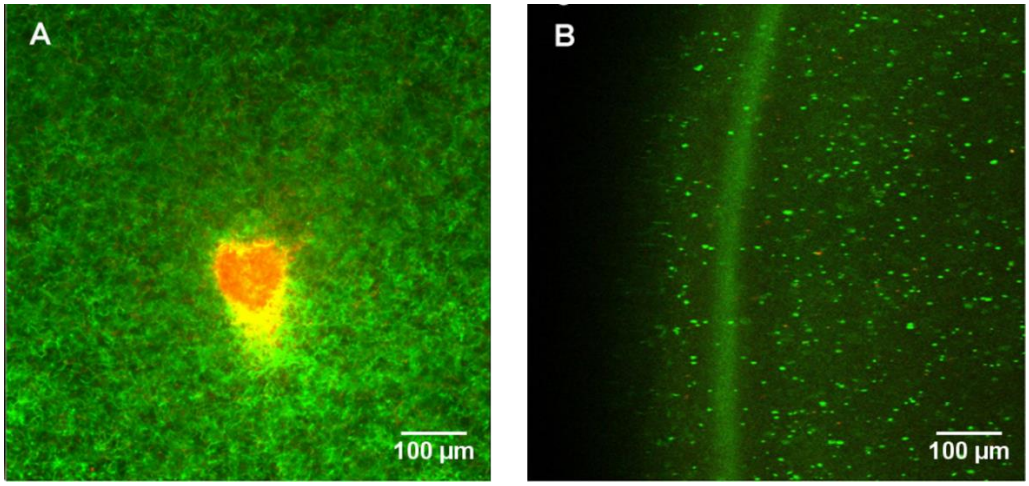

Figure 3.3. Typical spatial distribution of the live/dead bacteria within a cellulose pellicle grown on soft agar. Live bacteria are stained green while the dead ones are stained red. The centre of the pellicle (A) is marked by the presence of dead or dying cells while actively growing cells are seen at the edges of a pellicle (B). (*Scale bar: 100 µm*)

Figure 3.3 presents a characteristic bacteria population profile at the centre and edges of the pellicles. The centre region of the pellicle is marked by a dense red coloured spot indicating the predominance of dead bacterial cells within the region. The red spot is surrounded by an orange-yellow coloured zone typically because of varying intensities of green and red fluorescence indicating the presence of dead or dying cells. However, towards the edges of the pellicle, we observe a green coloured ring (Figure 3.3B) indicating that the region has high concentration of actively growing cells. The spatial distribution pattern of the bacterial population appears similar to that expected in the case of chemotactic bacteria exhibiting a Keller-Segel type growth[221]. Actively growing bacterial population keeps moving forward along the edges of the ring formed, leaving behind dead or dying cells particularly at the centre region where the inoculum was added. Based on our observations, we propose that the three strains in this study are capable of exhibiting chemotaxis and the pellicle formation could be an integral part of its chemotaxis. Although, the involvement of BC production with the bacterial movement has been previously observed by other research groups[225-227], this is the first observed direct correlation of the BC producing bacterial motility with chemotaxis.

3.3.2 Role of cellulose production in bacterial chemotaxis

To understand the importance of cellulose production to bacterial motility and its metabolic state, we grew the bacteria in the presence of cellulase in the soft agar medium. Cellulase is an enzyme known to degrade cellulose into smaller mono/oligosaccharide units[228]. We observed that the pellicles were formed on the first day but disintegrated by the second day. Subsequently, the bacteria grew in an unpredictable manner without following any concentric pattern distinct from the characteristic of bacteria showing chemotactic behaviour. The erratic growth corresponded to the disintegration of the cellulose fibres (Figure 3.2, bottom panel and Figure S1). For genuine chemotactic bacteria, we expected the bacteria to retain its ring formation despite the loss of the cellulose fibres. The observed inconsistent behaviour of the three BC-producing bacteria compared to those incubated in the absence of cellulase are shown in Figure 3.2 (top panel). Furthermore, under prolonged incubation in the presence of cellulase, the bacteria convert into non-cellulose producing metabolic state(s), where no pellicle formation is observed. Our results indicate that under the experimental conditions, cellulose production might be an integral part of the bacterial chemotaxis. Consequently, in the absence of the fibres to support its movement, the bacteria probably switch to a different set of metabolic machineries to support its survival. The causes of the switch between cellulose producing and non-producing metabolic states are not yet established and remain to be elucidated.

3.3.3 Preference in carbohydrate utilization by *Gluconacetobacter* bacteria

As we have established that chemotaxis is associated with the production of cellulose fibres, we expect that a higher rate of chemotaxis correlates with an increase in cellulose production. We test the applicability of the surface growth model as an easy platform for determining the impact of diverse environmental conditions on the growth of the bacteria. Briefly, the method quantifies growth effects by comparing the pellicle diameters in different experimental conditions. Developing the platform will be useful for cost effective screening of the growth conditions necessary for maximal cellulose production. To test the platform, we first performed the swim plate experiments in the presence of four different carbon sources (i.e. glucose, fructose, sucrose, and mannitol) at various concentrations. Glucose being one of the most widely used 6-carbon

monosaccharide easily utilized by all bacteria; Fructose on the other hand (an isomer of glucose with a 5-membered furan ring) was chosen to evaluate the impact of the altering geometries of the carbohydrate molecule. Sucrose was used to understand the impact of a disaccharide, while mannitol (an open chain monosaccharide) was used to evaluate the impact of open chain carbon source on bacterial growth.

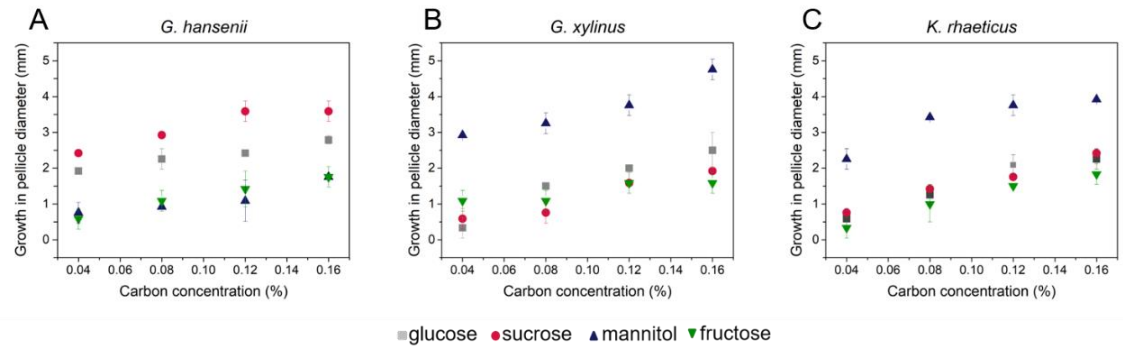

Figure 3.4. Observed growth of the different BC-producing strains grown under different carbon sources at different concentrations; (A) *Gluconacetobacter hansenii* 53582, (B) *Gluconacetobacter xylinus* 700178 and (C) *Komagataeibacter rhaeticus* iGEM.

The observed pellicle growth profiles, shown in Figure 3.4, present a few interesting points. First, the bacterial strains show obvious preferences towards the carbon sources used for their growth. *G. hansenii* 53582 strain showed preference towards sucrose with the order of preference towards other sources: Sucrose > Glucose > Fructose ≈ Mannitol. In contrast to *G. hansenii* 53582, both strains *G. xylinus* 700178 and *K. rhaeticus* iGEM show preference towards mannitol while their growth are unaffected by the other carbon sources. It is observed that the bacterial growth is proportional to sugar concentration Figure 3.4. However, for *G. hansenii* the growth reaches a plateau at 0.12 % (w/v) sucrose. These results indicate that our swim plate experiments provide quantitative prediction for cellulose production capacity in different carbon sources. Figure 3.5 presents the observed advantage in cellulose production capacity at 0.16 % (w/v) carbon source for different bacteria. The higher the observed area covered with cellulose by the different sources compared to glucose, the higher the growth rate and preference for the corresponding carbon source. Our platform thus allows quantification of the cellulose production between different sugars allowing to model bacterial growth under different scenarios.

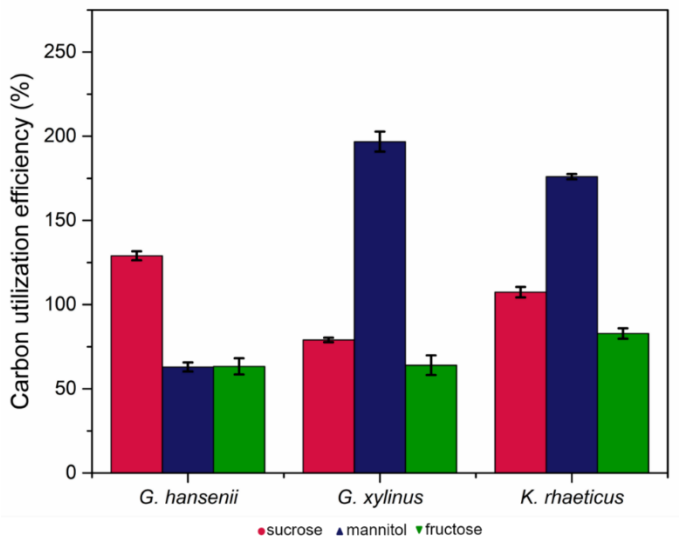

Figure 3.5. The impact of different carbon sources on the growth pattern of cellulose producing bacteria as derived from the swim plate experiments. Carbon utilization efficiency for each of the strain is calculated with respect to glucose.

3.3.4 Influence of pH in carbon utilization by bacteria

To test its applicability in testing other growth influencing factors, we challenged our platform for evaluating the impact of pH. Pellicle formation was tested over a varied pH range of 2-8. The impact of pH drop on the bacterial growth profile is summarised in Figure 3.6, where significant increase in bacterial growth is observed for all the strains grown on glucose at pH 5 compared to pH 6. Apart from glucose, *G. hansenii* exhibits significant increase in pellicle diameter for mannitol at pH 5 as well. Growth on sucrose and fructose supplemented media, on the other hand, barely affect *G. hansenii*. Interestingly, mannitol-fed *K. rhaeticus* shows a decrease in growth at pH 5 compared to that at pH 6. In addition, pellicle formation is only observed at pH 5 and 6, whereas other conditions show no signs of pellicle formation. This observation is in accordance to the growth patterns of the bacteria as observed by different research groups where cellulose production has been proposed to be optimum at $4 < pH < 7$[229,230]. In general, the BC producing strains are known to grow under mild acidic conditions however, the gluconic acid produced during subsequent cellulose production often tends to reduce the pH of the growth medium thereby making it difficult for further BC production[97,229]. These results therefore validate our platform for screening of BC producing conditions.

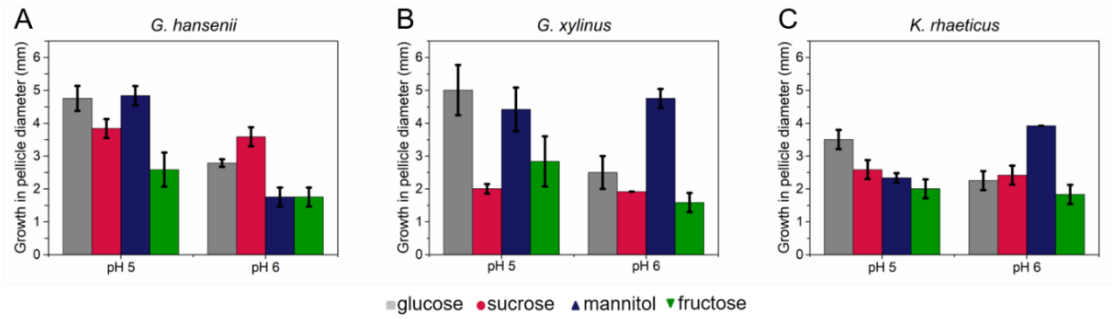

Figure 3.6. Testing the impact of pH on the growth or cellulose production capacity of the bacteria through the developed swim plate experimental platform. (A) *Gluconacetobacter hansenii* 53582, (B) *Gluconacetobacter xylinus* 700178 and (C) *Komagataeibacter rhaeticus* iGEM.

3.3.5 Correlation between swim plate platform and static cultures

For bioprocessing applications, it is necessary to extrapolate the observations on the platform to static cellulose production conditions. Identifying alternative carbon sources for desired bacterial growth conditions is important for improving yield. Our attention is particularly drawn to the fact that our bacteria show preferences for carbon sources other than glucose. *G. hansenii* was therefore grown in the presence of sucrose while *G. xylinus* and *K. rhaeticus* were grown in the presence of mannitol. For validation purposes, the yields obtained from the above carbon sources are compared to that obtained from glucose (Figure 3.7). Cellulose yields under static conditions agree well with the predictions obtained from our swim plate experiments where *G. hansenii* preferred sucrose over glucose, while mannitol is found to be the preferred carbon source for *G. xylinus* and *K. rhaeticus*.

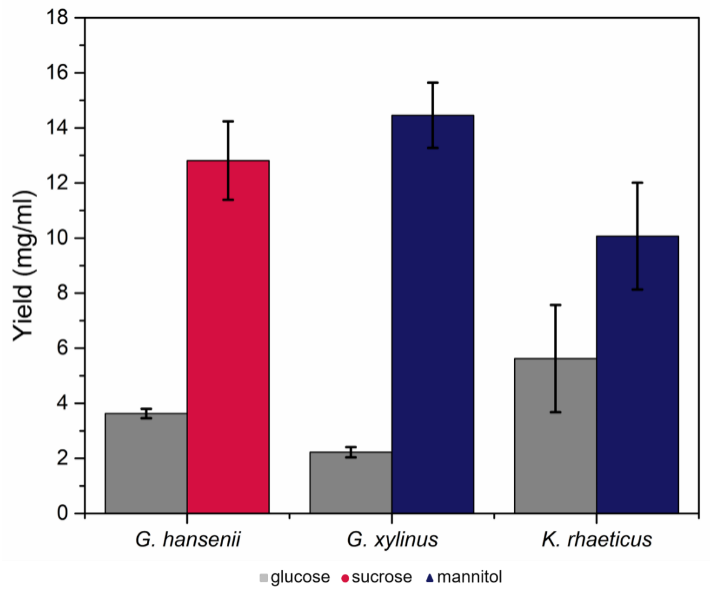

Figure 3.7. Comparison of the cellulose yields obtained using various static culture conditions. *G. hansenii* was grown in the presence of glucose and sucrose at 2 % (w/v); *G. xylinus* and *K. rhaeticus* were grown in glucose and mannitol at 2 % (w/v). The results show good correlation with the swim plate experiments.

3.4 Conclusions

The overall goal of the present work is to establish a simple analytical platform for BC production which can simultaneously shed new lights into the biology of the bacteria. Our particular interest is to compare the growth pattern with the Keller-Segel type growth primarily due to its compatibility with further mathematical modelling[231]. Preliminary results presented here (Figure 3.2 and Figure 3.3), suggest that the surface-growth pattern of the three bacterial strains in this study resemble Keller-Segel models consisting of actively growing cells at the edges of the pellicles leaving behind dead or dying cells in the central region[221]. Researchers working with bacterial cellulose have two distinct school of thoughts regarding the *G. xylinus* motility: (1) flagellate movement and (2) propulsion facilitated by inverse ejection force of the produced cellulose fibres[225,227]. Observations using our platform confirms the second school of thoughts. While others have reported cellulose-mediated motility without relating it to chemotaxis, we note an interesting correlation. In our experiments, we find that cellulose fibres are produced by the bacteria within the pellicles (Figure 2.3) and the organism deviates from its conventional chemotactic behaviour when incubated in presence of cellulase. Consequently, the observations bring up an obvious question mark

on the extent to which the bacteria adhere to the surface growth patterns observed in case of flagellate propulsion. A closer look into our experimental data reveals obvious differences between the movement of the three strains and flagellate movement. In the latter case, the velocity of the bacterial front remains independent of the sugar concentration within the growth media[221] which is the opposite of what we observed. The similar observations for all three strains imply that the chemotactic behaviour would be universal for cellulose mediated bacterial propulsion systems. Nevertheless, the BC producing strain growth remains associated with another interesting observation. On some occasions, the bacterial front achieves a terminal velocity characterized by a plateau in pellicle diameter despite increase in sugar content (Figure 3.4) thereby indicating a plausible limit of the extent of resources that can be allocated by the bacteria for exhibiting chemotaxis. Our experimental swim-plate platform indicates that obvious relationships do exist between pellicle diameter and sugar concentration, which can be used to derive empirical or semi-empirical growth models.

The good correlations between the observed trends in our swim-plate platform and that obtained in static cultures confirm that the platform developed is translatable to predictive models for bioreactor studies. Our proposed platform can be particularly useful to address some of the practical difficulties whilst studying the bacterial growth profile within bioreactors. For instance, the pH of the media plays a vital role in determining the cellulose productivities of the target organisms. However, owing to the development of cellulosic coats on the surface of the pH probe, it is difficult to monitor the dynamic changes of the medium pH during fermentation. In the present experimental platform, such problems can be easily eliminated since the pH of the media remains predetermined as the bacteria are moving towards fresh resources.

The combination of the biological knowledge and the platform has implications on the establishment of optimised bioprocessing strategies for BC large-scale production.

This chapter (including phrases and figures) have been reproduced from our published article 'A novel platform for evaluating the environmental impacts on bacterial cellulose production.' S.V. Vadanan, A. Basu, S. Lim; Scientific Reports, 8 (1) (2018),p. 5780, 10.1038/s41598-018-23701-y, with permission from Springer Nature. Copyright 2018.

Chapter 4

Introduction of Substituted Glucose Substrates to Investigate the Process of Polymerization and Crystallization in Exopolysaccharide Production

During cellulose biogenesis, cellulose synthase enzyme is unique to the whole process of BC production. The exceptional structure and properties of bacterial cellulose result from the extrusion of precursor polymeric molecules and their assembly outside the bacterial cells. The extruded polymeric molecules assemble with the help of inter/intra molecular hydrogen bonds between monomer units. By considering the substrate specificity of the enzyme complex and modification of the inter and intra molecular hydrogen bonds, modified carbohydrate polymers can be synthesised by bacteria. Disruption of the hydrogen bonds can be brought about by the introduction of substituted substrates. The substituted monomers tend to form new hydrogen bonds leading to new material properties. In this study, we intend to investigate the specificity and flexibility of the cellulose synthase complex and study their effects on polymerization and crystallization of cellulose fibres. With control over the structural properties of the polymer, newer sustainable strategies can be employed to produce functionalized biopolymers.

4.1 Introduction

Cellulose synthase enzyme complex is central to the process of cellulose production. BC is formed by the fermentation of sugars to form β-D glucose chains linked by β-1,4 glycosidic bonds[69]. During fermentation in the microorganism, carbon source is converted to the precursor product and the enzyme detects the precursor for extrusion. The exceptional material properties of BC are due to the result of the extrusion of the precursor glucan chains and their packing outside the cells[65]. The presence of hydroxyl groups and linear chains in cellulose form strong intramolecular and intermolecular hydrogen bonds leading to a highly crystalline form. Two intramolecular hydrogen bonds are present between glucan units (2-OH---O-6 and 3-OH---O-5) and one intermolecular bond (6-OH---O-3') between the chains as shown in the Figure 4.1. The hydrogen bonds in cellulose are generally modified or disrupted through physical and/or chemical treatments[64,232].

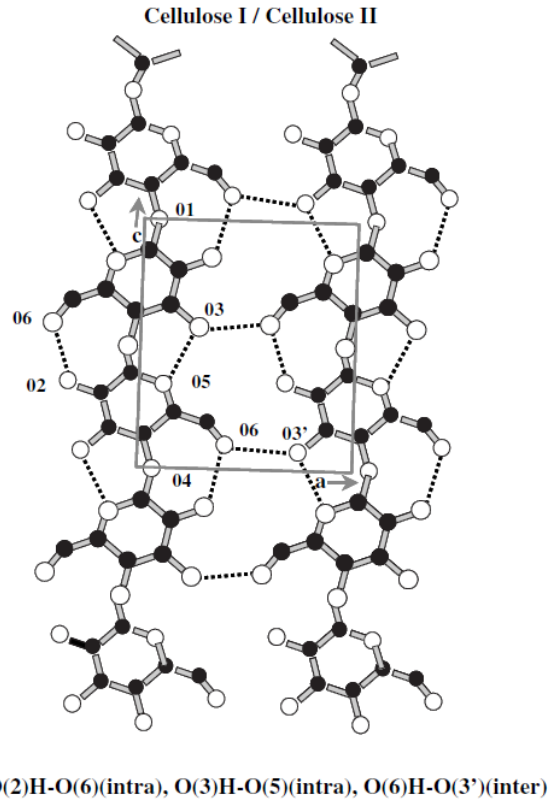

Figure 4.1 Intrachain and interchain hydrogen bonds present in cellulose from [233], © 1976, The American Chemical Society

Glucose and its derivatives were used as carbon sources to check for their direct incorporation by *G. hansenii* 53582 for modified cellulose production. Glucose was considered as the main carbon source for this study since most of the polysaccharides contain glucose as their main component and therefore, a rational target for direct formation of polyglucan chains by microorganisms. The three substrates used in combination with D-glucose are 3-O-methyl D-glucopyranose, methyl α D-glucopyranoside and N-acetylglucosamine (Figure 4.2)[234,235]. The rationale behind selecting the above substrates was to modify the inter and intramolecular hydrogen bonds present in bacterial cellulose during *de novo* synthesis.

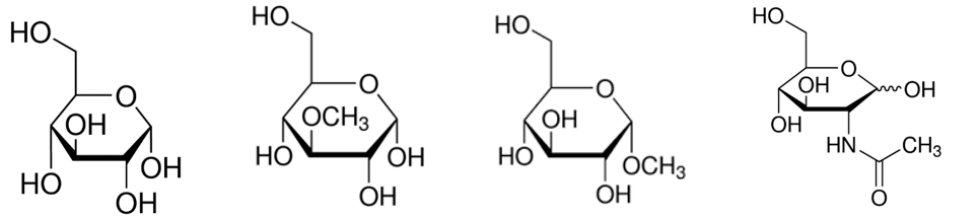

Figure 4.2 Various glucose analogues considered to interrupt hydrogen bonds in cellulose.

4.2 Materials and methods

4.2.1 Culture methods and organism

Gluconacetobacter hansenii ATCC 53582 was considered for this study, due to its preference towards glucose for cellulose production. Carbon sources were substituted into the culture medium according to the experimental study design. A pre-inoculum was prepared in petri-plates in HS media with 2% (w/v) of the desired sugar and allowed to grow for at least 2–3 days under static conditions at 26 °C. The BC pellicles formed were removed and the cell suspensions present in the dish were used as inoculum for the experimental studies.

4.2.2 Chemicals

Cells were cultured in a standard Hestrin and Schramm (HS) medium containing (w/v): 0.5% peptone, 0.5% yeast extract, 0.27% of sodium phosphate dibasic (Na_2HPO_4) and 0.12% of citric acid monohydrate[75]. Carbon sources such as D-glucose, 3-O- methyl D-glucopyranose, methyl α D-glucopyranoside and N-acetylglucosamine (all ≥99.5% purity) were substituted into the culture medium according to the experimental study design. Sodium hydroxide (≥97.0%, pellets) was used for cleaning cellulose.

All chemicals were purchased from Sigma Aldrich, unless specified otherwise.

4.2.3 Substituted glucose incorporation experiments

The samples were incubated in 12-well plates (Thermo Fisher Scientific, US) per the design mentioned in **Error! Reference source not found.**. Bacterial cells were ncubated with only HS medium (negative control), glucose 2% (w/v) and sterilized water (without HS medium), glucose 2% with HS medium (positive control) and fixed ratios of D- glucose with substituted glucose substrates (Table 4.1). The various substituted glucose substrates used for this study, 3-O-methyl D-glucopyranose, methyl α D-glucopyranoside and N-acetylglucosamine will be annotated as a, b and c respectively (Figure 4.2).

Table 4.1 Experimental design for the utilization of various substituted carbon sources.

Design	Source
	HS medium
	D-glucose 2% w/o HS
	D-glucose 2% + HS medium
1a/1b/1c	1.5% D-glucose: 0.5% a/b/c
2a/2b/2c	1% D-glucose: 1% a/b/c
3a/3b/3c	2% a/b/c

The bacterial cellulose pellicles obtained were treated in 0.5 M NaOH at 100 °C for 10 minutes to eliminate the entrapped cells and washed with deionized water until

the pH was neutral. The pellicles were subsequently freeze dried and weighted using a high precision balance. The dry weights were recorded for all the experimental conditions and represented as mean ± standard error.

4.2.4 Characterization of bacterial cellulose

Field emission scanning electron microscope (FESEM). JSM-6700F (JEOL, Japan) operating at an accelerating voltage of 1.5 V was used to observe the structural morphology of the ultrafine fibre network. FESEM analyses were performed on strips of freeze dried bacterial cellulose pellicle with area 3-4 mm^2. The samples were mounted on stubs with double sided carbon tape and sputter coated with platinum for 65 seconds, 20 A current in vacuum. A 10 nm film thickness was obtained through sputter coating. The coated samples were viewed at different magnifications. Thickness of the individual fibres was calculated and distribution of polymer in the BC matrix was analysed.

X-ray Diffraction (XRD). Bacterial cellulose crystal structure was analysed with D2 PHASER (Bruker, USA), benchtop x-ray diffractometer. The wavelength of the Cu/Kα radiation source was 0.154 nm, generated with an accelerating voltage of 30 kV and filament emission of 10 mA. The X-ray diffraction pattern was recorded between 5-30° (2θ). The freeze-dried samples were placed over circular discs and flattened out to obtain a very thin film for diffraction pattern measurement. The samples were scanned at a rate of 0.5 s per step. The X-ray diffractogram obtained was analysed and processed using EVA software V41.1.5.

Crystallinity index (CI) can be calculated from the obtained diffractogram using the following equation [236].

$$CI\ (\%) = \frac{Ic - Iam}{Ic} * 100$$

where, I_c and I_{am} correspond to the maximum intensity obtained for lattice diffraction plane (002) at 22.8° (2θ) and intensity of the minima at 18° (2θ) corresponds to amorphous cellulose, respectively.

The interplanar distance between the crystal planes or d-spacing was also computed based on Bragg's law [133].

$$\lambda = 2d\ Sin\theta$$

where, λ is the X-ray wavelength, d is the interplanar distance and θ is the Bragg's angle.

Fourier- transform infrared spectroscopy (FTIR). IR spectra was obtained using Spectrum One FTIR (Perkin Elmer, USA) equipped with potassium bromide (KBr) beam splitter and deuterated triglycine sulphate detector. The spectra were measured in transmission mode utilizing KBr discs. Freeze dried samples obtained were cut into fine pieces and mixed with KBr, this mixture was then hydraulic pressed to form transparent discs for the transmission of infrared light. The spectrum was obtained at room temperature with a resolution of 4 cm^{-1}, spectral range from 4000-400 cm^{-1} collected and averaged over 16 scans. The spectrum was baseline-corrected and optimized using Spectrum V5.0.1 software.

Thermogravimetric analysis (TGA). Phase transitions was recorded as weight loss function of temperature. Precision pans present in the analyser constantly measure weight of the sample under constant rate of temperature change. All measurements were done using TA instruments TGA Q500 equipment. Nitrogen gas with a flow rate of 60 ml/min was used during the experiments. TGA measurements were recorded from 30 ºC to 800 ºC, with step size of 5 ºC/min. DTG curves were obtained using the first derivative, rate of weight loss as a function of temperature. Analysis was done using the in-built TA Universal Analysis Software.

4.3 Results and discussion

4.3.1 Modified cellulose and dry weights

The pellicles after 7 days of incubation were cleaned, purified following the two-step cleaning process and freeze dried as shown in Figure 4.3.

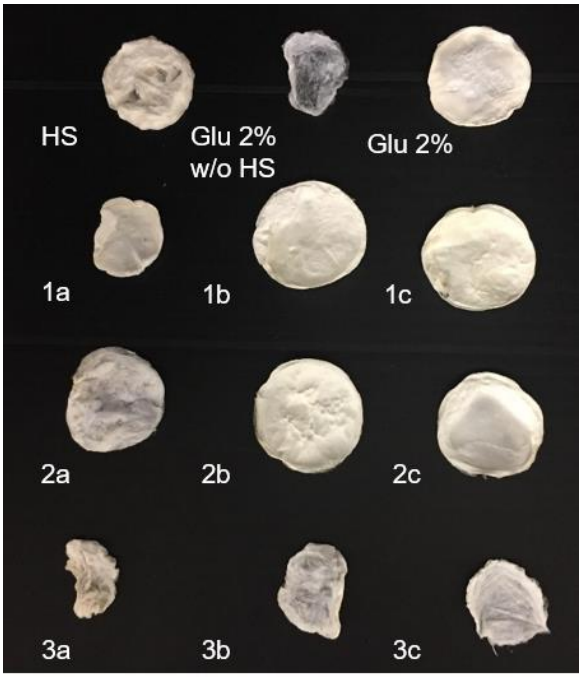

Figure 4.3 Cellulose pellicles obtained from various sources after 7 days of incubation.

Pellicles produced in combination with D- glucose or D- glucose alone appear full and round. The pellicles obtained from HS medium alone and in the absence of D-glucose appear to shrivel up and absorb moisture from the atmosphere. The pellicle obtained from D-glucose 2 %(w/v) in the absence of HS medium suggests that HS medium is an important component for cellulose production although it does not participate directly in cellulose production, it provides nutrition to the bacterial cells for growth and division. The freeze-dried pellicles were weighed to obtain dry weights for respective sources (Figure 4.3).

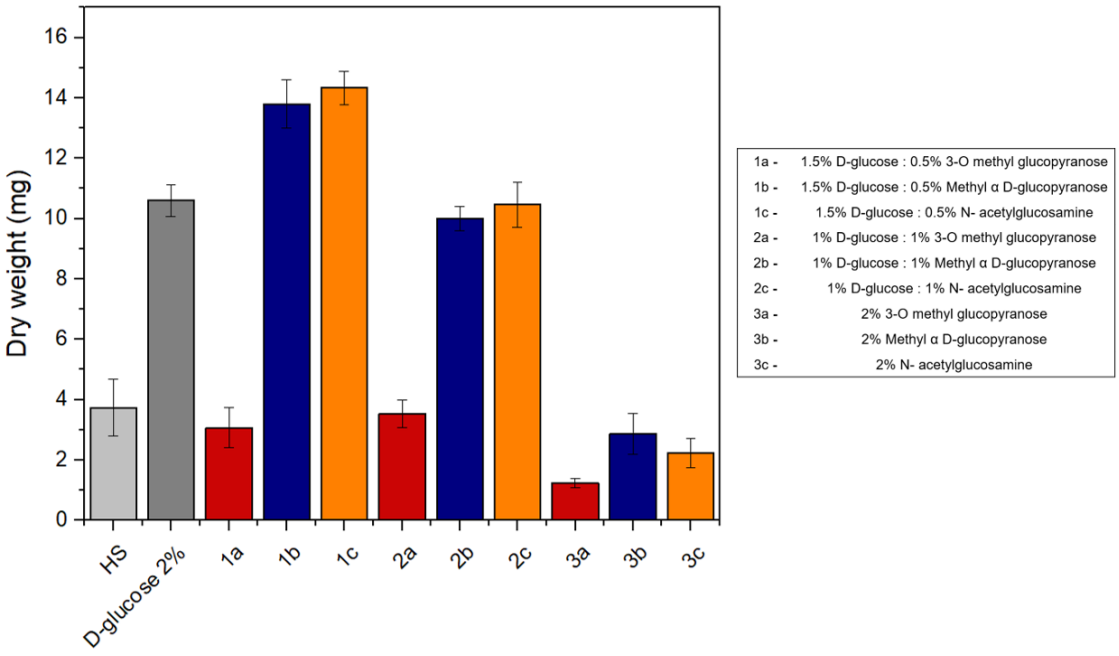

Figure 4.4 Dry weights of cellulose samples obtained by *G. hansenii* 53582 grown on HS media supplemented with 3-O methyl glucopyranose (series a), methyl α D-glucopyranoside (series b), or N-acetylglucosamine (series c) in the presence and absence of D- glucose.

Evidently the sample obtained from HS medium alone weighed less than 4 mg indicating carbon source is essential to produce a good yield of cellulose. D-glucose 2 %(w/v) with HS medium produced a yield of 3.5 mg/ml for 7 days of incubation in a 12-well plate. All samples that were incubated with 3-O-methyl D-glucopyranose did not produce a good yield of cellulose, suggesting that the enzyme complex of *G. hansenii* 53582 shuts down the moment they encounter this substrate. The microorganism does not possess the necessary enzymes required to modify the molecule to produce cellulose. The samples obtained from combinations 1b and 1c weighed more than the control sample (D-glucose 2 %(w/v)), suggesting that the presence of methyl α D-glucopyranoside and N-acetylglucosamine have enhanced the cellulose production mechanism of the bacteria to further synthesize polyglucan chains and thereby, increase its yield. A 2 %(w/v) decrease in the concentration of D-glucose yields about ≤0.95 mg/ml indicating that the presence of glucose is vital for the formation and assembly of cellulose chains. Hence, both the molecules can be used as an additive and not as a primary source for cellulose production.

4.3.2 Structural morphology of modified cellulose films

Cellulose morphology was analysed using FESEM. The distribution of fibre network across the cellulose pellicles for different carbon source combinations was observed. The gross morphology of all the samples are similar with no major change in fibre thickness or the fibre arrangement in the membrane. The average fibre thickness was measured to be between 30-40 nm across all the cellulose samples. The inset images for all the 3-series samples indicate that the absence of D-glucose leads to the production of short fibres in the form of nanowhiskers (Figure 4.5). These nanostructures are distributed randomly across the sample along with the common cellulose fibre network that we observe (Figure S2).

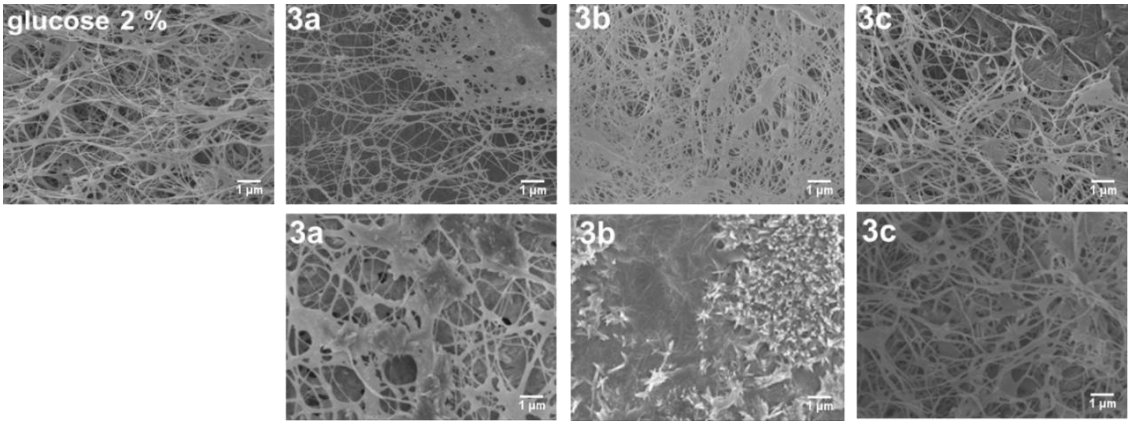

Figure 4.5 SEM images of different cellulose samples produced by *G. hansenii* 53582 from different glucose analogues grown in the absence of D- glucose (3 series). Top panel depicts the normal cellulose network and bottom panel depicts regions of nanocrystal formation in the same sample due to the absence of D-glucose. (*Scale bar: 1 µm*)

4.3.3 Direct incorporation of substituted glucose substrates in modified cellulose films

The various modified cellulose membranes were tested for their chemical structure differences due to the incorporation of substituted glucose substrates. The samples were investigated through FTIR and ^{1}H-NMR techniques.

4.3.3.1 Infrared spectrum of cellulose samples

FTIR spectrum of cellulose produced by *G. hansenii* 53582 obtained from different sources (Figure S3). Most of the bands observed in the infrared spectra of cellulose samples produced from different sources are similar. A strong broad band was observed at around 3400 cm^{-1} corresponding to all the bonded OH groups present in cellulose. The two small sharp bands at 2920 and 2850 cm^{-1} correspond to -CH stretching groups. The band at 1735 cm^{-1} is assigned to C=O deformation or stretching vibrations. In the fingerprint region of the spectrum, the bands 1460 and 1425 cm^{-1} correspond to C-C-H bending, CH_2 rocking/wagging and C-O-H bending modes. The bands at 1060 and 1030 cm^{-1} are assigned to skeletal ring stretches as well as C-O glycosidic and C-O alcoholic bonds stretch modes. Since the IR spectra from all the substituted glucose substrates had signature peaks overlapping with cellulose peaks, a sensitive technique was required for further analysis.

^{1}H-NMR was used to check for the incorporation of substituted glucose substrates into cellulose. Few samples were selected to check for their direct incorporation (Figure 4.6), signal acquired from cellulose obtained from D-glucose correlated with previous literature[234]. Similarly, all the signature peaks present in the various substituted glucose substrates were found in the corresponding cellulose films. This confirmed the direct incorporation of the monomers into cellulose without any modification. The enzyme cellulose synthase did not possess any machinery to modify/eliminate the substrates being incorporated into cellulose. ^{1}H-NMR clearly confirms the formation of new composites through *in-situ* fermentation strategy.

4.3.3.2 Disruption of hydrogen bonds in modified cellulose

Crystal structure investigation of various cellulose samples was analysed through the X-ray diffractograms obtained in Figure 4.7. The X-ray diffractograms correlated with the pellicle structure observed visually (Figure 4.3). The samples produced from HS medium and in the absence of D-glucose 2 %(w/v) were amorphous in nature due to the presence of a broad peak and absence of the signature crystalline peaks (Figure 4.7, top left). The cellulose samples produced from substrate ‘a’, 3-O-methyl D-glucopyranose either in the presence of or absence of D-glucose 2 %(w/v) combinations displayed amorphous and crystalline peaks. The samples obtained from D-glucose 2

%(w/v) and all the combinations with substrates ‘b’ methyl-α D-glucopyranoside and substrate ‘c’, N-acetylglucosamine in the presence of D-glucose produced crystalline cellulose.

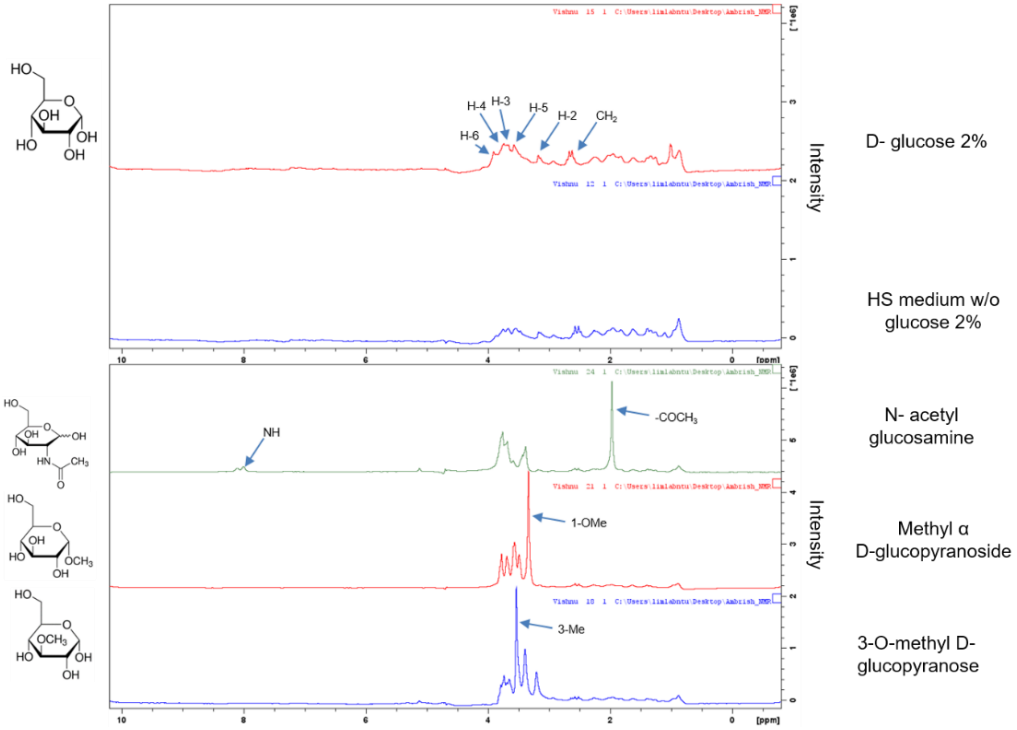

Figure 4.6 Confirmation of the direct incorporation of the substituted glucose substrates in the final modified cellulose.

X-ray diffractograms of pristine BC pellicles obtained from D-glucose 2 %(w/v) displayed all the crystalline planes of cellulose at 14.7° (1-10), 16.8° (110) and 22.7° (200) respectively (Figure 4.7, top left)[195,237].We can clearly observe from the various diffractograms, with decreasing D-glucose concentration there is a drop in crystallinity as indicated by the noise in the XRD curves. In complete absence of D-glucose, peaks 14.7° and 16.8° are not visible and the intensity of 22.7° peak was reduced as well. The presence of a small characteristic crystalline peak at 9.8° for all the substrate ‘c’ samples confirms the incorporation of N-acetylglucosamine into cellulose [238,239].

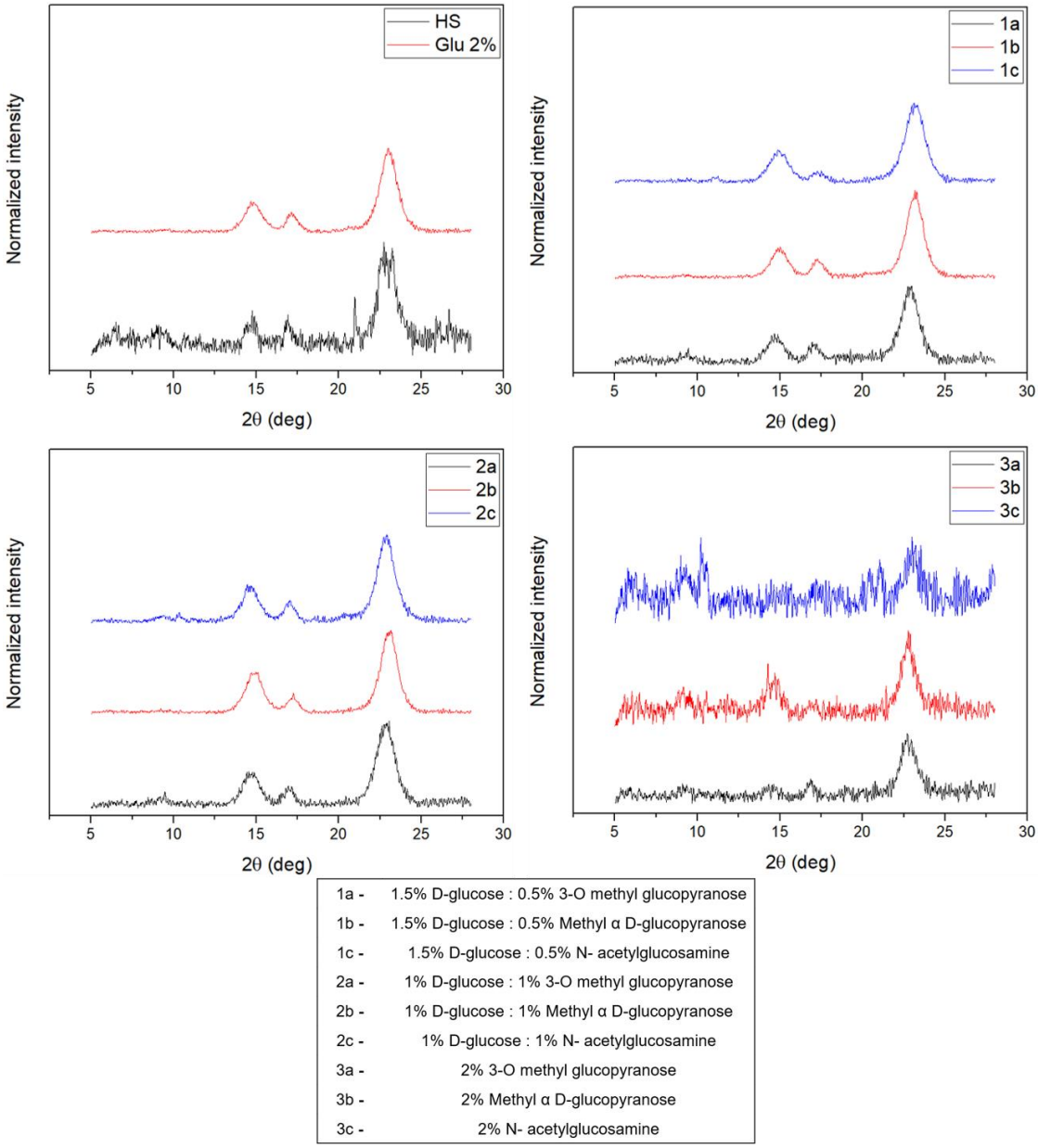

Figure 4.7 X-ray diffractograms of cellulose samples produced by *G. hansenii* 53582 using different glucose analogue concentrations.

The degree of crystallinity is the most imperative crystalline structure parameter. The stiffness of cellulose fibres increases with increasing the ratio between crystalline to amorphous regions. The crystallinity index (C.I) can be calculated using the Segal's method [236]. The index is calculated based on the peak intensity of the (002) plane and the minima at 18°, as this minimum corresponds to amorphous cellulose. The CI ratio and interplanar spacing between crystal planes is tabulated as below (Table 4.2). The CI for all the amorphous samples were not calculated due to the absence of 22° crystalline peak for (002) plane.

Table 4.2 Crystallinity index (CI) and d-spacing of cellulose samples obtained from different carbon sources. Reported values are average of three independent measurements.

Sample	C.I (%)	d-spacing (Å)
HS medium	72.75 ± 9.26	4.064 ± 0.009
D-Glucose 2%	94.98 ± 7.15	4.051 ± 0.003
1.5% D glucose: 0.5% 3-O- methyl D-glucopyranoside	81.79 ± 3.5	4.081 ± 0.012
1.5% D glucose: 0.5% methyl-α-D-glucopyranose	94.13 ± 6.75	4.055 ± 0.003
1.5% D glucose: 0.5% N-acetylglucosamine	91.62 ± 7.7	4.055 ± 0.01
1% D-glucose: 1% 3-O- methyl D-glucopyranoside	79.33 ± 0.17	4.077 ± 0.02
1% D-glucose: 1% methyl-α-D-glucopyranose	92.05 ± 4.88	4.057 ± 0.01
1% D-glucose: 1% N-acetylglucosamine	90.31 ± 6.03	4.071 ± 0.002

Clearly, cellulose obtained from D-glucose 2 % (w/v) showed highest crystallinity while the sample obtained from HS medium showed lowest crystallinity. With the absence of D-glucose there is a significant drop in the crystallinity of the cellulose samples obtained. A 2 %(w/v) decrease of D-glucose concentration results in 20-30% drop in crystallinity. The CI ratios calculated correlated with the dry weights of the various cellulose samples (Figure 4.4).

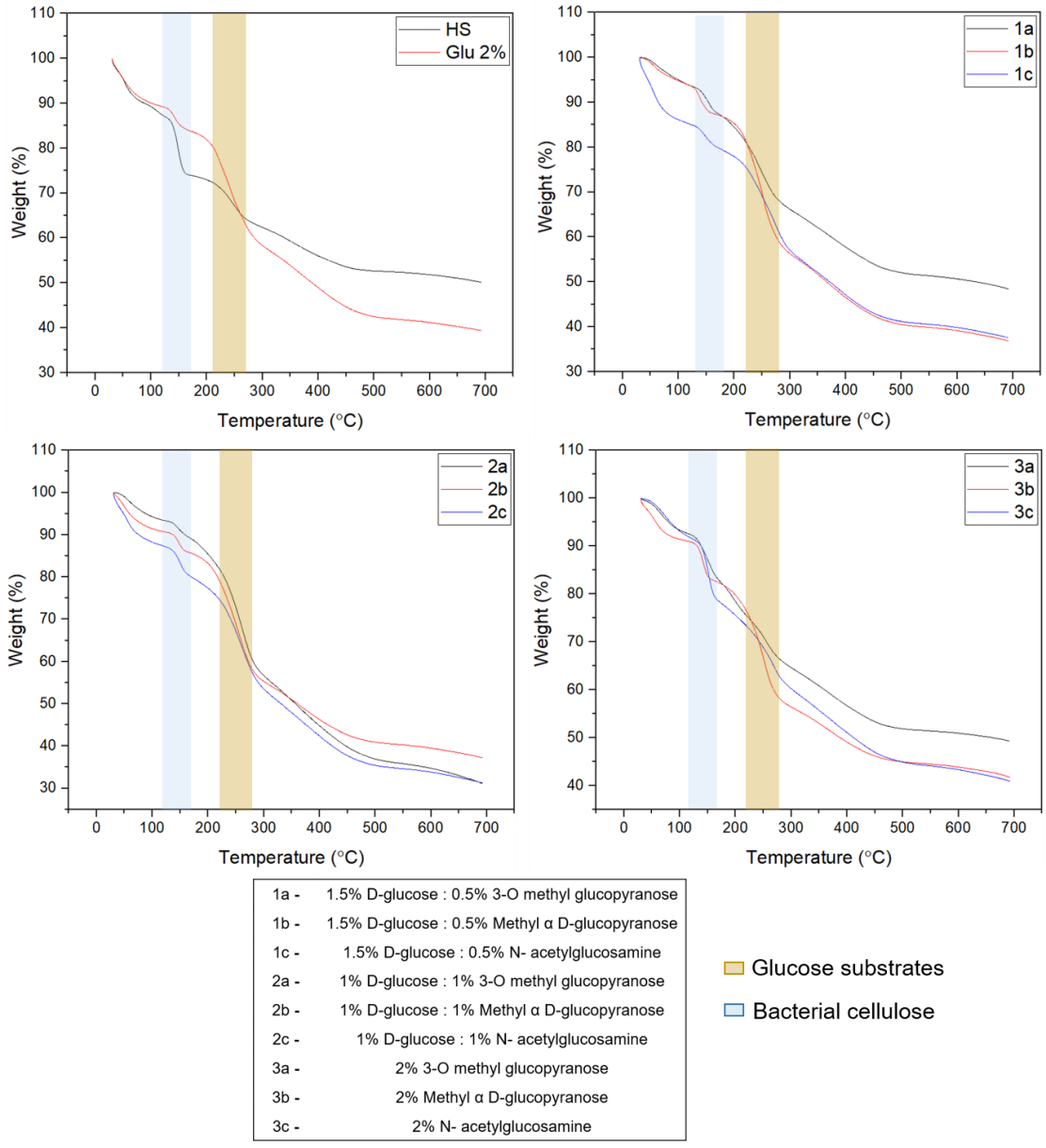

Figure 4.8 Thermal degradation of various cellulose films produced from substituted glucose substrates

4.3.3.3 Thermal degradation profile of BC produced from substituted glucose substrates

Thermal stability and thermal decomposition of the hybrid aerogels was analysed with TGA (Figure 4.8). The TG curves obtained can be distinctively divided into two sections. During the initial stage, a small weight loss at 80-150 °C for all cellulose samples occur due to the presence of moisture. The second stage involves a

sharp weight loss from 270-300 °C due to the disruption of the crystalline regions and decomposition of the various substituted glucan monomer units, which is about 20-40 wt.%. The onset of degradation at 220 °C in all the cellulose corresponds to the degradation of the functional groups followed by the disruption of the backbone structure [238-240]. For cellulose samples obtained from HS medium source (Figure 4.9, top left) and all the cellulose samples obtained in the absence of D-glucose (Figure 4.9, bottom right) there is significant weight loss observed in the first stage of about 10-15 wt.%. These pellicles tend to absorb moisture at a faster rate due to the absence of any crystalline peaks (Figure 4.7). Hence, correspond to higher weight loss due to the moisture present in the films.

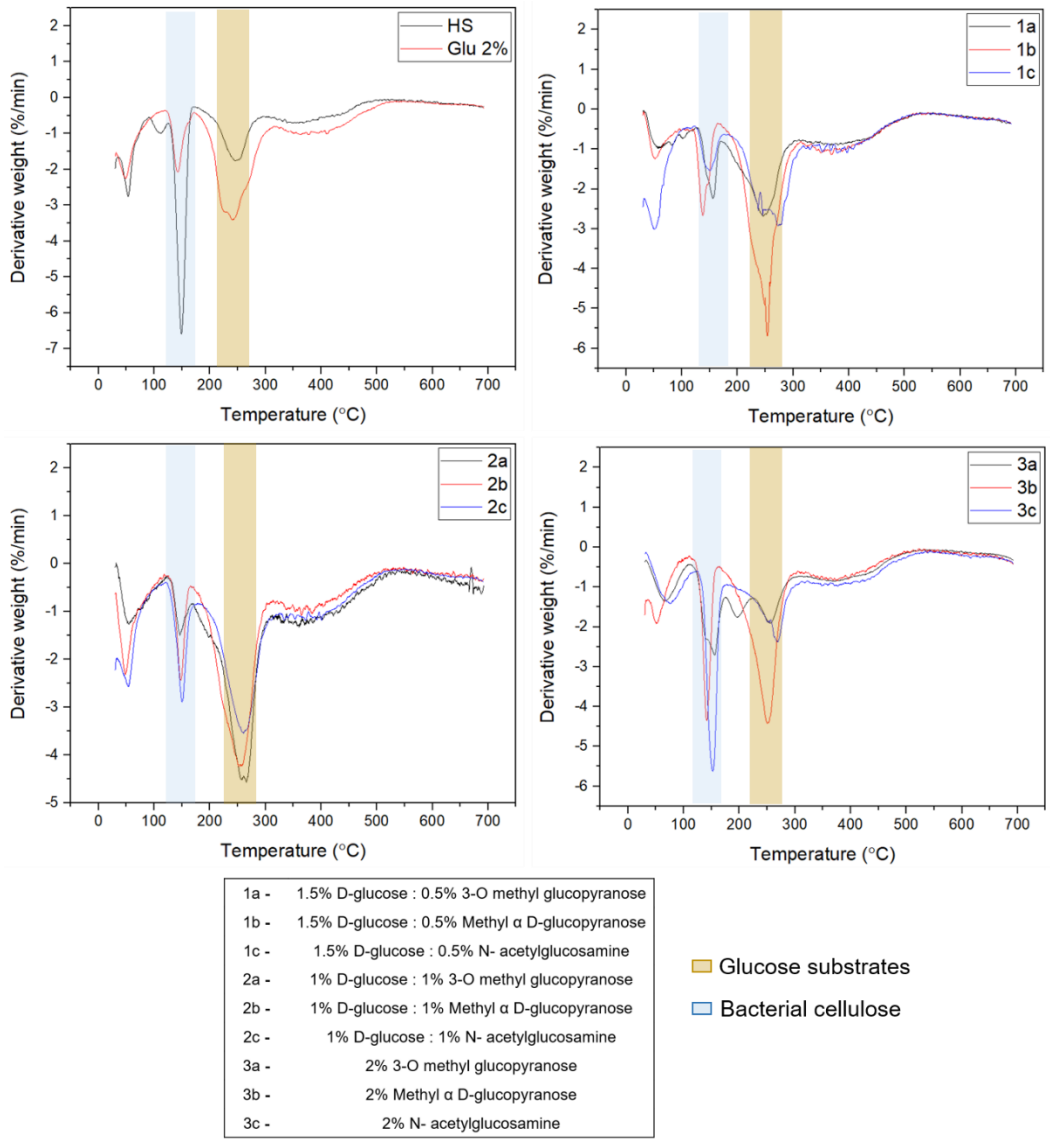

Figure 4.9 Differential weight profiles for various cellulose films

The first derivative (DTG) curves showed two distinct peaks corresponding to the two stages of weight loss as seen in Figure 4.9. The first peak at 120-150 °C corresponds to weight loss due to evaporation of water present in the samples. The second peak at 250 °C confirms the thermal degradation of the glucan backbone structure present in cellulose. For HS medium sample and all the samples obtained in the absence of D-glucose There is strong and sharp peak for the first weight loss stage, confirming higher moisture content present in these films. The second stage confirms the breakdown of all substituted glucose units present in the cellulose films.

4.4 Conclusion

Results obtained from various morphological and structural analysis suggest that the cellulose synthase enzyme and other enzymes have broad specificities with respect to recognising various molecules. There is a clear indication that the carbon sources were not modified post polymerization and assembly of cellulose chains. With the introduction of functional groups present in substituted glucose, the modified cellulose is functional and can be combined with other materials for various applications as indicated by NMR. The incorporation of functional glucose monomers serves as a potential functionalization strategy to produce new biopolymers during fermentation stage. This work requires further characterization tests and studies to understand the distribution of the functional groups along the polyglucan chains. This study serves as a promising approach for future BC functionalization and a step towards understanding the processes of polymerization and crystallization. The biological synthesis of functional cellulose does not require any physical and/or chemical treatment to enable the surface to be reactive and functional. The key understanding for this strategy is (i) design of various metabolic substrates and (ii) an awareness of the mechanism of substrate-enzyme complex and substrate resistance. Based on this theory, the yield can be enhanced, and the selection of metabolized substrates considered can be expanded.

Upon successful interruption of hydrogen bonds present in cellulose, new tunable functional materials can be designed to control the degradability of the composites. Degradability of a material increases with decreased crystallinity. With fair control over crystallinity of a material, novel biodegradable biopolymers can be synthesised *de novo* by the bacteria.

Chapter 5

Design of Bacterial Cellulose-Poly(3,4-Ethylenedioxythiophene) Polystyrene Sulfonate Conductive Aerogels as Flexible Electronic Substrates

Bacterial cellulose has emerged as an important biomaterial for fabrication of micro- and nanoelectronics in biomedical applications. The presence of biocompatible nanofibers with superior structural properties presents potential in innovative product design. Conductive polymer PEDOT:PSS has superior conductivity and biocompatibility but limited mechanical range. The intercalation of BC with PEDOT:PSS can essentially overcome the limitations of the conductive polymer and expand its applications. In this study, a facile design strategy was applied to develop BC-PEDOT:PSS conductive aerogels. The design strategy does not require the use of any harsh chemical treatments to functionalize cellulose. The polymer uniformly intercalates with the cellulose nanofibers to impart conductive properties to the functional material. The conductive aerogels exhibited high conductivity of 0.7 S/cm and low cytotoxicity in the presence of human dermal fibroblasts.

5.1 Introduction

The emergence of the development of functional biomaterials has garnered interest in medicine and bioengineering fields. From the fundamental viewpoint, the structure of cellulose exhibits high tensile strength, is chemically pure and thermally stable. Owing to these properties' cellulose is considered as a natural structure for applications in flexible electronics[50,241].

The ability to flex, heal, sense and stretch are few of the essential aspects of human skin. Hence, the choice of the substrate material being considered for flexible electronics is vital, as they significantly affect both electrical and mechanical functioning of the device. Flexible electronics is realized via: (i) synthesis of new materials as hybrids of soft materials with conductive fillers and (ii) smart engineering and design strategies[242]. The conventional materials consist of silicon and polymers that have very low tensile property, brittle, rigid, cytotoxic, absorb solvents over time and are toxic in nature leading to long environmental degradation times[242,243]. The reason for developing BC-based conductive materials is to replace the aforementioned, conventional materials used in organic electronics, sensors and wearable electronics. BC has been extensively combined with conductive polymers such as PAni, PPy and PEDOT:PSS through *in situ* and *ex situ* strategies. Due to the limitations of these two strategies, newer approaches were explored to develop conductive BC composites[1,42]. PEDOT:PSS was the preferred polymer due to its high conductivity, biocompatibility and resistance to oxidation as compared to other conductive polymers[244,245].

5.2 Materials and methods

5.2.1 Culture methods and organisms

Gluconacetobacter hansenii ATCC 53582 was considered for this study for cellulose production. A pre-inoculum was prepared in petri-plates in HS media with 2 %(w/v) of D-glucose and allowed to grow for at least 2–3 days under static conditions at 26 °C. The BC pellicles formed were removed and the cell suspensions present in the dish were used as inoculum for the experimental studies.

5.2.2 Chemicals

Cells were cultured in a standard Hestrin and Schramm (HS) medium containing (w/v): 0.5% peptone, 0.5% yeast extract, 0.27% of sodium phosphate dibasic (Na_2HPO_4) and 0.12% of citric acid monohydrate[75]. Carbon sources such as D-glucose, (≥99.5% purity) was added into the culture medium according to the experimental study design. Sodium hydroxide (≥97.0%, pellets) was used for cleaning cellulose. Poly(3,4-ethylenedioxythiophene)-poly(styrenesulfonate)- high conductivity grade (1.1% in H_2O,) was used for functionalization of cellulose. Ethyl alcohol (≥99.5% purity) was used to remove excess polymer.

All chemicals were purchased from Sigma Aldrich, unless specified otherwise.

5.2.3 Conductive cellulose design strategy

The bacterial cellulose pellicles obtained were treated in 0.5 M NaOH at 100 °C for 10 minutes to eliminate the entrapped cells and washed with deionized water until the pH was neutral. A flowchart describing the whole process of synthesis of BC-PEDOT:PSS aerogels is given below (Figure 5.1).

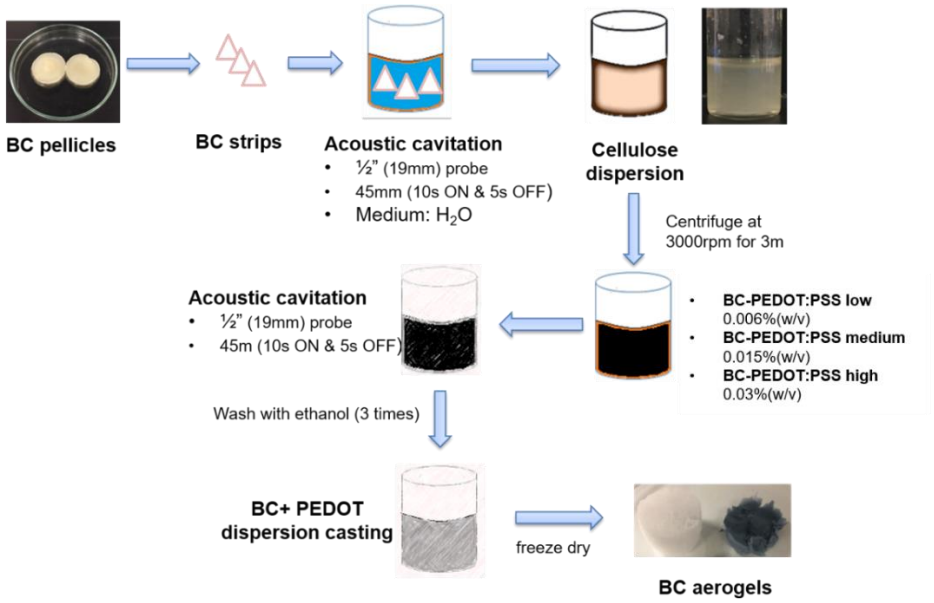

Figure 5.1 A flowchart describing the synthesis of bacterial cellulose- Poly(3,4-ethylenedioxythiophene)-poly(styrenesulfonate) conductive aerogels through acoustic cavitation.

The never-dried samples were disintegrated to form a uniform dispersion of cellulose fibres and different concentrations of PEDOT:PSS was mixed to form hybrid dispersions. The never dried BC pellicles obtained were cut into smaller strips and transferred into 40ml of milliQ water. The principle of acoustic cavitation was employed to disintegrate the tough cellulose strips with the help of Vibracell cell disrupter VC505, (Sonics & Materials Inc., Newtown, CT, USA) with maximum power output of 500 W, frequency 20 kHz at 40% amplitude for 45 minutes with 10 seconds' pulse ON and 5 seconds pulse OFF. Energy input was given through threaded end tip 1/2" containing a piezoelectric crystal with a probe diameter of 19 mm. Due to the collapse of cavitation bubbles produced in the liquid, sonic probe generates disruptive forces that tend disintegrate the bonds present in cellulose. After 45 minutes of ultrasonication, the cellulose dispersion obtained was centrifuged at 3000 rpm for 3 minutes to collect the disintegrated cellulose mass. The disintegrated cellulose mass is transferred to 20ml solutions containing different concentrations of PEDOT/PSS in H_2O (low: 0.006 %(w/v), medium: 0.015 %(w/v) and high: 0.03 %(w/v)). This mixture is further ultrasonicated for 45 minutes with the same conditions post which, the hybrid dispersion solution was washed with ethanol 100 %(v/v) to remove excess polymer (wash step is repeated 3 times). Finally, the dispersion mixture was cast into aluminium foils placed inside 24 well plates (Thermo Fisher Scientific, US) and freeze dried to obtain aerogels. The aerogels were subsequently freeze dried and weighted using a high precision balance. The dry weights were recorded for all the experimental conditions and represented as mean ± standard error.

5.2.4 Characterization of bacterial cellulose

FESEM, XRD, FTIR and TGA characterizations were followed according to Section 4.2.4

X-ray Photoelectron Spectroscopy (XPS). X-ray photoelectron spectroscopy (XPS) analysis was performed using an AXIS Supra spectrometer (Kratos Analytical, UK) equipped with a hemispherical analyser and a monochromatic Al K-alpha source (1487 eV) operated at 15 mA and 15 kV. The XPS spectra were acquired from an area of 700 x 300 μm2 with a take-off angle of 90°. Pass energy of 160 eV and 20 eV were used for survey and high-resolution scans, respectively. A 3.1 volt bias was applied to

the sample to neutralise charge build up on the sample surface. The binding energies (BEs) were charge-corrected based on the sp3 carbon C 1s at 284.8 eV.

Four probe resistivity. Conductivity of BC-PEDOT:PSS aerogels was obtained with the help of Four-point probe RM3000 (Jandel Engineering limited, England). BC-PEDOT:PSS aerogels were flattened before measurement, to ensure all the probes were in contact with the sample. The probes have a radius of 100 microns and are placed with a spacing of 1 mm between them. Once the probes contact the sample, the circuit is complete, and a current is passed through the sample. Based on the obstruction offered to the flow of current by the sample, sheet resistance values are calculated. In this case, sheet resistance (Ω/sq) was calculated assuming the sample was a thin film with uniform thickness throughout. Thickness of the film was calculated with the help of micrometer, it is measured at five different points and averaged out. Sheet resistivity (Ω/cm) was determined from thickness of the samples and their corresponding sheet resistance. Finally, electrical conductivity (S/cm) of the aerogels was calculated by just inversing the sheet resistivity value.

Cell viability assay (Resazurin dye assay). Resazurin assay is fluorometric assay that determines the metabolic capacity of live cells. The assay was conducted according to the protocol[246]. Primary human dermal fibroblasts (hDFs) were cultured in DMEM medium supplemented with 10 %(v/v) fetal bovine serum, 50 UmL^{-1} penicillin and 50 μgmL^{-1} streptomycin, in a humidified incubator at 37 °C with 5% CO_2. Cells (1×10^5 cells $well^{-1}$) were seeded at the bottom of the 12-well plates (TPP®) and allowed to adhere and grow for 24 h. After 24 h aerogels were introduced into the wells and tested for cell viability. Readings were taken every alternative day for a period of 7 days. For every reading, cells were incubated with resazurin dye for two hours and post which fluorescence signal was recorded. Viable cells with active metabolism can reduce resazurin into resorufin, a pink and fluorescent product. The quantity of the reduced product, resorufin is directly proportional to the number of viable cells. The resorufin product if quantified using the microplate reader, with 560 nm excitation and 590 nm emission.

5.3 Results and discussion

5.3.1 Cellulose aerogels and dry weights

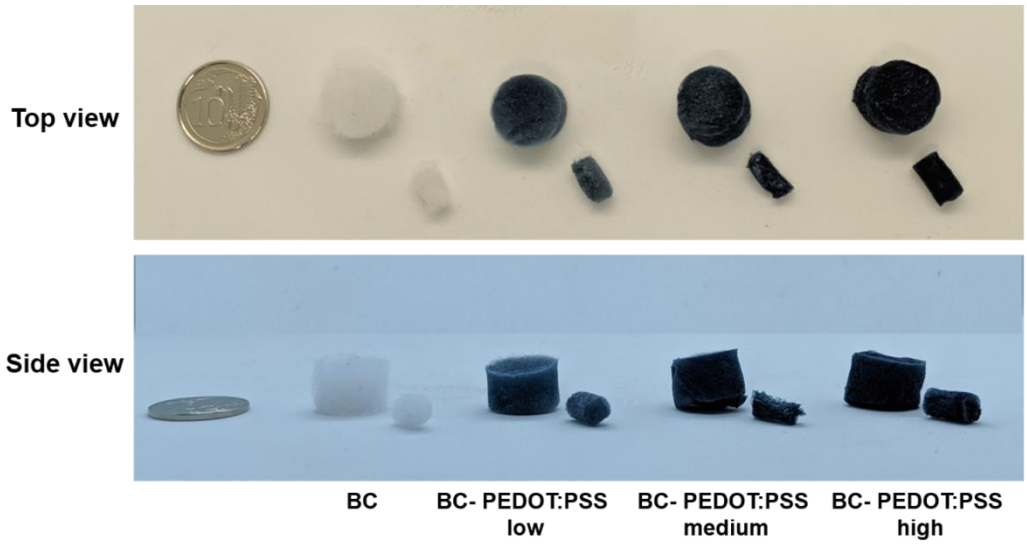

Figure 5.2 BC-PEDOT:PSS conductive aerogels; Cellulose nanofibers mixed with different concentrations of PEDOT:PSS and casted into different shapes

The aerogels will be referred to as BC-PEDOT:PSS low, BC-PEDOT:PSS medium and BC-PEDOT:PSS high for the three conductive polymer concentrations respectively (Figure 5.2). It is evident from the design strategy, various shapes and sizes can be casted. With increasing polymer concentration there is an increase in dry mass of the final aerogel, indicating the intercalation of the nanofibers with the conductive polymer (Table 5.1).

Table 5.1 Dry weights of various BC-PEDOT:PSS conductive aerogels with increasing polymer concentration

Sample	Dry Weight (mg)
BC	1.7 ± 0.1
BC-PEDOT:PSS low	3.3 ± 0.3
BC-PEDOT:PSS medium	6.9 ± 0.4
BC-PEDOT:PSS high	11.5 ± 0.4

5.3.2 Morphological study of BC-PEDOT:PSS aerogels

BC-PEDOT:PSS aerogels obtained were coated with Pt and observed using FESEM to study the morphological changes (Figure 5.3). BC control aerogel displayed the characteristic random porous fibre network as observed with normal cellulose pellicles after freeze drying, indicating that the process of ultrasonication did not destroy the core structure of BC. The pristine BC aerogel comprised of long cellulose fibres with high aspect ratio[163].

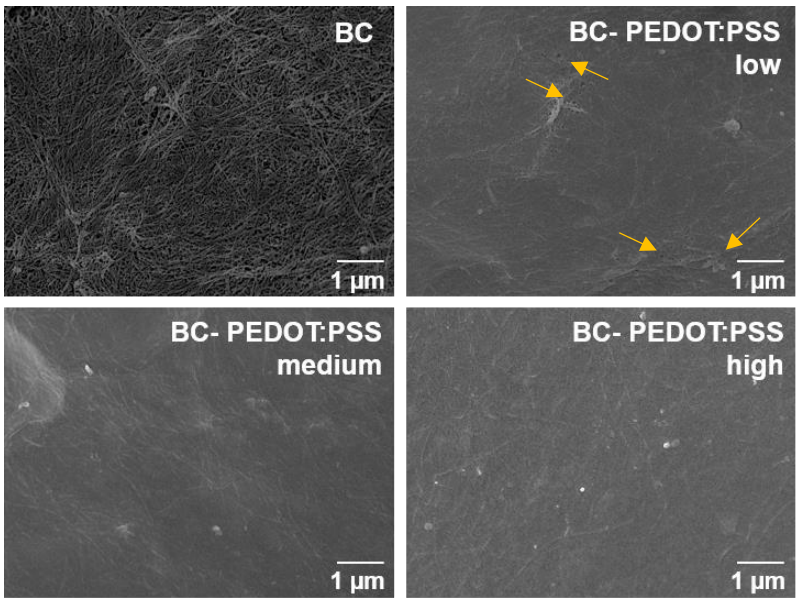

Figure 5.3 FESEM images of various BC-PEDOT:PSS aerogels obtained through different approaches (*Scale bar: 1 µm*).

With the increase in concentration of the polymer, the aerogel surface tends to become compact with the disappearance of the characteristic porous structure of cellulose network, indicative of the uniform distribution of polymer. The polymers densely adhere to the surface of long cellulose fibres and penetrate well into the matrix leading to high conductivity. The strong adhesion is assumed to arise from the interaction of the hydroxyl groups present in the glucan chains and the electronically charged PEDOT:PSS[181,195]. BC-PEDOT:PSS low aerogels (Figure 5.3, top right) did show distribution of minor pores across the surface but the higher concentration hybrid aerogels (Figure 5.3, bottom row) did not display any pores and the surface of the aerogels was even. This is the result of the strong interaction between excess polymer molecules inside the BC network.

5.3.3 Crystal orientation of BC-PEDOT:PSS aerogels

The introduction of PEDOT:PSS in between the cellulose layers can change the crystal structure of cellulose. New hydrogen bonds are formed between the polymer and cellulose fibre network, the characteristic intra and intermolecular hydrogen bonds present in cellulose chains are broken. X-ray diffractograms of pristine BC aerogels displayed all the crystalline planes of cellulose at 14.7° (1-10), 16.8° (110) and 22.7° (200) respectively[195,237]. With increasing polymer concentration, a right shift for 22° peak was observed suggestive of the change in the interplanar distance (Figure 5.4). The intensities of all the signature peaks reduced due to the introduction of amorphous PEDOT:PSS in the hybrid aerogel. We also, notice the appearance of a broad amorphous peak at 24.8° (020), indicative of the intercalation of the nanofibers with increasing polymer concentration. The broad peak corresponds to the presence of the amorphous PEDOT:PSS in the final hybrid aerogels[247].

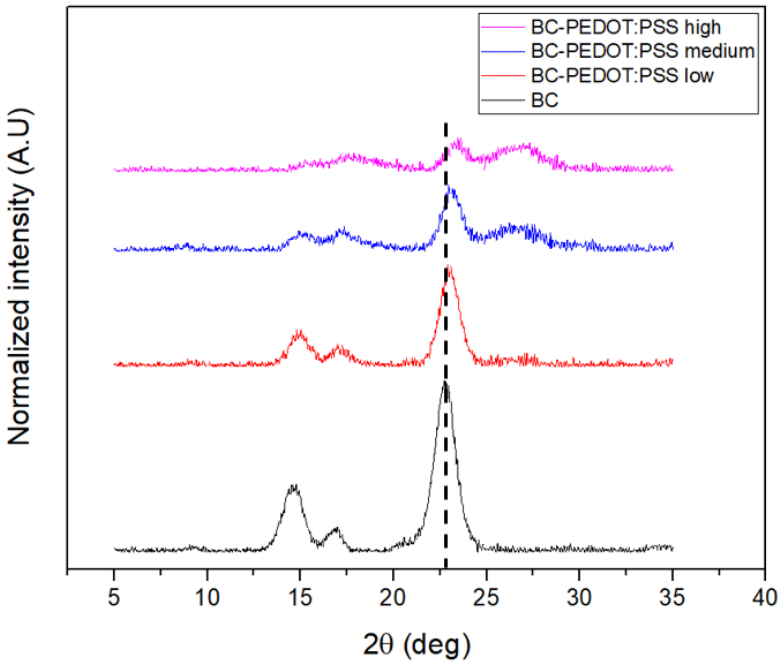

Figure 5.4 X-ray diffractograms of BC-PEDOT:PSS composites and PEDOT:PSS alone.

The CI ratio and d-spacing is calculated from the diffractograms to understand the impact of the introduction of the polymer to the crystal structure of BC (

Table **5.2**). The CI ratio and d-spacing were calculated based on the formulas under section 4.2.4 (X-ray diffraction methods).

Table 5.2 Crystallinity index and d-spacing of different BC aerogels.

Sample	Crystallinity (%)	d-spacing (Å)
BC	96.91 ± 2.45	3.91 ± 0.00
BC-PEDOT:PSS low	94.91 ± 1.75	3.86 ± 0.00
BC-PEDOT:PSS medium	86.94 ± 3.95	3.86 ± 0.00
BC-PEDOT:PSS high	72.71 ± 3.66	3.84 ± 0.04

We observe about 2-25% drop in crystallinity with the introduction of the polymers. PEDOT:PSS did not have any visible crystalline peak, so the relative crystalline area was not calculated. Only the crystalline peaks of BC were considered to calculate CI for the final hybrid. Drop in crystallinity values correlated with diffractograms obtained for the corresponding hybrid aerogels[248]. The d-spacing also, decreases due to the compressional stresses experienced by the BC samples with the introduction of polymer. The hydrogen bonds present in BC were disrupted leading to a new interplanar distance between the glucan chains[165].

5.3.4 Direct intercalation of PEDOT:PSS with BC matrix

FTIR spectra of the aerogels are presented in Figure 5.5. The FTIR spectrum of pristine BC aerogel has a broad region from 3200-3500 cm^{-1} corresponding to the -OH groups present in cellulose (-CH-OH and -CH_2-OH). The absorption bands at 1429, 1160 and 1050 cm^{-1} correspond to the H-C-H plane bending, -OH wagging vibration and C-O-C pyranose backbone ring vibration[165,249]. The FTIR spectrum of PEDOT:PSS contains absorption bands at 1157, 1121 and 1012 cm^{-1} assigned to S-O and S-C phenyl bonds present in the sulfonic acid groups. The peaks at 1356, 952, 845 and 704 cm^{-1} are assigned to C-C and C-S bonds present in the thiophene backbone structure[250,251]. The IR spectra of the BC-PEDOT:PSS hybrid aerogels attributed for all the signature peaks of BC and PEDOT:PSS indicated in the Figure 5.5 as shaded regions assigned to the

specific peaks. The big hydroxyl band of BC present at 3300 cm^{-1} is present in the hybrid aerogel as well, but the broadening of the peak clearly suggests the new hydrogen bonds formed between the conductive polymer and the hydroxyl groups of BC matrix[195,252]. The other prominent absorption bands at 1340, 948, 860 and 710 cm^{-1} arise from S-O, C-C and C-S bonds present in thiophene backbone and sulfonic groups. The broad peak at 1050 cm^{-1} corresponds to the merging of the pyranose skeletal rings present in BC with PEDOT:PSS.

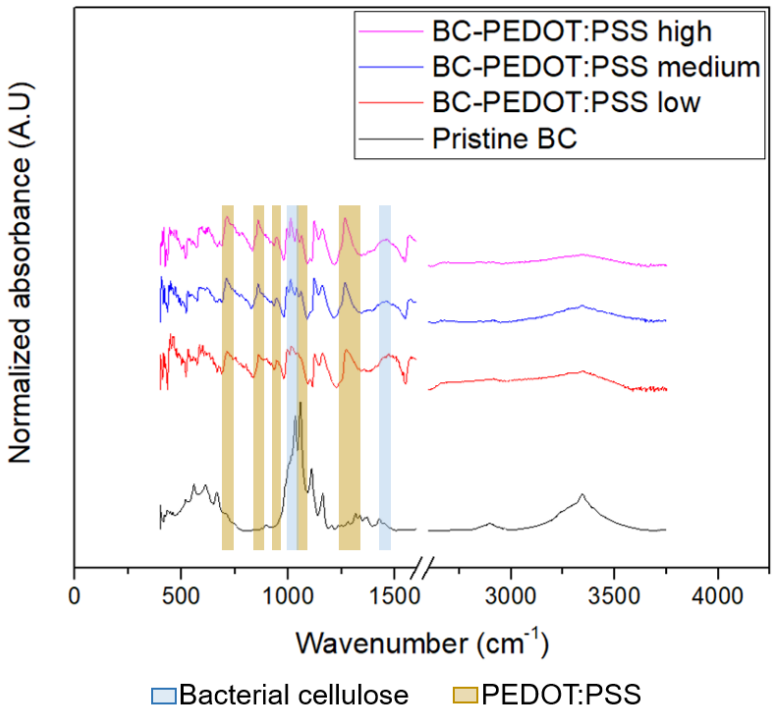

Figure 5.5 The IR spectrum of BC aerogels indicating the presence of PEDOT:PSS polymer.

5.3.5 Surface chemistry of BC-PEDOT:PSS aerogels

XPS was used to analyse the surface chemistry of the conductive aerogels. Table 5.3 shows the atomic compositions of the various conductive aerogels. The atomic concentrations of carbon and sulphur increased with increasing polymer concentration whereas, the oxygen atom concentration decreased. The hydroxyl groups present in BC matrix were involved in the interactions with the ionic polymer.

Table 5.3 The atomic composition of the BC aerogel and BC-PEDOT:PSS conductive aerogels

Atom (%)	BC	BC-PEDOT:PSS low	BC-PEDOT:PSS medium	BC-PEDOT:PSS high
Carbon	61.03 ± 1.36	68.25 ± 2.56	71.34 ± 2.84	69.65 ± 1.82
Oxygen	38.97 ± 1.36	26.34 ± 2.59	23.09 ± 2.46	23.67 ± 1.75
Sulphur		5.41 ± 0.10	5.56 ± 0.41	6.68 ± 0.07

The C1s and O1s core-level spectra of pristine BC and the C1s, O1s and S2p core-level spectra of the BC-PEDOT:PSS aerogels are shown in Figure 5.6. The C1s core-level of BC can be resolved to three peaks by deconvolution, C1 at 285 eV, C2 at 286.6 eV and C3 at 288.2 eV assigned to non-functionalized carbon (C-C, C-H), carbon linked to oxygen atom by a simple bond (C-O) and carbon linked to two oxygen atoms by a simple bond (O-C-O) respectively. Similarly, the O1s core-level of BC is resolved to two peaks, O1 at 533.1 eV and O2 at 533.8 eV assigned to the hydroxyl groups in cellulose (-OH) and oxygen linked to a carbon by a simple bond (O-C) respectively[253,254]. The C1s peak for PEDOT:PSS originated with a strong peak at 284.1 eV and a shoulder at 286.2 eV. The presence of a strong peak is due to the saturation and conjugation of carbon atoms present in PEDOT and PSS chains. The shoulder corresponds to C-O-C bonds present in the thiophene rings of PEDOT. The O1s core-level with peaks at 531.7 eV and 532.3 eV correspond to oxygen atoms in the sulfonate group of PSS chains and oxygen atoms present in the thiophene backbone respectively. Likewise, the S2p core-levels have an energy splitting of 1.2 eV and 1:2 intensity ratio with $S2p_{3/2}$ and $S2p_{1/2}$ peaks. Both the S2p peaks have contributions from a spin split doublet[255]. The peaks at 161.0 eV and 163.2 eV belong to the sulphur atoms present in PEDOT and the peaks at 165.7 eV and 167.9 eV originate from the attachment of electropositive sulphur atom with the highly electronegative oxygen atoms present in the sulfonate groups of PSS chains[255-257].

The core-level spectra of C1s and O1s of the hybrid aerogels shifts right to lower binding energy as compared to the pristine BC. This right shift arises from the presence of the counter ion, PSS in the conductive polymer[258,259]. The sulphur atom in PSS is highly electropositive as it surrounded by three electronegative oxygen atoms. With increasing polymer concentration, we notice a trend in the right shift for C1s and O1s core-levels indicative of the higher concentration of PSS in the hybrid aerogel.

Similarly, for S2p core-level we notice an increase in the intensity of S2 peak corresponding to sulphur atoms in PSS chains.

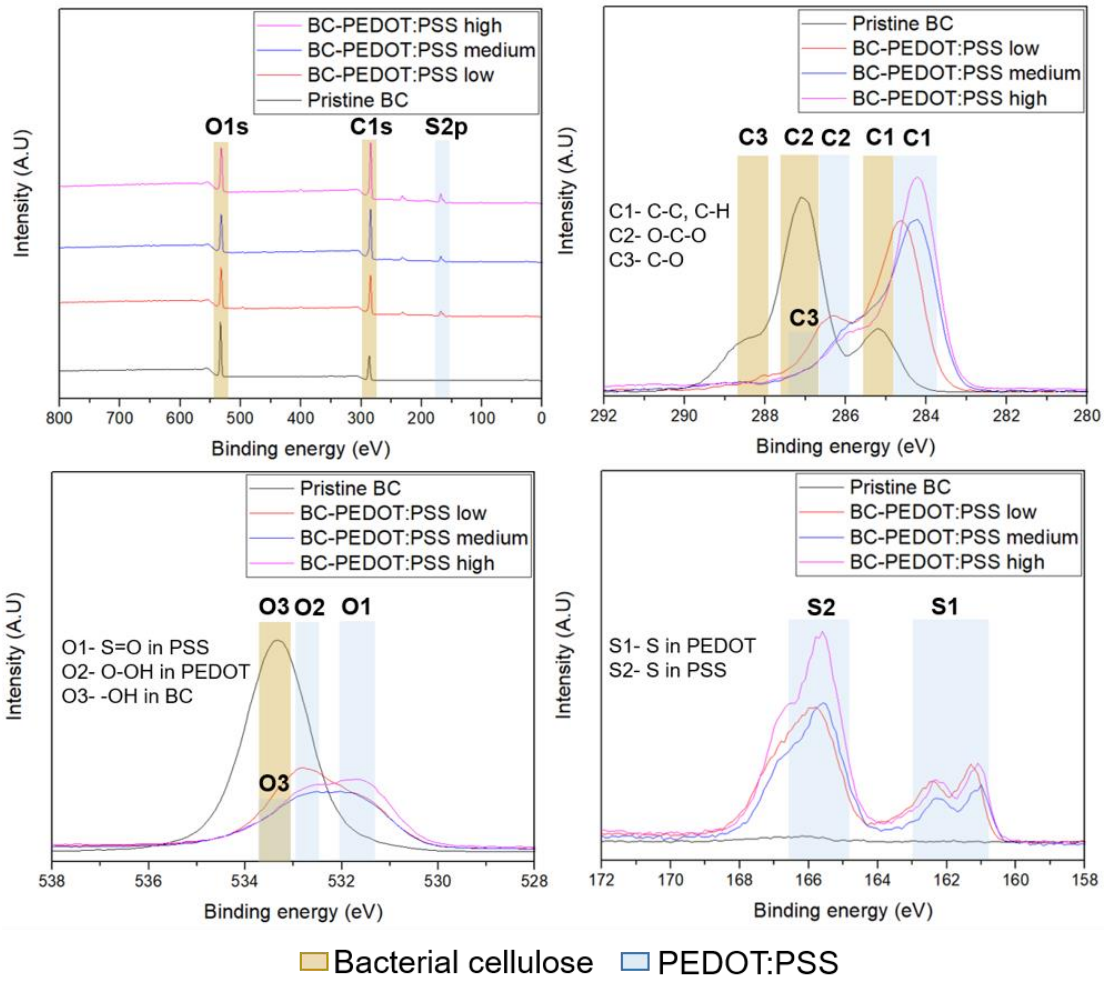

Figure 5.6 XPS spectra of BC-PEDOT:PSS aerogels with a) Survey scan, b) C1s spectra, c) O 1s spectra, d) S 2p spectra

5.3.6 Thermal stability and degradation profile of BC-PEDOT:PSS aerogels

Thermal stability and thermal decomposition of the hybrid aerogels was analysed with TGA (Figure 5.7). The TG curves obtained can be distinctively divided into two stages. During the initial stage, a small weight loss at 50-100 °C for pure BC as well as BC-PEDOT:PSS aerogels occur due to the presence of moisture which makes up about 14 wt.% approximately. The second stage involves a sharp weight loss from 320-380 °C due to the disruption of the crystalline regions and decomposition of amorphous BC into D-glucopyranose monomer units, which is about 70 wt.%. The

second stage for the hybrid aerogels occurs over 240-400 °C, earlier than that of pure BC. The onset of degradation at 240 °C in hybrid aerogels corresponds to the degradation of sulfonate groups in PSS with weight loss of 5-9 wt.%. With temperatures greater than 300 °C, the carbon atoms present in PEDOT backbone oxidize, contributing to 15-20 wt.% loss[260,261]. The hybrid aerogels are thermally stable at 200 °C. The mass loss of pure BC occurs at 80 °C higher than that of the BC present in BC-PEDOT:PSS aerogels due to the weak hydrogen bonds between BC and polymer.

The first derivative (DTG) curves showed two distinct peaks at 240 °C and 360 °C that confirm the thermal degradation observed in pure BC and hybrid aerogels. The two sharp endothermic peaks correspond to the degradation of the crystalline regions present pure BC and the BC present in hybrid aerogels.

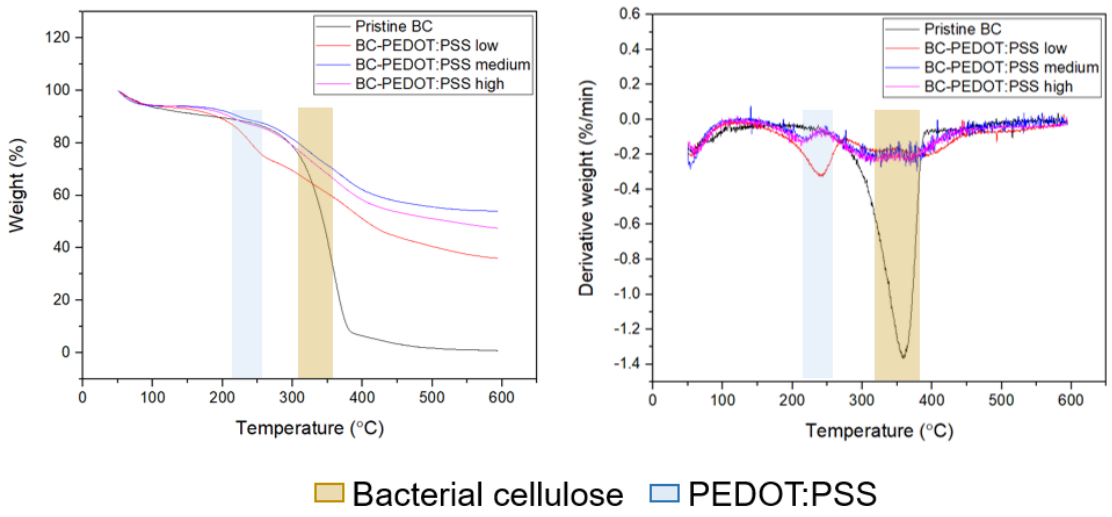

Figure 5.7 (Left) TGA curve of BC-PEDOT:PSS aerogels (right) DTG curves highlighting the degradation temperatures.

5.3.7 Electrical conductivity of BC-PEDOT:PSS aerogels

Pristine BC samples are not conductive in nature, they are insulators with very high resistance values[162]. With the introduction of PEDOT:PSS, BC samples turned conductive (Table S1). Conductive BC aerogels with a low concentration of PEDOT:PSS exhibited 0.7 S/cm of conductivity when measured with the 4-Probe equipment. PEDOT:PSS not only intercalates with the cellulose nanofibers but also, fills the gaps present in the matrix due to the strong electrostatic interactions. The electrical conductivity of the hybrid aerogels is enhanced due to the homogeneous dispersion, high

content of conductive fillers in the matrix and the formation of long conducting pathways in the two-dimensional morphology of the hybrid aerogels[262]. We notice that there is no further increase in the electrical conductivity with increasing polymer concentration. This can be attributed to the saturation capacity of the BC membranes for further incorporation of the conductive polymer. It is evident from the table (Table 5.4) that the electrical conductivity obtained in this work is high as compared to other BC conducting composites[162,181,186,241,263-265]. Some of the high conductivity values obtained by others, compared to the ones obtained in this study, are due to a very high concentration of the conducting polymer deposited on the BC matrix. In some reactions, harsh chemicals were used for the polymerization of monomers and temperatures of about 70 °C were required for the deposition. In this work as mentioned previously in Section 5.2.3, the reaction is carried out in a water based system and at ambient room temperatures.

Table 5.4 Conductivity values of BC based composites from previous work compared to conductive aerogels developed in this work.

Substrate	Composite material	Process	Conductivity	Journal
BC	PEDOT:PSS	Ex situ deposition	6 S/cm (34% PEDOT:PSS, with specific conductivity of 850 S/cm)	Carbohydrate Polymers (2015)
BC	Polyaniline	Oxidative polymerisation	8.2×10^{-4} S/cm	Cellulose (2012)
Wood cellulose	Polythiophene	Oxidative polymerisation	1.3×10^{-4} S/cm	Carbohydrate Polymers (2019)
BC	Polyaniline	Oxidative polymerisation	5×10^{-2} S/cm	Physical Chemistry B (2011)
BC	PEDOT:PSS	Oxidative polymerisation	1.5 S/cm (5 days reaction)	Mater Sci: Mater Electron (2016)
Filter paper	Polyaniline	Oxidative polymerisation	2×10^{-3} S/cm	Synthetic Metals (2005)
BC	PEDOT:PSS	Oxidative polymerisation	0.26 S/cm	Synthetic Metals (2015)
BC	Polyaniline with p-TSA dopant	Oxidative polymerisation	1.3 S/cm	Current Applied Physics (2011)
BC	Polyaniline without p-TSA dopant	Oxidative polymerisation	0.8 S/cm	Current Applied Physics (2011)
Bamboo	Polyaniline	Oxidative polymerisation	1×10^{-3} S/cm	BioResources (2015)
BC	Polypyrrole- $FeCl_3.6H_2O$	Oxidative polymerization	2.7 S/cm (80% Ppy content)	Carbohydrate Polymers (2013)
BC	Polypyrrole- Ammonium Persulphate	Oxidative polymerization	1.2×10^{-2} S/cm (33% Ppy content)	Carbohydrate Polymers (2013)
BC	PEDOT:PSS	Oxidative polymerisation	1.2×10^{-3} S/cm	ACS Appl. Mater. and Interfaces (2015)
BC	**PEDOT:PSS**	**Acoustic cavitation**	**0.7 S/cm (40% PEDOT:PSS content)**	**This work**

5.3.8 Cell viability in the presence of BC-PEDOT:PSS aerogels

Studies have shown bacterial cellulose to be biocompatible when either used as a scaffold or as an implanted material[146,147,266]. In addition to biocompatibility, cellulose possesses unique mechanical properties making it well suited for biomedical applications. Assessment of cell proliferation of PEDOT:PSS films alone or when doped with other polymers confirmed the cytocompatibility of the PEDOT:PSS[267,268]. Similarly, PEDOT:PSS aerogels were evaluated for cytotoxicity in the presence of human dermal fibroblasts (HDFa) cells (Figure 5.8). The findings reveal that over the course of 7 days of incubation, the viability of BC-PEDOT:PSS aerogel with lower polymer concentration was similar to the pure BC group as observed in other studies[269-271]. With higher polymer concentrations the cells did not proliferate in the presence of the hybrid aerogels suggesting toxic nature of higher polymer concentrations. BC-PEDOT:PSS low aerogels did not inhibit the proliferation of the HDFa cells over the incubation period. Furthermore, pure BC displayed inhibition to cell proliferation post 5 days, but the BC-PEDOT:PSS low aerogels continued to support cell proliferation. A lower polymer concentration was sufficient to achieve biocompatibility without compromising the electrical conductivity of the hybrid aerogel.

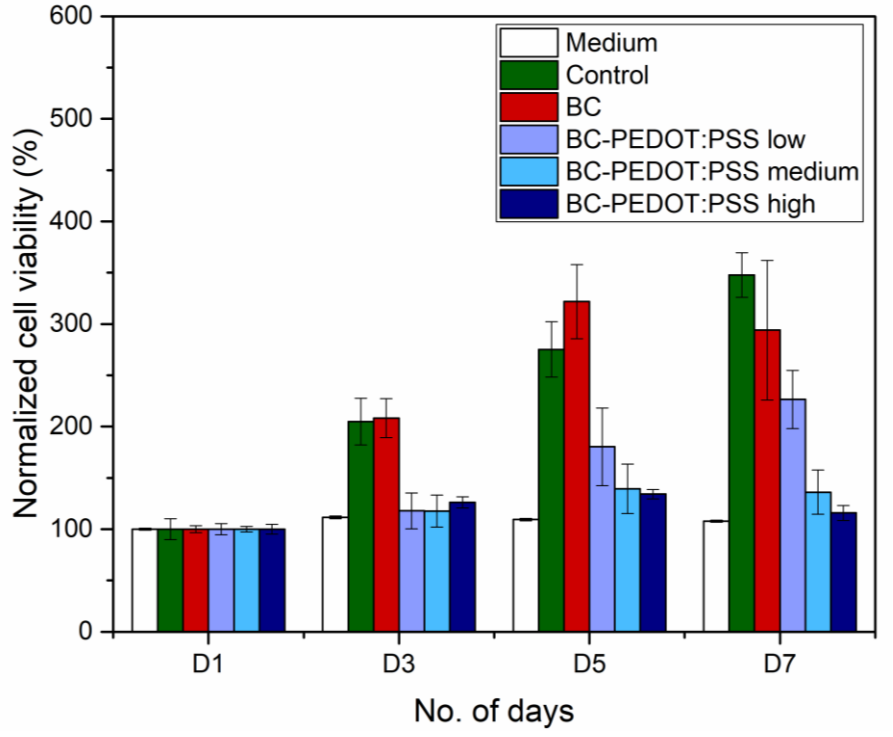

Figure 5.8 Resazurin cell viability assay of BC-PEDOT:PSS aerogels in the presence of HDFa cells.

5.4 Conclusions

We have developed a green strategy to prepare electroconductive 3D aerogels comprising of bacterial cellulose and PEDOT:PSS polymer. Our design strategy enables uniform intercalation of the polymer with BC nanofibers, as not observed in *in-situ* and *ex-situ* approaches. Acoustic cavitation facilitates even distribution of the polymer with fibres and strong adherence of the polymer to cellulose nanofibers. It also allows for tuning of coating thickness and pore size distribution as seen in FESEM. Chemical incorporation of PEDOT:PSS in the hybrid aerogels was confirmed by the strong absorption bands across the IR spectrum. XPS validated the intercalation of the cellulose nanofibers with the conductive polymer due to the chemical shift in the binding energy of carbon and oxygen atoms core-levels. Likewise, the preferential orientation of the (200) plane was shifted right with the introduction of the polymer in the hybrid aerogels. The disruption of the hydrogen bonds in native BC caused a drop in crystallinity and change in d-spacing due to the polymer. The hybrid aerogels were found to be thermally stable at 200 °C. When the aerogels were evaluated for their cytocompatibility in the presence of HDFS cells, higher polymer concentration hybrid aerogels proved to be toxic to the cells. With 72 h of incubation, BC-PEDOT:PSS low aerogels did not inhibit cell proliferation and the cells were found to be viable and comparable to the control group. Four-probe resistivity measurements indicated higher polymer concentration in the hybrid aerogels did not necessarily enhance the electrical conductivities as expected. This also confirmed the limitation of BC's capacity to intercalate with the polymer due to the depletion of the hydroxyl groups in the final aerogels. BC-PEDOT:PSS low aerogels were found to be intrinsically crystalline, cytocompatible and exhibited high electroconductivity, suggesting these hybrid materials are potential substrates for flexible electronics applications.

Our simple design strategy and optimization adopted for obtaining a hybrid conductive biopolymer for use in the development of biomedical devices, is unquestionably low-cost, facile, and highly efficient approach. This will pave way for replacing and reducing the usage of synthetic polymers, carbon nanotubes and other carbon-based materials obtained usually by expensive and complex methods. This draws us to the possibility of applying simple methods to convert bio-based materials into novel products almost at par or in some cases even better than the existing substrates

used. Hence, aids in the reduction of environmental wastes caused due to the production materials or inefficient disposal of existing devices which is of greatest concerns given the present energy crises across the world.

Chapter 6

Synthesis of Magnetic Bacterial Cellulose Membranes Inspired by a Novel Bioengineering Approach

The significant role of biopolymers for biomedical applications has driven research into encouraging development of novel products through innovative strategies. Bioinspired design methods enable the self-assembly of multifunctional biomaterials devoid of any structural disruption. As a proof of concept, in this work we demonstrated that the entrapped recombinant Escherichia coli in cellulose matrix aided in functional display. The recombinant E. coli contained the genetic circuit, amyloid proteins CsgA tagged with short functional m6A peptide domains, responsible for in situ magnetite nanoparticle nucleation. The functional amyloid CsgA proteins were secreted extracellularly by E.coli and self-assembled in the cellulose matrix. The injection of functional amyloid proteins into cellulose facilitated magnetite nanoparticle decoration across the matrix. Through this bioengineered design we were able to achieve a maximum magnetization of 40 emu g^{-1}. The functional magnetic membranes demonstrated biocompatibility and accelerated the process of wound healing in the presence of magnetic field. This work lays the foundation for developing novel functional materials by combining living systems with non-living components.

6.1 Introduction

The performances of materials are defined from the nano to micro scale by their chemical composition, structural morphology, penetrability, crystallinity and hierarchical structural design[212]. In this regard, bacterial cellulose has earned considerable interest in material science due to its unique material properties. The biocompatibility, biodegradability and high water-holding capacity of BC make it a suitable candidate for wound healing applications[142,146]. Functionalizing cellulose through sustainable approaches has led to new design strategies. Bioengineering has been employed to biological systems to produce functionalized materials. This design approach uses synthetic biological tools to engineer bacteria, the novel chassis for material functionalization[206,207].

Incorporation of functional amyloid proteins to anchor BC fibrils is a possibility to be explored. CsgA proteins secreted by recombinant *E. coli* are highly robust functional amyloid nanofibers with a diameter of approximately 4–7 nm and exist as extended tangled networks encapsulating the cells. They are formed from the extracellular self-assembly of the amyloid protein CsgA, a small 13-kDa protein[272,273]. A homologous outer-membrane protein, CsgB, nucleates assembly of CsgA and anchors the nanofibers to the bacterial surface[272,274]. The amyloid protein system exhibits numerous features that make it an ideal platform for synthesizing the type of materials engineered by synthetic biology. Functional amyloid fibres formed by CsgA are extremely robust, can withstand boiling in detergents and extended incubation in solvents, thereby increasing their potential utility in harsh environments[272,275]. They can be used in a broad and modular way for the display of various functional peptides throughout the BC scaffold[209].

A variety of peptides for the nucleation of metal nanoparticles are available at our disposal for their display along with amyloid proteins[209]. One such peptide domain is the magnetite forming m6A peptide which is part of the long MMS6 protein found in magnetotactic bacteria, *Magnetospirillum magneticum* AMB-1. The m6A peptide acts as a nucleation site for the formation of the iron oxide nanoparticles thereby imparting magnetic property to the membrane[276,277]. It is a short peptide of only 12 amino acids (DIESAQSDEEVE) with a molecular weight of 1.4 kDa[278]. The m6A peptide aids in

controlled nucleation of magnetite nanoparticles and synthesizes cubo-octahedral magnetite nanoparticles in the reaction solution of iron sulphate[277,279].

Magnetite (Fe_3O_4) nanoparticles are one of important iron oxides that can be found in nature. Magnetite exhibits high magnetizations as compared to other iron oxide ores[280]. The high magnetization and color of magnetite nanoparticles arises from its crystal structure, inverse spinel with a unit cell consisting of 32 oxygen atoms in a face centered cubic. The black color obtained post synthesis, is due to the intervalence charge transfer between Fe^{2+} and Fe^{3+} ions and the high magnetization is due to occupation of Fe^{2+} and Fe^{3+} atoms in tetra and octahedral sites in its crystal structure respectively[281,282]. They are widely studied for their applications in various fields such as magnetic resonance imaging (MRI), drug delivery, hyperthermia, wound healing, immunoassays, energy, rocket fuels, ferrofluids and storage devices, but its applications can be limited if shape and size are not controlled. Various surface modifications on magnetite can play a crucial role in its properties and applications[283,284].

6.2 Materials and methods

6.2.1 Plasmid construction

pBbE8k plasmid containing curli forming subunits csgB, csgA, csgC, csgE, csgF and csgG was kindly obtained from Prof. Neil Joshi's laboratory, Harvard University. Gibson assembly method was employed for inserting m6a peptide (DIESAQSDEEVE) followed by GSGGSG linker to the C-terminus of the csgA subunit. The plasmid map is supplemented in Figure S4.

6.2.2 Culture method and organisms

Culture method and organism used for cellulose production was according to Section 5.2.1.

Escherichia coli PQN4 cells harbouring genes encoding amyloid fusion protein CsgA tagged with the m6A peptide domain was inoculated in lysogeny broth with chloramphenicol (Cm) and kanamycin for overnight at 37 °C at 180 rpm. The overnight cultures were used as pre inoculum for CsgA protein expression.

CsgA protein expression. The overnight cultures was transferred to fresh LB medium with chloramphenicol and kanamycin and 2 %(w/v) glucose. They were cultured at 37 °C and 180 rpm until they reached an optical density (OD_{600}) of 0.6 to 0.8. The cells were pelleted at 4000 xg and gently resuspended in an induction medium (LB without glucose, containing 0.5 %(w/v) arabinose with Cm and kanamycin).

Functional bacterial cellulose. Cellulose films harvested post five days of incubation, were dropped inside the induction medium. Culture medium was left overnight at 30 °C and 180 rpm for CsgA fusion protein expression. Pellicles were removed from the induction medium the following day. They were washed 3 times in purified water and heated with 1% NaOH at 100 °C for 10 minutes to remove the entrapped bacteria. The pellicles were rinsed again 3 times and lyophilized. Samples were then stored for further characterizations.

6.2.3 Chemicals

All chemicals related to cellulose production was according to Section 5.2.2.

Lysogenic broth, Chloramphenicol, Kanamycin, L-arabinose was used for *E.coli* growth and CsgA protein expression. Iron (ii) sulphate heptahydrate, Potassium hydroxide, Potassium nitrate and Poly(ethylene glycol) (≥97.0%, pellets) was used for magnetite nanoparticle synthesis. Curcumin, an amyloid specific dye for protein confirmation. Ethyl alcohol (≥99.5% purity) was used for solvent exchange in cellulose films.

All chemicals were purchased from Sigma Aldrich, unless specified otherwise.

6.2.4 Magnetic cellulose membranes design strategy

Cellulose from *Gluconacetobacter* bacteria will offer the scaffold for the membrane design and help in entrapping recombinant *E. coli* bacteria. The recombinant *E. coli* bacteria contains the genetic circuit for functional display. The functional peptide, m6A, will aid in the localization and growth of magnetite nanoparticles as shown in the Figure 6.1. The short m6A peptide was genetically engineered into the N-terminus of the CsgA amyloid protein as show in the Figure S4. The never dried

functional membranes are solvent exchanged overnight in 20 %(v/v) ethylene alcohol to allow better penetrability for nanoparticle synthesis[285]. The solvent exchanged hybrid membranes was dropped in a reaction volume (20 ml) containing 400 mM potassium nitrate (KNO_3), 100 mM potassium hydroxide (KOH) and 1 %(w/v) poly(ethylene glycol) (PEG) used as a surfactant. The entire mixture was capped, and continuous N_2 gas was bubbled for 5 minutes to remove any oxygen present. Iron (ii) heptahydrate (30mM) solution was introduced dropwise into the mixture with the help of a syringe pump at 100 µL/min with a reaction time of 20 minutes[277]. The nanoparticle synthesis was carried out in a silicone oil bath set to 80 °C and the mixture was stirred with the help of a magnetic stirrer to ensure there is even distribution of the magnetite nanoparticle across the matrix. Post nanoparticle synthesis, the magnetic membranes are washed with water 3 times to ensure there is excess chemicals or nanoparticles on the membrane. The membranes were subjected to freeze drying and stored for further characterizations. Two sample models were prepared, first one was pure BC membrane with magnetite nanoparticles will be referred to as BC(Fe_{30mM}) and the second was the functional hybrid membrane containing magnetite nanoparticles which will be referred to as BC-m6A(Fe_{30mM}).

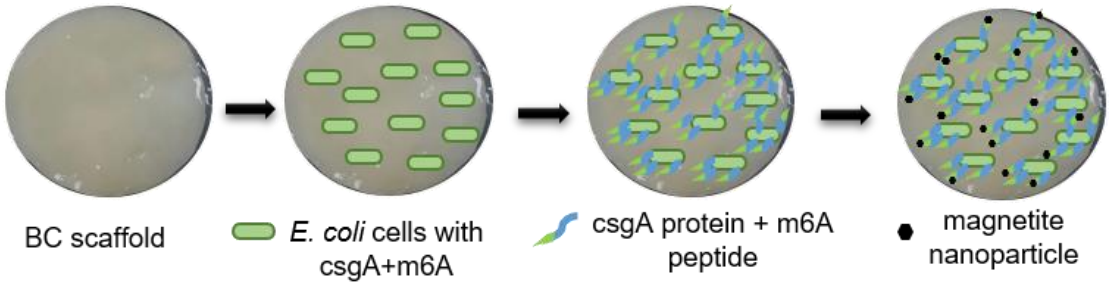

Figure 6.1 Co-cultivation of G. xylinus and E. coli to develop bioinspired magnetic membranes

6.2.5 Characterization of bacterial cellulose

FESEM , XRD, FTIR, TGA was conducted according to Section 4.2.4 and Cell viability assay and XPS was according to Section 5.2.4

Confocal light microscopy. Amyloid specific curcumin dye was used to confirm the presence of amyloid fusion protein, CsgA-m6A in the final bioengineered cellulose membrane. The membrane was incubated in 25µM curcumin dye for 15 minutes and rinsed with water to remove excess dye. Green fluorescence obtained with 432 nm excitation and 510 nm emission filter set. Samples were placed on glass slides and images were recorded using Zeiss LSM 800 confocal microscope at 20x magnification. The images were processed using Zen software (blue edition).

Vibrating sample magnetometer (VSM). Magnetic measurement of magnetic cellulose films was obtained using vibrating sample magnetometer. The magnetic property was obtained by measuring the magnetization (M) versus applied magnetic field (Oe) under a maximum field of 20 kOe. The MH curves were acquired at room temperature using Lake Shore Cryotronics, 8600 series VSM. The hysteresis curves were analysed using the 8600 series inbuilt software.

Scratch test. Scratch wound assay was followed according to the protocol[286]. Primary human dermal fibroblasts (hDFs) were cultured in DMEM medium supplemented with 10 %(v/v) fetal bovine serum, 50 UmL^{-1} penicillin and 50 μgmL^{-1} streptomycin, in a humidified incubator at 37 °C with 5% CO_2. Cells (25×10^3 cells $well^{-1}$) were seeded at the bottom of the 96-well plates (TPP®) and allowed to adhere and grow for 24 h to form a confluent monolayer. With the help of Accu Wound 96 (Acea Biosciences Inc.) we created uniform scratches of 1mm at the centre of the well. Each well was washed three times with prewarmed (37 °C) PBS to remove detached cells from the scratch site. The wells were then replenished with fresh DMEM containing 1% FBS. The various functional cellulose based films were introduced and monitored for 48H. Wound closure was captured with a 10× objective using a light microscope. Each wounded area was captured at 0, 24, 36 and 48 h post scratch. Wound closure was quantified using ImageJ software (developed by Wayne Rasband, National Institutes of Health, Bethesda, MD; provided in the public domain at *http://rsb.info.nih.gov/ij*).

6.3 Results and discussion

6.3.1 Bioengineered magnetic cellulose membranes and confirmation of the amyloid protein

CsgA(m6A) fusion proteins were successfully incorporated into the BC matrix as confirmed by confocal microscopy (Figure S6). Biosynthesized functional cellulose membranes were successful in nucleating higher concentration of magnetite nanoparticles across the cellulose matrix. From the Figure 6.2 it is evident the BC functional membranes were able to disperse the iron oxide nanoparticles better as indicated by the intense black colour. Magnetic membranes were obtained at much lower reaction temperatures and without any structural disruption by the use of strong solvents[287,288]. The BC membranes did demonstrate limitations in nanoparticle templating (Figure 6.2) due to the limited distribution of pores and the availability of hydroxyl groups for nucleation and growth. The bottom side is limited to the process of nanoparticle synthesis as they are not in direct contact with the iron salt that is injected. The bulk material is not black but the nanostructural morphology of the material under SEM confirmed the presence of magnetite nanoparticles on either side of the cellulose films (Figure 6.3). Further optimization of the mixing and reaction conditions would eliminate these issues and lead to a more uniform material formation.

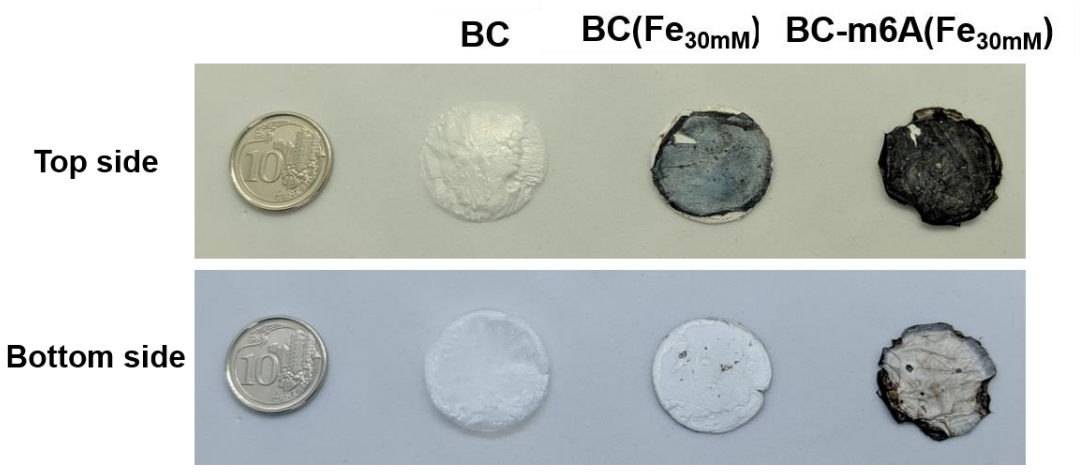

Figure 6.2 Bioinspired BC-m6A membranes with magnetite nanoparticles decorated across the membrane.

6.3.2 Morphological study of magnetic cellulose membranes and nanoparticle size distribution

The morphology of the magnetic membranes was investigated by FESEM, whose pictures are shown in Figure 6.2. The SEM images confirm the higher density of magnetite nanoparticles present in the BC-m6A membranes as compared to BC membranes coated with nanoparticles. The structural morphology cellulose fibres in functional membranes did not alter with the introduction of the fusion amyloid proteins. The nanofiber thickness was 30-40 nm about the same as the control pure BC membrane.

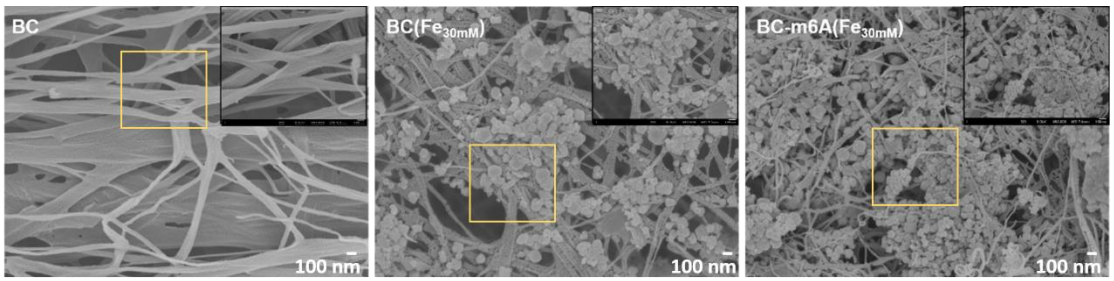

Figure 6.3 Structural morphology of various cellulose membranes. (a) BC, (b) magnetic BC and (c) magnetic BC-m6A (*Scale bar: 100 nm*).

We observe with BC membranes alone there is aggregation of nanoparticles and/or large nanoparticles as seen by the wide particle size distribution with a mean of 82.4 nm in Figure 6.4. The presence of m6A peptide domains in the functional BC membranes aids in controlled magnetite nucleation and growth. A narrow size distribution with a mean size of 47.0 nm (Figure 6.4) of the nanoparticles across the matrix we can achieve high saturation magnetization[289,290]. The presence of PEG as a surfactant prevented the magnetite particles from agglomerating and maintain an optimum size and shape which was not observed in the absence of the capping agent (Figure S5)[291,292].

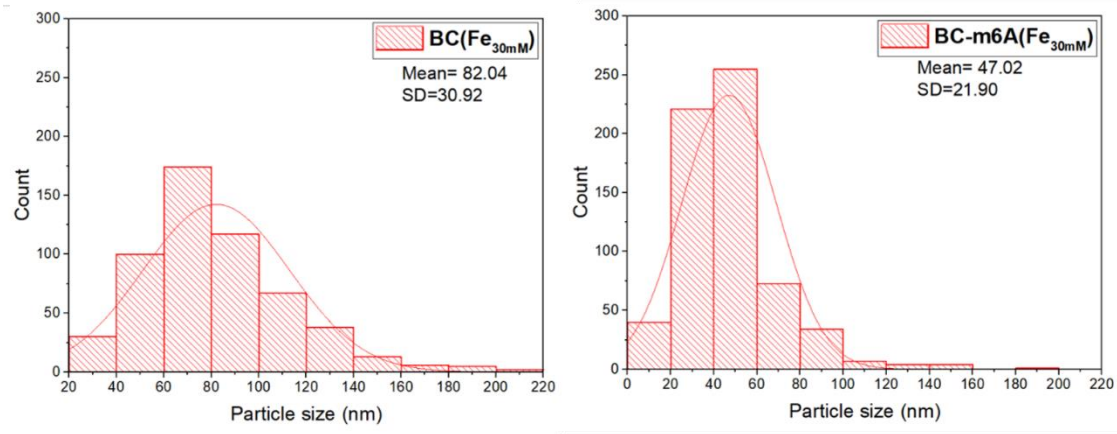

Figure 6.4. Size distribution of magnetite nanoparticles in BC and BC-m6A membranes. Particle size measured using Image J software and plotted using Origin software.

6.3.3 Crystal orientation of magnetic cellulose membranes

Table 6.1 The crystallinity index and d-spacing of BC and magnetic cellulose membranes.

Sample	Crystallinity (%)	d-spacing (Å)
BC	99.75 ± 0.31	3.80 ± 0.06
BC(Fe_{30mM})	98.83 ± 1.35	3.85 ± 0.02
BC-m6A(Fe_{30mM})	98.16 ± 0.14	3.91 ± 0.00

The XRD patterns of pure BC and magnetic BC membranes are shown in Figure 6.5. The pristine BC sample displayed all the characteristic crystalline phases corresponding to the three main diffraction peaks at 14.7° (1-10), 16.8° (110) and 22.7° (200) respectively[195,237]. All the characteristic Bragg peaks of Fe_3O_4 of nanoparticles were present in the functional BC membranes whereas in the BC membranes with nanoparticles, either some peaks were missing, or the intensity of the peaks was too low (Figure 6.5). The signature peaks of Fe_3O_4 was located at 2θ= 18.6º, 30.6º, 36.1º, 37.7º, 43.8º, 54.4º, 58.0º and 63.7º corresponding to (111), (220), (311), (222), (400), (422), (511) and (440) reflections of the face-centred cubic magnetite structure[285,293].

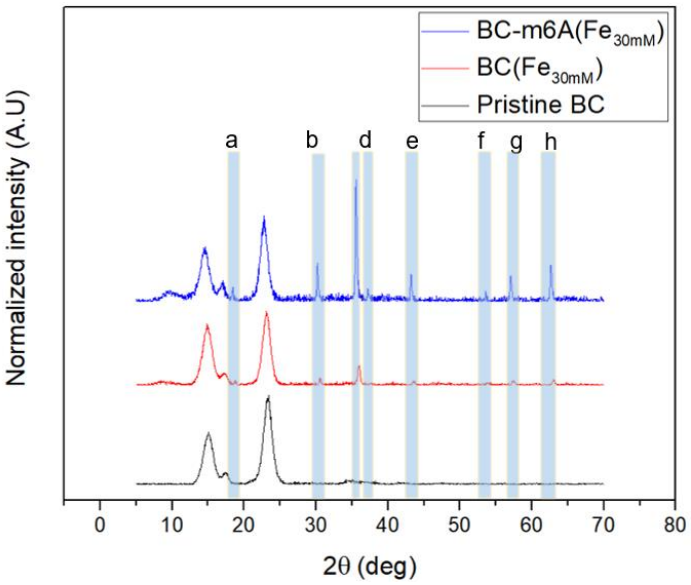

Figure 6.5 XRD diffractograms of BC and magnetic cellulose membranes indicating the presence of magnetite nanoparticles

The calculated d-spacing matched with the experimental d-spacing values obtained from the bioengineered functional membranes confirming the magnetite crystal structure (Table 6.2)[294]. There was a gradual drop in the crystalline peaks corresponding to BC with the introduction of magnetite nanoparticles in the final membranes. This could also be the result of drop in the crystallinity of the magnetic BC membranes as compared to pure BC films. The drop in crystallinity coincides with increased d-spacing for the functional magnetic membrane confirming the magnetite nanoparticle synthesis Table 6.1. This drop in crystallinity is commonly found in BC based composites due to the partial or complete disruption of the hydrogen bonds present in the BC films[295-297]. With only about 1-2 % drop in crystallinity, we were able to preserve the inherent BC structure. An advantage of the bioengineered strategy is the controlled synthesis of the magnetite nanoparticles preventing the formation of other oxide phases as compared to other *in situ* amethods[288,298].

Table 6.2 Calculated d-spacing compared to experimental d-spacing for magnetite nanoparticles present in BC and BC-m6A membranes

Database			**BC(Fe_{30mM})**	**BC-m6A(Fe_{30mM})**
2θ (deg)	d_{cal} (Å)	(hkl)	d_{exp} (Å)	d_{exp} (Å)
18.6	4.8	111	4.7	4.8
30.6	2.9	220	2.9	2.9
36.1	2.5	311	2.5	2.5
37.7	2.4	222	-	2.4
43.8	2.1	400	2.1	2.1
54.4	1.7	422	1.7	1.7
58.0	1.6	511	1.6	1.6
63.7	1.5	440	1.5	1.5

6.3.4 Direct intercalation of amyloid protein with cellulose in magnetic cellulose membranes

FTIR spectra of the magnetic membranes are presented in Figure 6.6. The FTIR spectrum of pristine BC aerogel has a broad region from 3200-3500 cm^{-1} corresponding to the -OH groups present in cellulose (-CH-OH and -CH_2-OH). The absorption bands at 1429, 1160 and 1050 cm^{-1} correspond to the H-C-H plane bending, -OH wagging vibration and C-O-C pyranose backbone ring vibration[165,249]. The FTIR spectrum of PEG coated magnetite nanoparticles contains absorption bands at 580, 870 and 1100 cm^{-1} assigned to Fe-O vibration in magnetite, C-H rocking and C-O stretch in ether groups of PEG chains respectively[295,296]. There is a small absorption band at 630 cm^{-1} for the BC membranes containing nanoparticles, represents the Fe-O bond vibrations

found in maghemite, caused due to the partial oxidation of magnetite[299]. The IR spectra of the BC-m6A membrane attributed for all the signature peaks of BC and the functional domain as indicated in the Figure 6.6. The broad hydroxyl group of pure BC was at 3446 cm^{-1} whereas we notice a shift in the hydroxyl peak of BC films deposited with magnetite nanoparticles, with the peak positioned at 3404 cm^{-1} instead (Figure S7). The shift was because of the interaction of Fe^{2+} precursor with the hydroxyl groups of cellulose due to electrical dipole bonding. The OH groups present in cellulose behave as anchoring sites for the iron precursors to deposit and also creates regions where the nanoparticles form clusters. However, we notice a very small shift in the hydroxyl peak for BC-m6A membranes, 3444 cm^{-1}. The presence of m6A functional domains prevented aggregation of the iron ions and controlled the synthesis of nanoparticles on the cellulose matrix and homogeneous distribution of the same. Hence, *in situ* precipitation methods can lead to the electrostatic interaction of the iron precursors with -OH groups of cellulose, causing the agglomeration of the nanoparticles[157,296], but this can be avoided with our bioengineered approach.

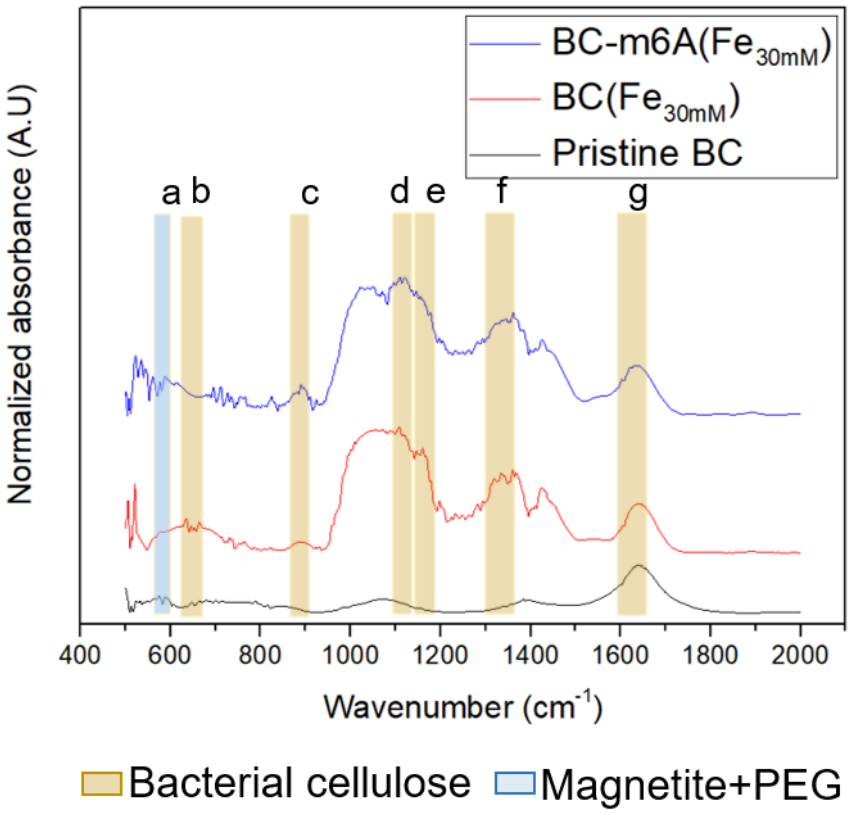

Figure 6.6 The IR spectra obtained for BC and various magnetic membranes

6.3.5 Surface chemistry of magnetic cellulose membranes

XPS was used to analyse the surface chemistry of the magnetic membranes. Table 6.3 shows the atomic compositions of the various conductive aerogels. The atomic concentrations of oxygen and iron increased with increasing nanoparticle concentration.

Table 6.3 The atomic composition of BC and magnetic BC membranes

Atom (%)	**Pristine BC**	**BC(Fe_{30mM})**	**BC-m6A(Fe_{30mM})**
Carbon	65.93 ± 2.56	64.85 ± 1.64	57.65 ± 1.34
Oxygen	34.00 ± 2.66	33.62 ± 1.36	36.31 ± 0.70
Iron		1.52 ± 0.69	6.04 ± 0.68

The C1s and O1s core-level spectra of pristine BC and the C1s, O1s and Fe2p core-level spectra of the magnetic membranes are shown in Figure 6.7. The C1s core-level of BC comprised of three peaks by deconvolution, C1 at 284 eV, C2 at 285.6 eV and C3 at 287.2 eV assigned to non-functionalized carbon (C-C, C-H), carbon linked to oxygen atom by a simple bond (C-O) and carbon linked to two oxygen atoms by a simple bond (O-C-O) respectively. Similarly, the O1s core-level of BC is resolved to two peaks, O1 at 531.7 eV and O2 at 532.6 eV assigned to the hydroxyl groups in cellulose (-OH) and oxygen linked to a carbon by a simple bond (O-C) respectively[253,254].

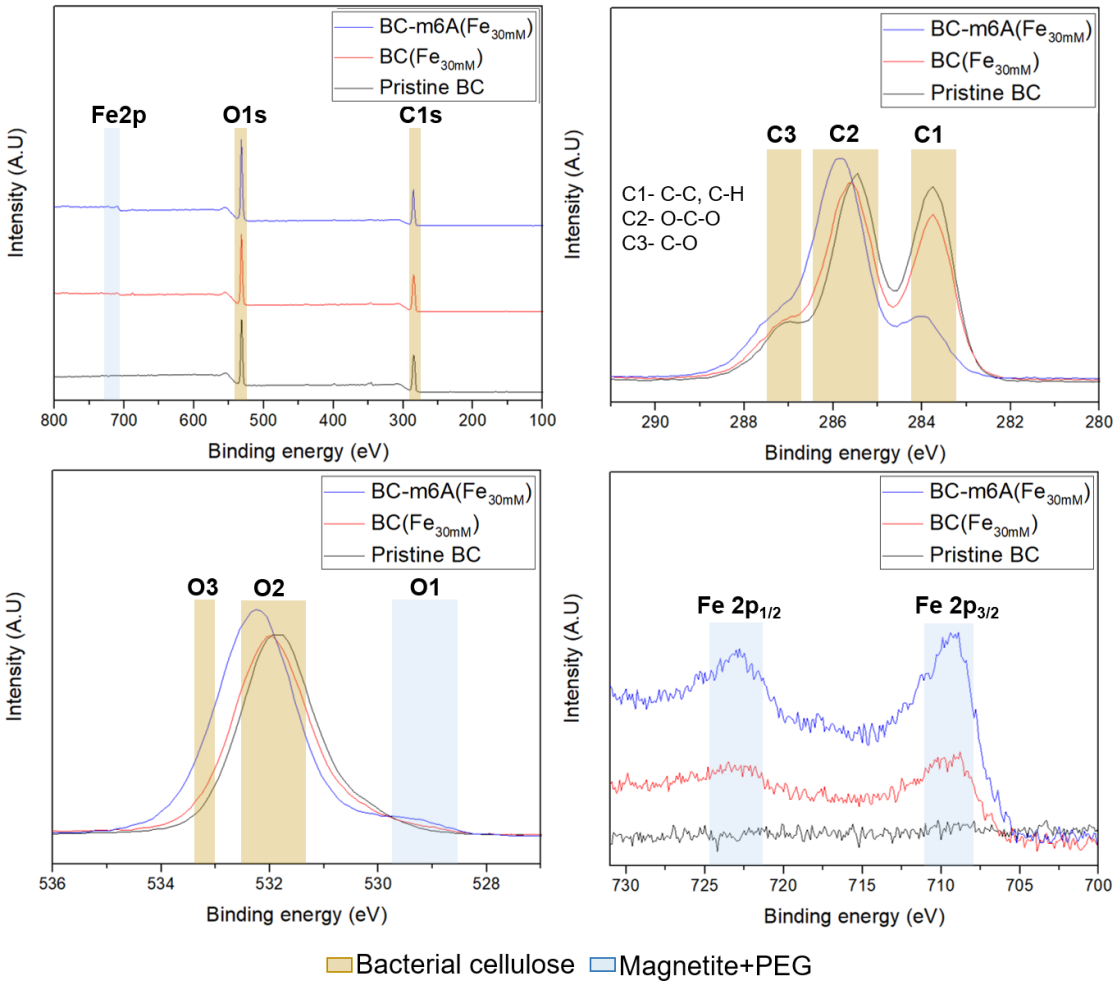

Figure 6.7 XPS spectra of magnetic BC membranes with a) survey scan, b) C 1s scan, c) O 1s scan, d) Fe 2p

The Fe2p peaks are located at the same binding energy as the normal BC membranes deposited with nanoparticles, but in higher intensity. We also, do not observe any satellite peak at 718 eV characteristic of maghemite. The $Fe2p_{3/2}$ was deconvoluted for the magnetic membranes to obtain the Fe^{2+} and Fe^{3+} peaks, and their respective areas were calculated. The stoichiometric ratio for Fe_3O_4 is represented as 0.33:0.67 $(Fe^{2+}:Fe^{3+})^{300}$. The results obtained for BC and BC-m6A membranes are 0.11:0.89 and 0.27:0.73 respectively (Table 6.4). The stoichiometric ratio obtained for BC-m6A membranes is close to the theoretical ratio of magnetite nanoparticles.

Table 6.4 The experimental stoichiometric ratio of Fe^{2+} and Fe^{3+} series for magnetic BC and magnetic BC-m6A membranes

Sample	Binding energy (eV)	Fe^{2+} Area (%)	Binding energy (eV)	Fe^{3+} Area (%)
BC(Fe_{30mM})	710.7	17.6	713.1	19.6
BC-m6A(Fe_{30mM})	710.7	25.7	713.1	35.2

6.3.6 Thermal stability and degradation profile of magnetic cellulose membranes

Thermal stability and thermal decomposition of the hybrid aerogels was analysed with TGA. The TG curves obtained can be distinctively divided into two stages. During the initial stage, a small weight loss at 50-100 °C for pure BC as well as magnetic BC magnetic membranes occur due to the presence of moisture which makes up about 14-16 wt.% approximately. The second stage involves a sharp weight loss from 320-380 °C caused due to a sequence of reactions, starting with degradation of BC including decomposition, dehydration and depolymerization of glucan chains. During these reactions, CH_2-OH and -OH groups are thought to be removed[285]. The main decomposition temperature ranges for magnetic membranes occur between 240-400 °C and 400-700 °C earlier than that of pure BC. The onset of degradation at 240 °C in magnetic membranes corresponds to the desorption and evaporation of the PEG coating with loss of 30-40 wt.%. As combustion of PEG takes place, a transformation of magnetite to maghemite is observed, but it is masked by the significant degradation of PEG molecules as seen in the DTG curves (Figure 6.8). The third weight loss is due to the transformation of maghemite to hematite as observed by the DTG at higher temperatures (Figure 6.8)[295,301].

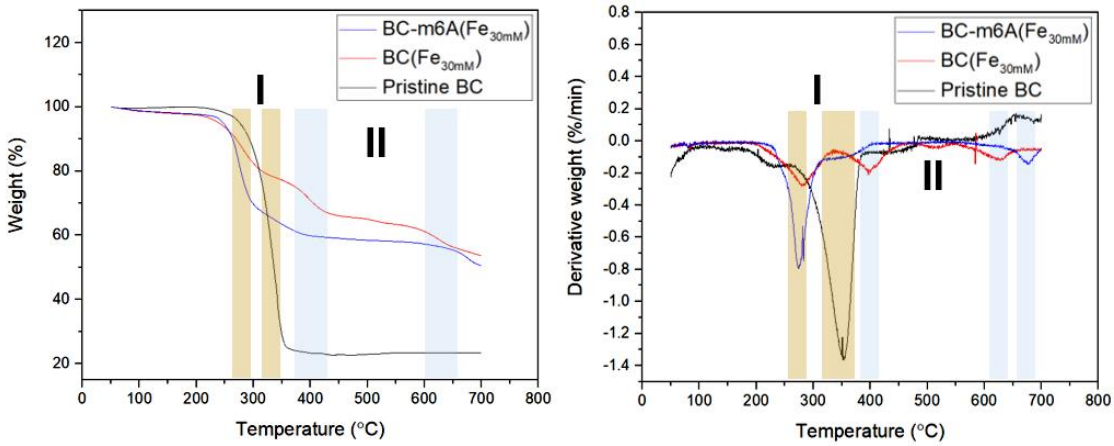

Figure 6.8 (Left) TGA curve of BC and magnetic cellulose membranes (right) DTG curves highlighting the degradation temperatures.

The first derivative (DTG) curves showed two distinct peaks at 240 °C and 360 °C that confirm the thermal degradation observed in pure BC and magnetic membranes. The two sharp endothermic peaks correspond to the degradation of the crystalline regions present pure BC and the transformation of iron oxides during combustion process.

6.3.7 Magnetic behavior of cellulose membranes

Magnetic M *versus* H curves at room temperature was measured for all the membranes (Figure 6.9). As expected, the pristine BC film did not demonstrate any magnetic behaviour. With the incorporation of magnetite nanoparticles both the magnetic membranes displayed superparamagnetic behaviour. Superparamagnetic behaviour is characterized by the lack of hysteresis loop and low/no coercivity. The saturation magnetization (M_s) of BC-m6A was four times greater than BC films deposited with nanoparticles. The high M_s of 40 $emug^{-1}$ was due to the higher concentration of magnetite nanoparticles homogeneously dispersed across the matrix, as observed in FESEM. The M_s of ferrofluids is between 60-70 $emug^{-1}$. The drop in M_s corresponds to nanoparticle size and surface modification methods, in this case PEG molecules used as surfactants. The Ms values obtained in this study for BC-m6A membranes was considerably higher than other research work[293,297,302,303]. Only two other research studies have reported higher M_s values than the current work, 60 emu/g[295] and 50 emu/g[285], but both the works have incorporated a large concentration of

nanoparticles into cellulose matrix to the extent of complete drop in intensities of the characteristic cellulose crystalline phases. Such a high concentration could render the functional material mechanically unstable, due to low crystallinity. The functional magnetic membrane developed from the bioengineered approach did not compromise the structural architecture of the cellulose network.

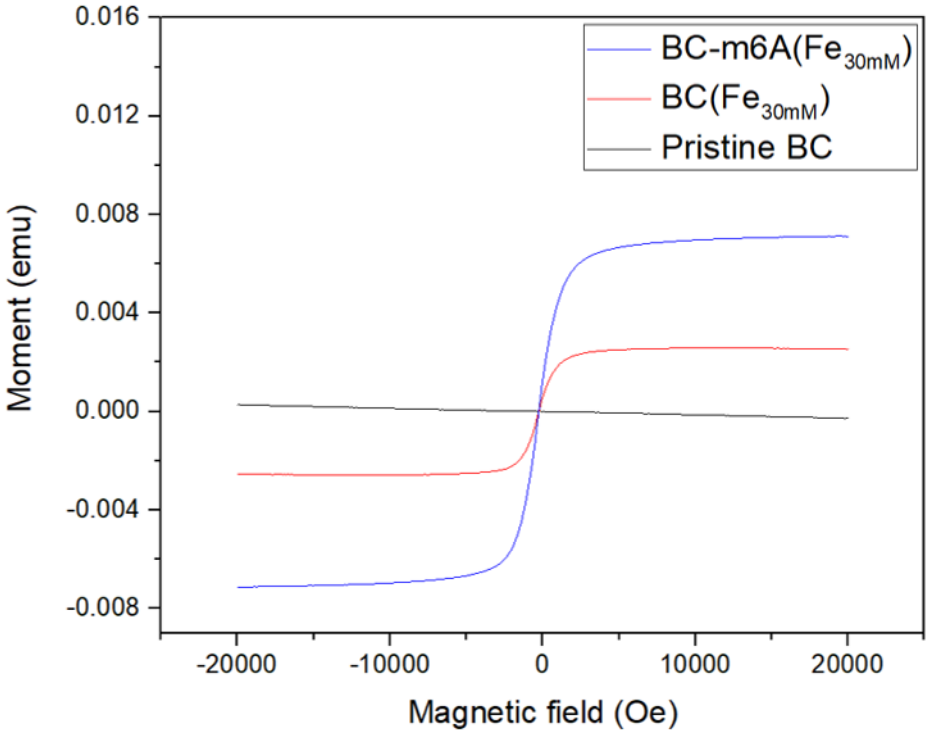

Figure 6.9 VSM measurements of magnetic BC and magnetic BC-m6A membranes

6.3.8 Cell viability in the presence of magnetic cellulose membranes

Findings have shown bacterial cellulose to demonstrate biocompatibility when either used as a scaffold or as an implanted material[146,147,266]. Assessment of cell proliferation of magnetite nanoparticles alone or when doped in combination with other materials confirmed the cytocompatibility of the magnetite and their potential in biomedicine[304,305]. Likewise, bioengineered magnetic cellulose membranes designed in this study were evaluated for cytocompatibility in the presence of human dermal fibroblasts (HDFa) cells (Figure 6.10). Our results reveal that over the course of 7 days of incubation, the cell viability of functional magnetic membranes was comparable to the control group as observed in other studies[306-310]. As expected, cellulose films alone

did enhance proliferation of cells, due to its morphological, chemical, and biocompatible properties[145,310,311]. The presence of PEG coating on magnetite nanoparticles assisted in cell proliferation in the magnetic membranes as observed in similar works[296,312,313]. The functional magnetic membranes exhibited cytocompatibility and hence, were put to test in a simulated wound healing application test.

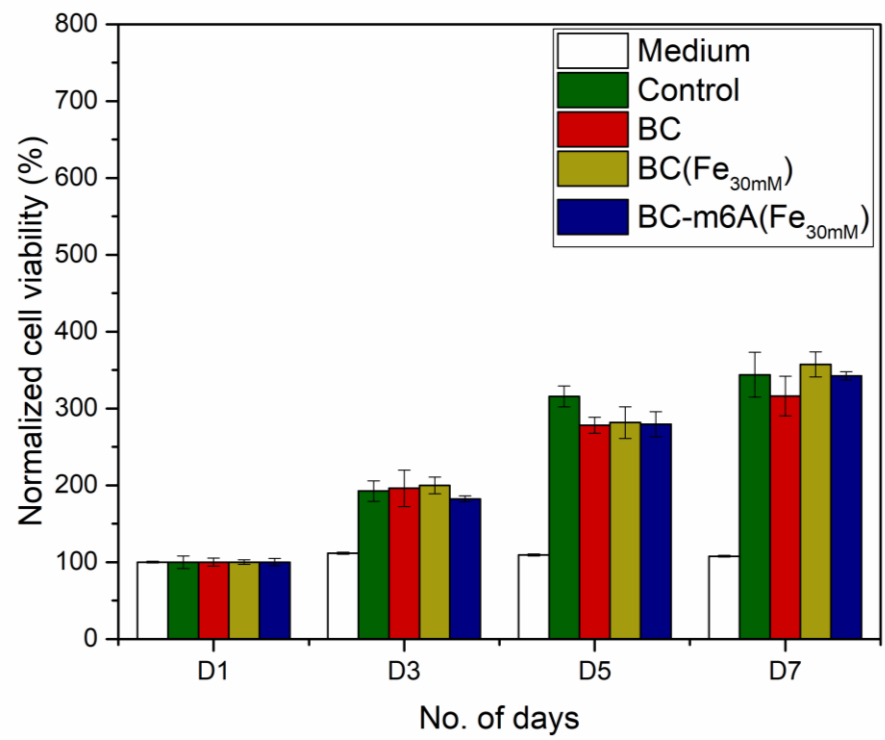

Figure 6.10 Resazurin cell viability assay of various cellulose based membranes in the presence of HDFa cells

6.3.9 Scratch test for simulated wound healing

Wound healing is a complex cellular response process. It involves the activation of a number of cells responsible for wound closure. Fibroblast cells are involved in the repair of structure and function at the wound site. Hence, functional bioactive materials that can accelerate fibroblast growth and migration can improve wound healing rate[314]. Results from the scratch test assay are given below (Figure 6.11 and Figure 6.13 and Figure 6.13). Scratch test assay was conducted to test the migration and proliferation capacity of the fibroblast cells in the presence of the functional magnetic membranes. We also tested if the application of static magnetic field stimulated the cells for enhanced migration.

The fibroblast cells migration was captured using the light microscope attached to a camera, and the distance was measured at 0, 24, 36 and 48 hrs after the scratch was created in the presence and absence of static magnetic field (10 mT).

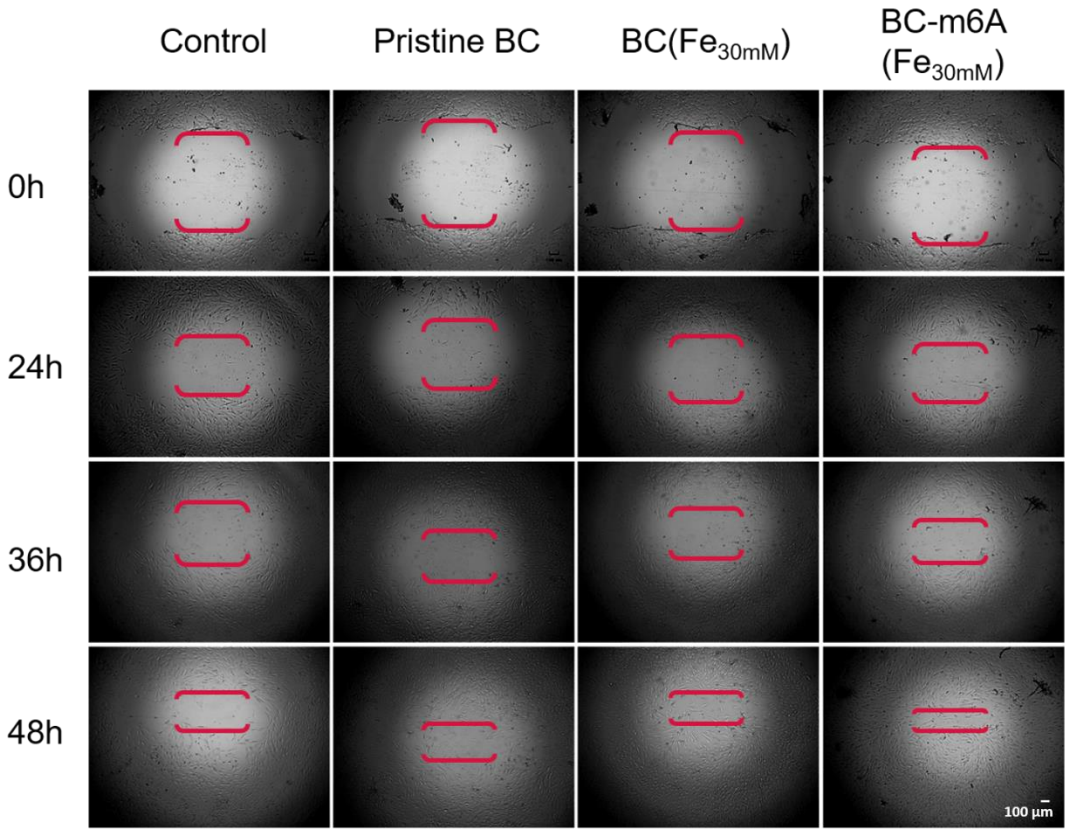

Figure 6.11 Simulated wound healing via scratch test in the presence of various cellulose membranes and absence of magnetic field (*Scale bar: 100 µm*)

About 1 mm wide scratch was created and the effect of various membranes was analysed. The migration of HDFa cells was significant in the presence of functional magnetic membranes compared to the other sets in the absence of a static magnetic field (Figure 6.11). We observed a 30% improvement in cell migration for functional BC membranes compared to the control group (Figure 6.12). The magnetite nanoparticles present in the functional BC, exhibit superparamagnetic behaviour as seen in Figure 6.9. Each nanoparticle in the absence of any magnetic field behave as single magnetic domains that provide cues to the cells for enhanced adhesion, migration, and proliferation. In addition to magnetic properties, the incorporation of nanoparticles into the matrix can change the surface roughness and stiffness of the scaffold[315]. The cellular

behaviour is clearly influenced by these mechanical signals induced by the presence of magnetite nanoparticles, as discussed in other literature[316,317].

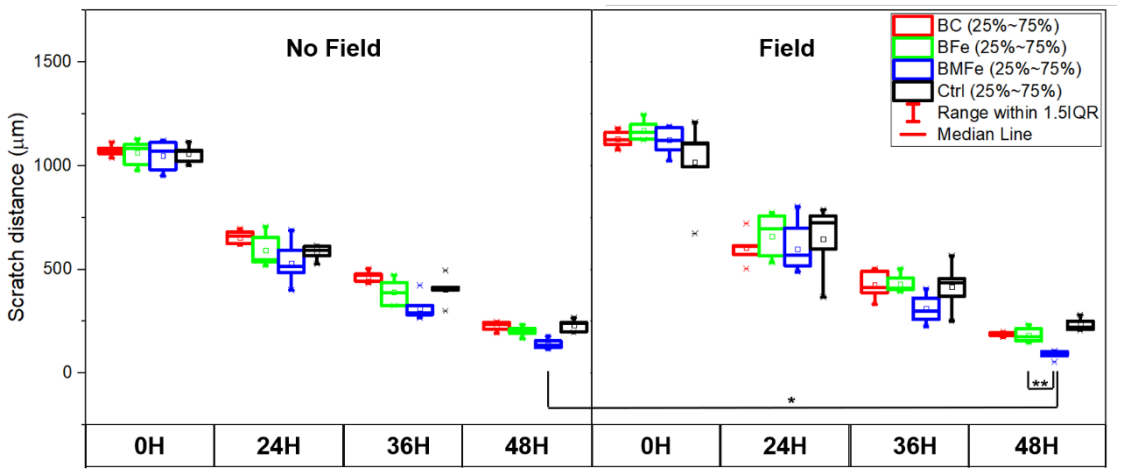

Figure 6.12 Wound width at different time points in the presence and absence of 10 mT magnetic field (*p < 0.01 and **p < 0.004) (BC- Bacterial cellulose, BFe- BC(Fe_{30mM}) BMFe- BC-m6A(Fe_{30mM}) and Ctrl- HDFa cells)

In the presence of a 10 mT static magnetic field, there is an obvious improvement in cell migration post 48 hrs of incubation (Figure 6.13). The control group did not improve much even in the presence of magnetic field due do the direct effect of magnetic field on the cellular activity in the absence of magnetite nanoparticles (Figure 6.12)[315]. With the incorporation of magnetite nanoparticles and stimulation of cells with magnetic field, we improved cell migration by 44% for the same bioengineered functional membranes (Figure 6.12).

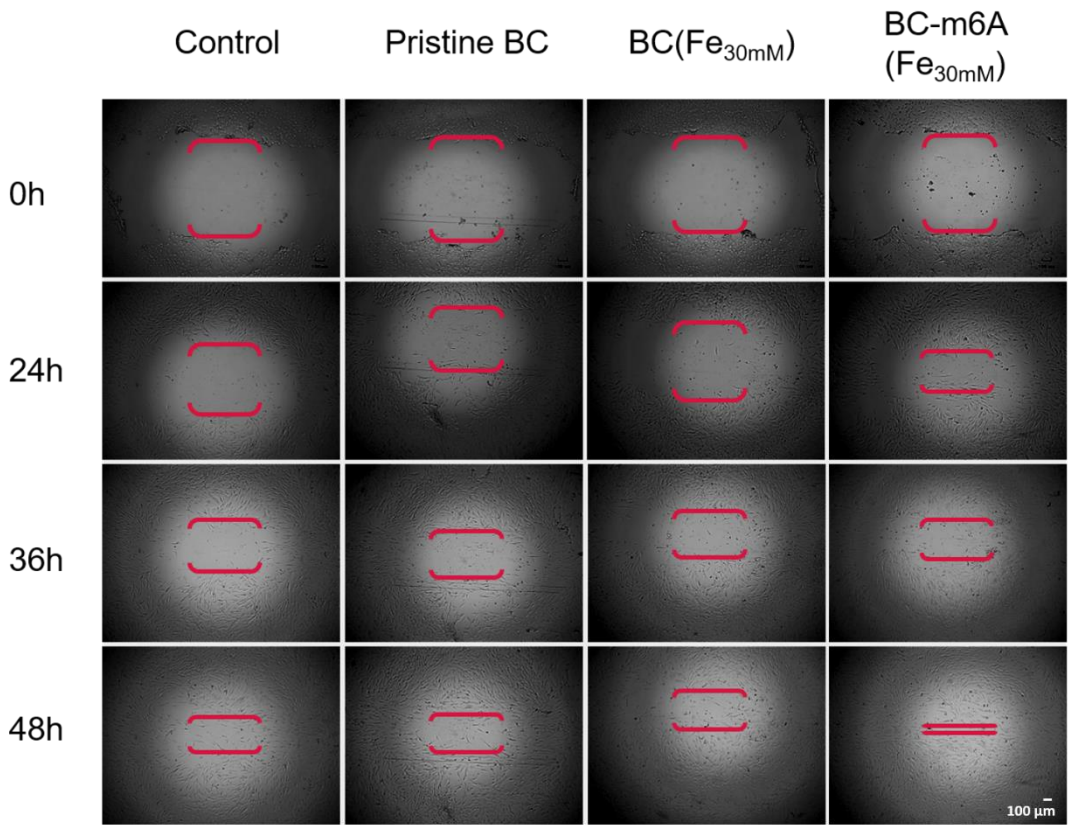

Figure 6.13 Simulated wound healing via scratch test in the presence of various cellulose membranes and presence of 10 mT static magnetic field

Direct magnetic actuation can deliver controlled forces that assist in regulation of the different cellular functions[304]. In this way, with the help of the magnetically responsive bio engineered membranes, we were able to direct the cell migration to the scratch zone efficiently[318]. Application of magnetic field in the presence of nanoparticle incorporated bioengineered membranes improved wound healing by 61% when compared to the control group in the absence of magnetic field[319,320]. Hence, with the help of magnetic responsive materials we can provide local mechanical stimuli that can amplify the cellular functions for enhanced wound healing[321].

6.4 Conclusion

The biological approach employed in this study is synonymous to a bottom up approach wherein, the bacteria are responsible for providing the base matrix as well as incorporating functionality to the matrix. The bioengineered functional cellulose membranes are comprised of bacterial cellulose and amyloid fusion protein CsgA

genetically tagged with m6A peptide domain. The resulting BC scaffold network maintained its ability to trap recombinant *E. coli* bacteria within its matrix. This supports the uniform intercalation of the amyloid protein with BC nanofibers, as not observed in previous cellulose composite design approaches. The m6A peptide domains added functionality to the cellulose matrix without any harsh chemical or mechanical processes.

BC-m6A membrane displayed intense black colour post magnetite synthesis suggesting a high density of Fe_3O_4 nanoparticles in the matrix. FESEM helped confirmed the high density of nanoparticles across the matrix. The presence of m6A peptides helped control the size of nanoparticles being synthesised. Chemical incorporation of Fe_3O_4 was confirmed by the absorption band of Fe-O for the BC-m6A membrane. XPS validated the interaction of the cellulose matrix with the magnetic nanoparticles due to the chemical shift in the binding energy of carbon and oxygen atoms core-levels. Likewise, the preferential orientation of the (200) plane was shifted left with the introduction of the nanoparticles in the matrix. The introduction of Fe_3O_4 nanoparticles in the BC matrix caused a gradual drop in crystallinity and change in d-spacing. The BC-m6A were found to be thermally stable at 200 °C. VSM measurements indicated significantly high saturation magnetization of 40 $emug^{-1}$ for BC-m6A membrane, four times higher than normal *ex situ* BC doping. The magnetic membranes were evaluated for their cytocompatibility in the presence of HDFS cells, BC-m6A membrane was comparable to the control group. With 72 h of incubation, BC-m6A membrane did not inhibit cell proliferation and the cells were viable. The BC-m6A membrane displayed exceptional wound healing capabilities in the presence of the magnetic field. The membrane improved wound healing by 61% for a given time. The BC-m6A membrane was intrinsically crystalline, cytocompatible and exhibited high saturation magnetization, suggesting these functional membranes are potential substrates for biomedical applications.

In the present situation of energy crises, there is pressing need for sustainable development, clean and green solutions to meet the energy demands. The membrane developed in this study requires very few chemicals, demonstrates its importance as a key to sustainability and an environmentally friendly material, highlighting its potential in a myriad of practical applications.

Chapter 7

Conclusion and Future work

7.1 Conclusion

BC research has led to important advancement in recent years with the potential of even greater achievements yet to come.

In this thesis, we focussed on developing tools to understand the organism better, optimization of culture conditions for improved cellulose production and structural modification of the exopolysaccharide. With the surface growth platform, we were able to able to appreciate the biologics of the organism and the influence of environmental factors on the organism for cellulose production. Three wild-type bacterial strains were considered for the study and we observed good correlation between our swim-plate platform results and static culture experiments. With the help of this analytical platform we can further understand the behaviour of the bacteria under controlled environmental conditions and its effect on cellulose production. Similarly, the platform can be employed to test the environmental conditions for cellulose production at small scale before translating to bioreactors for scale-up production. The platform does possess certain limitations in its applicability. Vessel dimensions have been found to be important for BC production, the platform cannot employ this factor in screening. Similarly, dissolved oxygen detection is a challenge using this platform. A variation of the platform has to be further developed to overcome the limitations stated above.

The formation and assembly of cellulose chains extruded by the bacteria was interrupted with the introduction of different molecules. Various substituted glucose molecules were deliberately chosen to interfere with the hydrogen bonds, and the interruption was found to be successful as observed through X-ray diffractograms and NMR. XRD analysis clearly showed the effect of substituted groups on crystal plane arrangement as D-glucose concentration is reduced. For the last series, with the absence of D-glucose a broad peak was observed for all the three substrates, indicating the presence of functional groups. The d-spacing values calculated based on the peak

position of (002) plane clearly increased with the absence of D-glucose. ^{1}H NMR confirmed that the bacteria possess an enzyme complex capable of detecting broad range of molecules and produce modified cellulose with the presence of functional groups incorporated in the polyglucan chains. Through this study we can control and alter the structure of the polymer for display of various desired properties as per the applications needs. With the preliminary results there were indications of a co-polymer hybrid material, but further characterisations required to further understand the process of polymerisation and crystallization. The limitations of this work was the inability to calculate the distribution of the substituted glucose monomers across the backbone polyglucan chain.

BC based functional materials have become an important part of cellulose research. These materials impart new features to BC, besides improving on the prevailing properties. Properties such as purifying, antimicrobial, biocompatibility, separating, biosensing, conducting and many other application-directed properties have been introduced into BC composites. BC-PEDOT:PSS aerogels obtained through an environment friendly synthetic approach, displayed good intercalation between cellulose layers and PEDOT:PSS polymer through FESEM. With increasing concentration of polymer, the surface morphology became compact with the disappearance of pores. X-ray diffractograms confirmed the presence of polymer with increasing concentration due to peak shift of the (002) plane. Four-probe resistivity measurements reported high conductivity values of 0.7 S/cm for BC-PEDOT:PSS aerogels, characteristic of good semiconductor materials. Though we were able to achieve good conductivity values when compared to previous literature, the mechanical properties of BC was compromised. Due to the process of disintegration by acoustic cavitation, the inherent hydrogen bonds present in BC were broken irreversibly contributing to low mechanical strength and thereby, limiting its applicability. Also, the practical application of the aerogels could have been evaluated in a real-time analysis.

Bioinspired magnetic cellulose membranes developed in the thesis is the first of its kind. The membranes were developed without the use of any chemicals or mechanical treatments. Bacteria were employed to functionalize bacterial cellulose matrix. It displayed very high saturation magnetization of 40 $emug^{-1}$ through the VSM measurement. The membranes were found to be cytocompatible and aided in accelerated

wound closure in the presence of the magnetic field. The magnetite nanoparticles were found to be integrated well into the BC matrix without altering the structural integrity through XPS and XRD analysis. By overcoming the limitation mentioned in the previous chapter without compromising the structural integrity of the BC film, functional materials were developed. Though, the films displayed good functionality, distribution of the functional display is not controlled. Further process optimisation required to have a controlled functional display across the BC membrane. The applicability of the films could have been tested against certain primary cell lines for its use as wound dressing material in the future.

In summary, the goals set out while venturing into this research work have been met with noteworthy results and insights. From culturing the bacteria using novel platform strategies to obtaining materials with superior properties was achieved in due course. The different aims of this study assisted towards the understanding of culture conditions for a strain, to manipulate the process of exopolymer formation and assembly, and production of new bacterial cellulose-based materials with desirable properties for niche applications. The design approach and types of dopant materials used provide insight into the future progress of BC based functional materials for biomedical applications.

7.2 Future work

The role of cellulose synthase enzyme could be explored further to understand the process of BC production. The overexpression of each subunit and its effect on BC production and structural formation can be investigated (Figure 7.1). A platform could be developed for a quick screening of the cellulose producing mutants to assess the effect of subunit overexpression. This screening strategy could lead to the identification of both modified and non-modified cellulose producing strains with efficient cellulose producing capability.

Cellulose mutants overexpressing subunits individually and in combinations can be generated using Gibson DNA assembly methods. The subunit overexpression can be confirmed by purifying the membrane fractions of the bacterial cells and assessing the protein composition using SDS-PAGE analysis and mass spectrometric techniques.

Upon confirmation of the over-expression of the subunits, the engineered stains can be subjected to a platform screening.

The platform screening would miniaturize the culture environment of a regularly grown bacterial strains of 10 ml or larger reactions to a 96-well plate assay. Thus, allowing short growth periods and quick substrate utilization hence reducing the time required for realizing full cellulose producing potential. This screening platform could help screen through all the single subunit mutants and subunits expressed in combinations. The amount of cellulose produced could be assessed by using fluorescent dyes that bind to cellulose such as congo red and calcofluor. This also eliminates the additional steps required to purify, dry and weigh the cellulose obtained. To standardize the platform however, the congo red dye could be used to measure cellulose production fluorometrically and the values could be correlated to the dry weight of cellulose. The growth of the bacteria can be monitored using optical density measurements or redox indicator dyes such as resazurin could be used to monitor bacterial growth with the help of fluorescence output proportional to the growth of cells. Serial dilutions of bacterial cells grown on petri plates to obtain colony forming units can be compared to the fluorescence values obtained in plate assay for standardization.

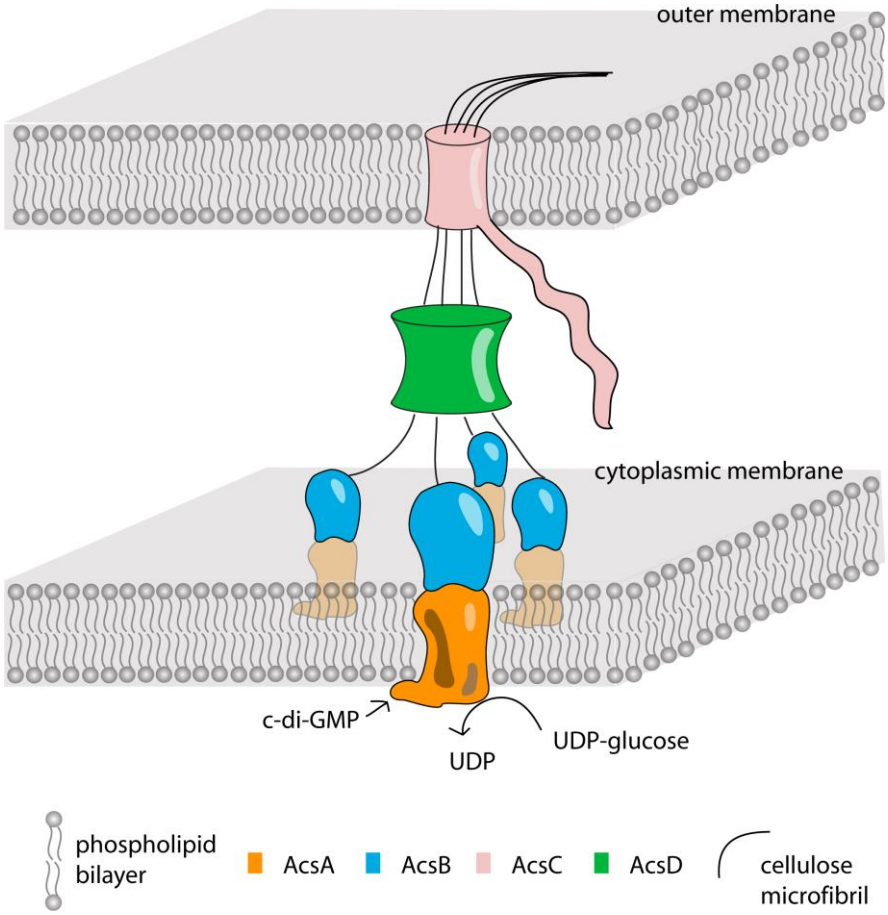

Figure 7.1 Schematic representation of cellulose synthase sub-units in *G. hansenii*. Reprinted with permission from [322], © 2016, PLoS One.

The BC based functional materials developed in this thesis could be further explored to cater to applications in biomedical field. The conductive aerogels can be used to design wearable electronics with responsive circuits for healthcare monitoring. The inherent mechanical property of BC combined with its conductive behavior can replace the conventional stiff and brittle materials used for developing such wearables. For the next phase of progress, the conductive aerogels developed can be used as substrates to design flexible electronic circuits. Materials that retain their electrical conductivity when subjected to bending and elastic stretching have gained huge attention in recent times for flexible electronics. The conductive BC developed in this work could further be analyzed for its ability to retain its conductivity upon multiple stretch and bend cycles. The desirable outcome would be no increase in resistance post bending and stretching. BC:PEDOT/PSS composites could be subjected to repeated cycles of

stretching and bending and analyzed for any differences in their conductive behavior which could be easily measured by 4 probe analyzers.

The magnetic membranes developed in this work showed good potential as wound healing materials in the presence of a magnetic field. Further investigations into the alignment of cells in the presence of the magnetic membrane and field are imperative to understand the process of wound healing and scar formation. The underlying mechanism of this observation would be interesting to probe for the response of various cell lines in the presence of the material and field. This will shed some light for the further development of the material in medical applications.

Bioinspired design strategies can be employed to develop novel nanophotonic materials. Bioinspired nanophotonic are derived from the biophotonics field, where organic-inorganic complexes represent the functions of the natural living systems[323,324]. Optical materials and devices possess certain important optical properties via efficient control of light through reflection, absorption, scattering, interference, diffraction, transmission (bulk material transparency) and in combinations of these properties[325]. Routine and extensive use of conventional plastic polymers such as polypropylene (PP), polyethylene (PE) and polyethylene terephthalate (PET) have caused serious environmental issues. These polymers have been used to fabricate optical devices, but possess poor thermal stability, high coefficient of thermal expansion. Other materials such as glass and poly (methyl methacrylate) have excellent optical clarity, good processability but low strength and storage modulus[323,324,326]. We can replace the conventional materials with bacterial cellulose for the fabrication of optical devices from renewable sources[327]. The functional cellulose materials can be developed through sustainable approach keeping in mind the current environmental and economic crisis[328]. Newer synthetic routes with less energy intensive and less chemical oriented, and more biomass derived materials (Figure 7.2) for the development bioinspired optics.

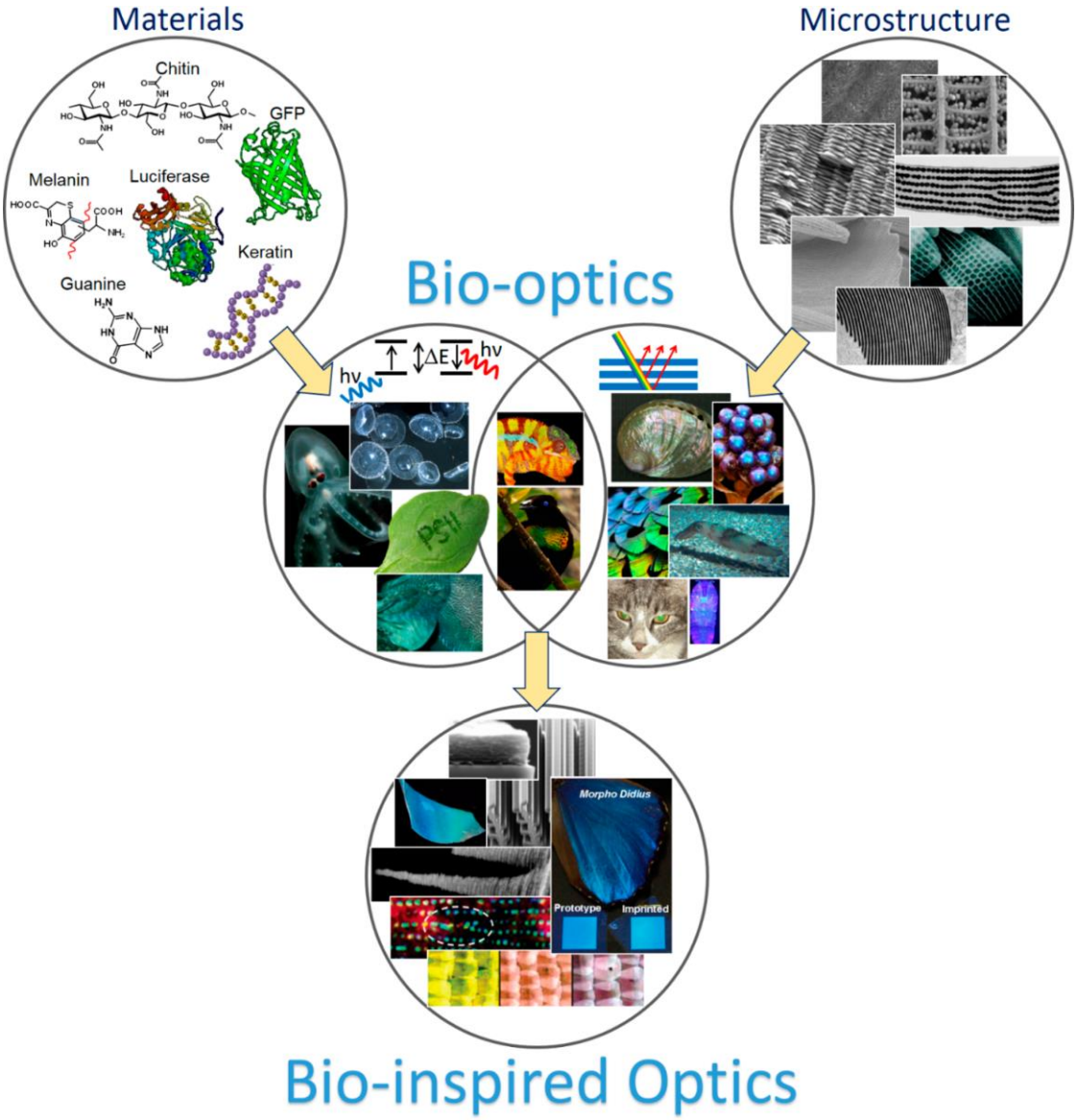

Figure 7.2 Schematic showing the process of biomimicry in optical materials: material-structure-function relationship and bioinspired materials. Reprinted with permission from 307,© 2017, American Chemical Society

Variations of the design strategy mentioned in Chapter 5, can be employed to BC network to develop novel nanophotonic devices. Co-culture of cellulose producing *Gluconacetobacter* bacteria with recombinant *E. coli* bacteria can produce a novel hybrid of polysaccharide-protein complex with functional displays. The live functional membrane will incorporate both living systems with inorganic compounds to design materials with various functionalities. The design strategy can be further explored by simplifying the culturing conditions for the two bacteria and co-culturing them together in the same nutrition medium. *E. coli* being more robust in terms of nutrient requirement

can be tuned to grow slowly in modified medium more favorable for the growth of *G. xylinus* hence increasing the specific growth of the cellulose producing bacteria that can make the polysaccharide scaffold. Lowering the growth of *E. coli* helps produce the recombinant protein being expressed in it at a slower rate for its incorporation into the extending polysaccharide scaffold. The development of this bacterial consortium can greatly reduce cost, time and resources used to produce the functional cellulose membranes.

G. xylinus bacteria can provide the scaffold for the membrane design and help in entrapping recombinant *E. coli* bacteria. The recombinant *E. coli* bacteria contain the genetic circuit tuned to produce extracellular amyloid proteins, CsgA with specific metal-chelating peptides[329,330]. The cellulose-csgA integrated display can behave as a template for future molecular programming of the bacterial extracellular matrix material by genetically cloning metal chelating peptides to the domains of the amyloid protein CsgA. The living functional membrane can be placed in metal salt solutions to produce metallo-organic complexes for various optical applications. This inorganic nanoparticle templating can provide the membrane with excellent optical properties. This functional material may find application as a bioinspired optical display membrane, wearable circuits, catalytic films or as semiconductor devices.

Appendix

I. Supplementary Information

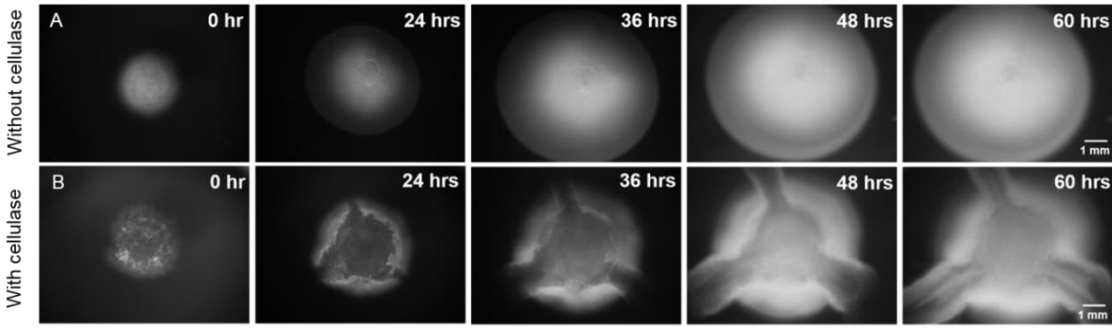

Figure S1. Typical growth patterns of G. xylinus 700178 bacteria grown in the absence (A) and in the presence (B) of cellulase at different time points during incubation.

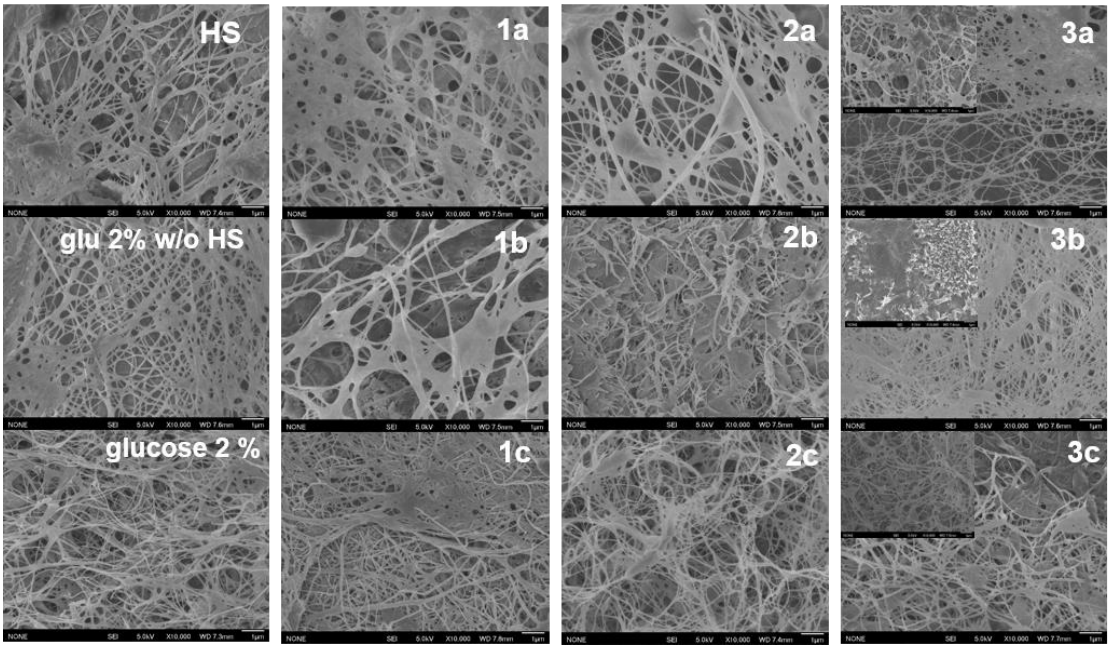

Figure S2. SEM images of different cellulose samples produced by G. hansenii 53582 from different glucose analogs; (inset- all 3-series samples show the formation of short fibres in the cellulose network)

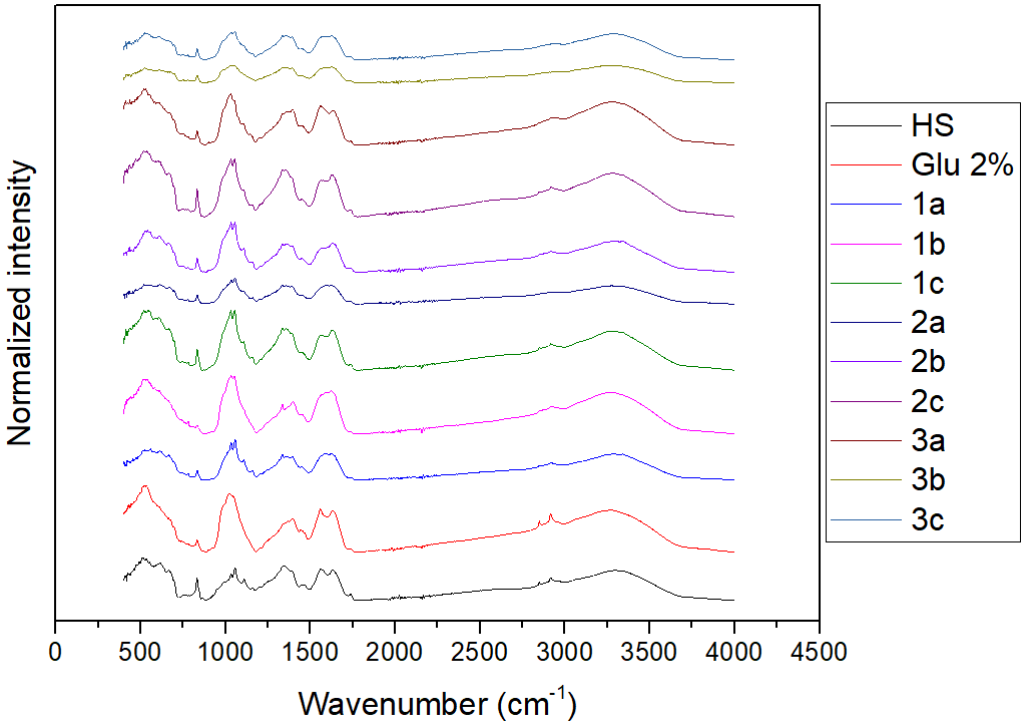

Figure S3. IR spectra of cellulose films obtained from various substituted glucose substrate

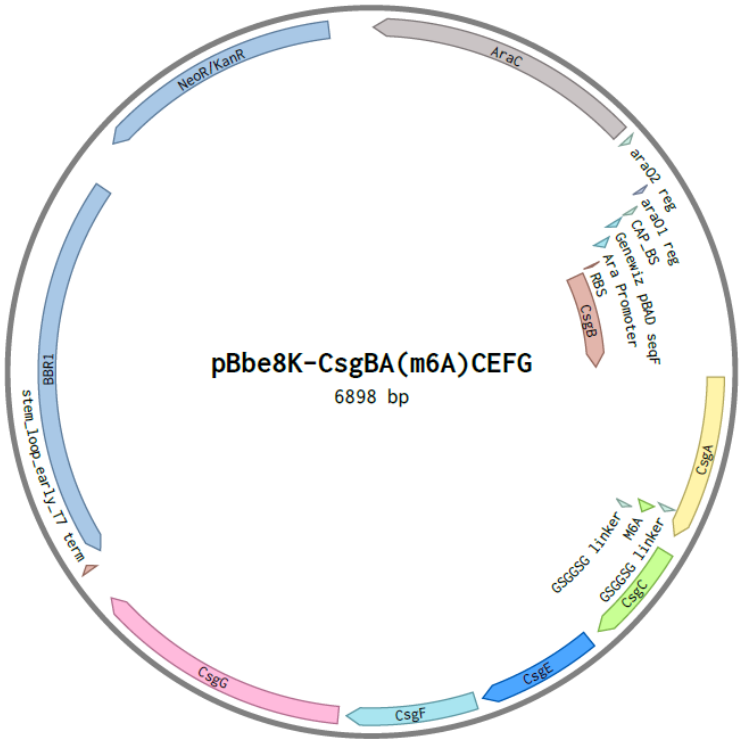

Figure S4. Plasmid map of pBbe8k plasmid containing curli forming subunits. M6A peptide with GSGGSG linker has been fused to the C-terminus of csgA subunit.

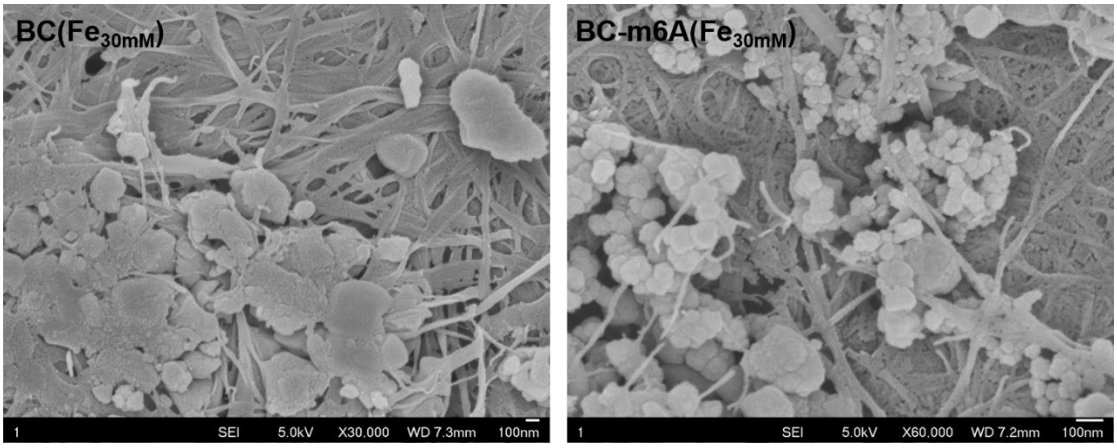

Figure S5. Structural morphology of cellulose films coated with uncapped magnetite nanoparticles

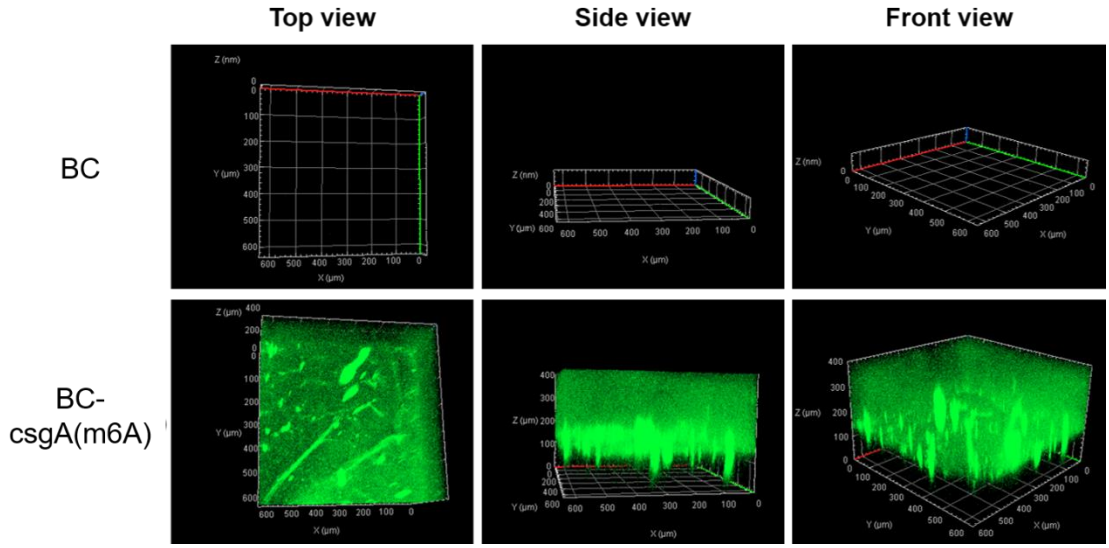

Figure S6. Green fluorescence confirming the presence of csgA(m6A) fusion protein in the cellulose matrix with amyloid protein-specific curcumin dye.

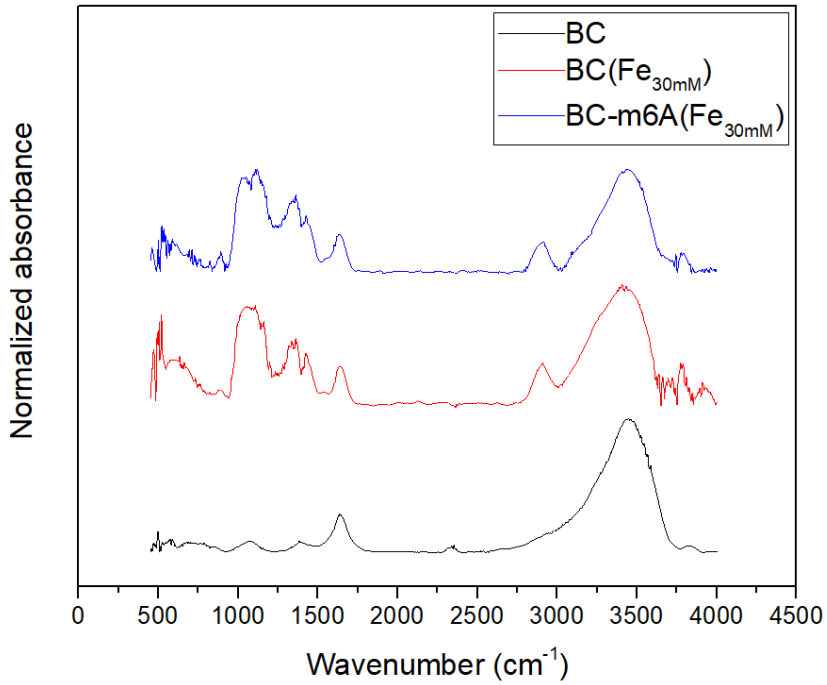

Figure S7. IR spectra of cellulose films coated with magnetite nanoparticles

Table S1. Four-probe conductivity values of various BC-PEDOT/PSS composites.

Sample	Sheet resistance (Ω/□)	Conductivity (S/cm)
BC	Out of range	
BC-PEDOT:PSS low	94.5 ± 21.6	0.7 ± 0.2
BC-PEDOT:PSS medium	113.9 ± 40.4	0.6 ± 0.2
BC-PEDOT:PSS high	141.4 ± 18.4	0.5 ± 0.1
Bare PEDOT/PSS	166.6 ± 22.8	0.4 ± 0.1

II. List of Publications

1. **S.V. Vadanan**, A. Basu, S. Lim; A novel platform for evaluating the environmental impacts on bacterial cellulose production. Scientific Reports, 8 (1) (2018),p. 5780, *10.1038/s41598-018-23701-y*.

2. Basu, A., **Vadanan, S. V.** & Lim, S. Rational design of a scalable bioprocess platform for bacterial cellulose production. *Carbohydr Polym* **207**, 684-693, doi:10.1016/j.carbpol.2018.10.085 (2019).

III. List of Figures

IV. List of Tables

V. Abbreviations

$(NH_4)_2SO_4$	Ammonium sulphate
Ag	Silver
BC	Bacterial cellulose
c-di-GMP	Cyclic diguanylic acid
Ch	Chitosan
CI	Crystallinity index
CMC	Carboxymethyl cellulose
CNT	Carbon nanotube
CS	Cellulose synthase
CSL	Corn steep liquor
DMEM	Dulbecco's Modified Eagle Medium
DNA	Deoxyribonucleic acid
DO	Dissolved oxygen
DOE	Design of Experiments
EPS	Exopolysaccharides
FDA	Food and Drug Administration
FESEM	Field emission scanning electron microscope
$FeSO_4.7H_2O$	Ferrous sulphate heptahydrate
FTIR	Fourier transform infrared spectroscopy
GK	Glucokinase
GO	Graphene oxide
GRAS	Generally recognised as safe
H_3BO_3	Boric acid
HA	Hydroxyapatite
HDFa	Primary Human Dermal Fibroblasts
HS	Hestrin and Schramm
KH_2PO_4	Potassium dihydrogenphosphate
LiOH	Lithium hydroxide
LPS	Lipopolysaccharides
$MgSO_4.7H_2O$	Magnesium sulphate heptahydrate
MH	Magnetic hysteresis

MMT	Montmorillonite
Na_2HPO_4	Disodium hydrogen phosphate
NaCl	Sodium chloride
NaOH	Sodium hydroxide
NMNO	N-methyl morpholine N-oxide
NMR	Nuclear magnetic resonance
NPs	Nanoparticles
OD	Optical density
OH	Hydroxyl group
P3HB	poly(3-hydroxybutyrate)
PANI	Polyaniline
PBS	Phosphate buffered saline
PDMS	Polydimethylsiloxane
PEDOT:PSS	Poly(3,4-ethylenedioxythiophene) polystyrene sulfonate
PEG	Poly(ethylene glycol)
PGI	Phosphoglucose isomerase
PGM	Phosphoglucomutase
PL	Polylysine
Ppy	Polypropylene
PVA	Polyvinyl alcohol
RNA	Ribonucleic acid
TEBV	Tissue engineered blood vessels
TEMPO	2,2,6,6-Tetramethylpiperidin-1-yl)oxyl
TGA	Thermogravimetric analysis
UDP	Uridine diphosphate
UDPGlc	Uridine diphophoglucose
VSM	Vibrating-Sample Magnetometer
w/v	weight by volume
XPS	X-ray photoelectron spectroscopy
XRD	X-ray diffraction

VI. References

1 Figueiredo, A. R. P., Vilela, C., Neto, C. P., Silvestre, A. J. D. & Freire, C. S. R. Bacterial Cellulose-Based Nanocomposites- Roadmap for innovative materials. *Nanocellulose Polymer Nanocomposites: Fundamentals and Applications.*, 17-62, doi:10.1002/9781118872246.ch2 (2014).

2 Ruka, D. R., Simon, G. P. & Dean, K. M. Bacterial Cellulose and Its Use in Renewable composites. *Nanocellulose Polymer Nanocomposites: Fundamentals and Applications.*, 89-130, doi:10.1002/9781118872246.ch4 (2014).

3 Fajardo, A. R., Pereira, A. G. B. & Muniz, E. C. in *Eco-friendly Polymer Nanocomposites: Chemistry and Applications* (eds Vijay Kumar Thakur & Manju Kumari Thakur) 43-71 (Springer India, 2015).

4 Shi, Z. *et al.* Electroconductive natural polymer-based hydrogels. *Biomaterials* **111**, 40-54, doi:10.1016/j.biomaterials.2016.09.020 (2016).

5 Guiseppi-Elie, A. Electroconductive hydrogels: synthesis, characterization and biomedical applications. *Biomaterials* **31**, 2701-2716, doi:10.1016/j.biomaterials.2009.12.052 (2010).

6 Huang, J.-C., Shetty, A. S. & Wang, M.-S. Biodegradable plastics: A review. *Advances in Polymer Technology* **10**, 23-30, doi:10.1002/adv.1990.060100103 (1990).

7 Shah, A. A., Hasan, F., Hameed, A. & Ahmed, S. Biological degradation of plastics: a comprehensive review. *Biotechnol Adv* **26**, 246-265, doi:10.1016/j.biotechadv.2007.12.005 (2008).

8 Yates, M. R. & Barlow, C. Y. Life cycle assessments of biodegradable, commercial biopolymers—A critical review. **v. 78** (2013).

9 Holzapfel, B. M. *et al.* How smart do biomaterials need to be? A translational science and clinical point of view. *Adv Drug Deliv Rev* **65**, 581-603, doi:10.1016/j.addr.2012.07.009 (2013).

10 Pattanashetti, N. A., Heggannavar, G. B. & Kariduraganavar, M. Y. Smart Biopolymers and their Biomedical Applications. *Procedia Manufacturing* **12**, 263-279, doi:10.1016/j.promfg.2017.08.030 (2017).

11 Van de Velde, K. & Kiekens, P. Biopolymers: overview of several properties and consequences on their applications. *Polymer Testing* **21**, 433-442, doi:10.1016/s0142-9418(01)00107-6 (2002).

12 Eder, M., Amini, S. & Fratzl, P. Biological composites-complex structures for functional diversity. *Science* **362**, 543-547, doi:10.1126/science.aat8297 (2018).

13 Liu, Y., Ren, J. & Ling, S. Bioinspired and biomimetic silk spinning. *Composites Communications* **13**, 85-96, doi:10.1016/j.coco.2019.03.004 (2019).

14 Del Valle, L. J., Diaz, A. & Puiggali, J. Hydrogels for Biomedical Applications: Cellulose, Chitosan, and Protein/Peptide Derivatives. *Gels* **3**, doi:10.3390/gels3030027 (2017).

15 Torres, F. G., Commeaux, S. & Troncoso, O. P. Starch-based biomaterials for wound-dressing applications. *Starch - Stärke* **65**, 543-551, doi:10.1002/star.201200259 (2013).

16 Jayakumar, R., Prabaharan, M., Sudheesh Kumar, P. T., Nair, S. V. & Tamura, H. Biomaterials based on chitin and chitosan in wound dressing applications. *Biotechnol Adv* **29**, 322-337, doi:10.1016/j.biotechadv.2011.01.005 (2011).

17 Lesnikowski, Z. DNA as Platform for New Biomaterials. Metal-Containing Nucleic Acids. *Current Organic Chemistry* **11**, 355-381, doi:10.2174/138527207780059358 (2007).

18 Pandian, G. N. & Sugiyama, H. Nature-Inspired Design of Smart Biomaterials Using the Chemical Biology of Nucleic Acids. *Bulletin of the Chemical Society of Japan* **89**, 843-868, doi:10.1246/bcsj.20160062 (2016).

19 Majeed, K. *et al. Potential materials for food packaging from nanoclay/natural fibres filled hybrid composites*. Vol. 46 (2012).

20 Shavandi, A. *et al.* Polyphenol uses in biomaterials engineering. *Biomaterials* **167**, 91-106, doi:10.1016/j.biomaterials.2018.03.018 (2018).

21 Richards, M., Dahiyat, B. I., Arm, D. M., Brown, P. R. & Leong, K. W. Evaluation of polyphosphates and polyphosphonates as degradable biomaterials. *J Biomed Mater Res* **25**, 1151-1167, doi:10.1002/jbm.820250908 (1991).

22 Melke, J., Midha, S., Ghosh, S., Ito, K. & Hofmann, S. Silk fibroin as biomaterial for bone tissue engineering. *Acta Biomater* **31**, 1-16, doi:10.1016/j.actbio.2015.09.005 (2016).

23 Xiang, L. *et al.* Gate-controlled conductance switching in DNA. *Nat Commun* **8**, 14471, doi:10.1038/ncomms14471 (2017).

24 Chang, C. & Zhang, L. Cellulose-based hydrogels: Present status and application prospects. *Carbohydrate Polymers* **84**, 40-53, doi:10.1016/j.carbpol.2010.12.023 (2011).

25 Shen, X., Shamshina, J. L., Berton, P., Gurau, G. & Rogers, R. D. Hydrogels based on cellulose and chitin: fabrication, properties, and applications. *Green Chemistry* **18**, 53-75, doi:10.1039/c5gc02396c (2016).

26 U.S. Congress. Office of Technology Assessment, Biopolymers: Making Materials Nature's Way-Background Paper, OTA-BP-E-102 (Washington, DC: U.S. Government Printing Office, September 1993).

27 Ulery, B. D., Nair, L. S. & Laurencin, C. T. Biomedical Applications of Biodegradable Polymers. *J Polym Sci B Polym Phys* **49**, 832-864, doi:10.1002/polb.22259 (2011).

28 Mudhoo, A., Mohee, R., Unmar, G. D. & Sharma, S. K. Degradation of Biodegradable and Green Polymers in the Composting Environment. **0**, 332-364, doi:10.1039/9781849733458-00332 (2011).

29 Stevens, E. S. How green are green plastics? . *Biocycle*, 42-45 (2002).

30 Miller, S. A. Sustainable Polymers: Opportunities for the Next Decade. *ACS Macro Letters* **2**, 550-554, doi:10.1021/mz400207g (2013).

31 Muhammadi, Shabina, Afzal, M. & Hameed, S. Bacterial polyhydroxyalkanoates-eco-friendly next generation plastic: Production, biocompatibility, biodegradation, physical properties and applications. *Green Chemistry Letters and Reviews* **8**, 56-77, doi:10.1080/17518253.2015.1109715 (2015).

32 Klemm, D., Heublein, B., Fink, H. P. & Bohn, A. Cellulose: fascinating biopolymer and sustainable raw material. *Angew Chem Int Ed Engl* **44**, 3358-3393, doi:10.1002/anie.200460587 (2005).

33 Sutherland, I. W. Bioplastic and Biopolymer production. *Biotechnology* **5**, 152-176 (2007).

34 Rehm, B. H. Bacterial polymers: biosynthesis, modifications and applications. *Nat Rev Microbiol* **8**, 578-592, doi:10.1038/nrmicro2354 (2010).

35 Dake, M. in *Microbial Factories: Biodiversity, Biopolymers, Bioactive Molecules: Volume 2* (ed Vipin Chandra Kalia) 29-56 (Springer India, 2015).

36 Nwodo, U. U., Green, E. & Okoh, A. I. Bacterial exopolysaccharides: functionality and prospects. *Int J Mol Sci* **13**, 14002-14015, doi:10.3390/ijms131114002 (2012).

37 Yildiz, H. & Karatas, N. Microbial exopolysaccharides: Resources and bioactive properties. *Process Biochemistry* **72**, 41-46, doi:10.1016/j.procbio.2018.06.009 (2018).

38 Schmid, J., Sieber, V. & Rehm, B. Bacterial exopolysaccharides: biosynthesis pathways and engineering strategies. *Front Microbiol* **6**, 496, doi:10.3389/fmicb.2015.00496 (2015).

39 Cannon, R. E. & Anderson, S. M. Biogenesis of bacterial cellulose. *Crit Rev Microbiol* **17**, 435-447, doi:10.3109/10408419109115207 (1991).

40 Freitas, F., Alves, V. D. & Reis, M. A. Advances in bacterial exopolysaccharides: from production to biotechnological applications. *Trends Biotechnol* **29**, 388-398, doi:10.1016/j.tibtech.2011.03.008 (2011).

41 Ullah, H., Santos, H. A. & Khan, T. Applications of bacterial cellulose in food, cosmetics and drug delivery. *Cellulose* **23**, 2291-2314, doi:10.1007/s10570-016-0986-y (2016).

42 Shah, N., Ul-Islam, M., Khattak, W. A. & Park, J. K. Overview of bacterial cellulose composites: a multipurpose advanced material. *Carbohydr Polym* **98**, 1585-1598, doi:10.1016/j.carbpol.2013.08.018 (2013).

43 Islam, M. U., Ullah, M. W., Khan, S., Shah, N. & Park, J. K. Strategies for cost-effective and enhanced production of bacterial cellulose. *Int J Biol Macromol* **102**, 1166-1173, doi:10.1016/j.ijbiomac.2017.04.110 (2017).

44 Horecker, B. L. The biosynthesis of bacterial polysaccharides. *Annu Rev Microbiol* **20**, 253-290, doi:10.1146/annurev.mi.20.100166.001345 (1966).

45 Sharon, N. Polysaccharides. *Annual Review of Biochemistry* **35**, 485-520, doi:10.1146/annurev.bi.35.070166.002413 (1966).

46 Moon, R. J., Martini, A., Nairn, J., Simonsen, J. & Youngblood, J. Cellulose nanomaterials review: structure, properties and nanocomposites. *Chem Soc Rev* **40**, 3941-3994, doi:10.1039/c0cs00108b (2011).

47 Lavoine, N., Desloges, I., Dufresne, A. & Bras, J. Microfibrillated cellulose - its barrier properties and applications in cellulosic materials: a review. *Carbohydr Polym* **90**, 735-764, doi:10.1016/j.carbpol.2012.05.026 (2012).

48 Dufresne, A. Nanocellulose: a new ageless bionanomaterial. *Materials Today* **16**, 220-227, doi:10.1016/j.mattod.2013.06.004 (2013).

49 Iguchi, M., Yamanaka, S. & Budhiono, A. Review Bacterial Cellulose- a masterpiece of nature's art. *Journal of Materials Science* **35**, 261-270 (2000).

50 Ummartyotin, S. & Manuspiya, H. A critical review on cellulose: From fundamental to an approach on sensor technology. *Renewable and Sustainable Energy Reviews* **41**, 402-412, doi:10.1016/j.rser.2014.08.050 (2015).

51 Brown, A. J. The Chemical Action of Pure Cultivations of Bacterium Aceti. *J. Chem. Soc. Trans.* **49**, 172 (1886).

52 Lee, K. Y., Buldum, G., Mantalaris, A. & Bismarck, A. More than meets the eye in bacterial cellulose: biosynthesis, bioprocessing, and applications in advanced fiber composites. *Macromol Biosci* **14**, 10-32, doi:10.1002/mabi.201300298 (2014).

53 Hestrin, S., Aschner, M. & Mager, J. Synthesis of cellulose by resting cells of Acetobacter xylinum. *Nature* **159**, 64-65 (1947).

54 Gromet, Z., Schramm, M. & Hestrin, S. Synthesis of Cellulose by Acetobacter xylinum. Part 2: Preparation of freeze-dried cells capable of polymerizing glucose to cellulose *Biochem. J.* **67**, 679 (1957).

55 Chawla, P. R., Bajaj, I., B., Survase, S. A. & Singhal, R. S. Microbial Cellulose Fermentative Production and Applications. *Food Technol. Biotechnol.* **47**, 107-124 (2009).

56 Lynd, L. R., Weimer, P. J., van Zyl, W. H. & Pretorius, I. S. Microbial cellulose utilization: fundamentals and biotechnology. *Microbiol Mol Biol Rev* **66**, 506-577, table of contents, doi:10.1128/mmbr.66.3.506-577.2002 (2002).

57 Lisdiyanti, P., Navarro, R. R., Uchimura, T. & Komagata, K. Reclassification of Gluconacetobacter hansenii strains and proposals of Gluconacetobacter saccharivorans sp. nov. and Gluconacetobacter nataicola sp. nov. *Int J Syst Evol Microbiol* **56**, 2101-2111, doi:10.1099/ijs.0.63252-0 (2006).

58 Yamada, Y. & Yukphan, P. Genera and species in acetic acid bacteria. *Int J Food Microbiol* **125**, 15-24, doi:10.1016/j.ijfoodmicro.2007.11.077 (2008).

59 Crotti, E. *et al.* Acetic acid bacteria, newly emerging symbionts of insects. *Appl Environ Microbiol* **76**, 6963-6970, doi:10.1128/AEM.01336-10 (2010).

60 Saxena, I. M., Lin, F. C. & Brown, R. M., Jr. Cloning and sequencing of the cellulose synthase catalytic subunit gene of Acetobacter xylinum. *Plant Mol Biol* **15**, 673-683, doi:10.1007/BF00016118 (1990).

61 Kojima, Y., Tonouchi, N., Tsuchida, T., Yoshinaga, F. & Yamada, Y. The Characterization of Acetic Acid Bacteria Efficiently Producing Bacterial

Cellulose from Sucrose: The Proposal of Acetobacter xylinum subsp. nonacetoxidans subsp. Nov. *Biosci Biotechnol Biochem* **62**, 185-187, doi:10.1271/bbb.62.185 (1998).

62 Florea, M. *et al.* Engineering control of bacterial cellulose production using a genetic toolkit and a new cellulose-producing strain. *Proc Natl Acad Sci U S A* **113**, E3431-3440, doi:10.1073/pnas.1522985113 (2016).

63 Basu, A., Vadanan, S. V. & Lim, S. A Novel Platform for Evaluating the Environmental Impacts on Bacterial Cellulose Production. *Scientific Reports* **8**, 5780, doi:10.1038/s41598-018-23701-y (2018).

64 Jonas, R. & Farah, L. F. Production and application of microbial cellulose. *Polymer Degradation and Stability* **59**, 101-106 (1998).

65 McNamara, J. T., Morgan, J. L. & Zimmer, J. A molecular description of cellulose biosynthesis. *Annu Rev Biochem* **84**, 895-921, doi:10.1146/annurev-biochem-060614-033930 (2015).

66 Yamanaka, S. & Sugiyama, J. Structural modification of bacterial cellulose. *Cellulose* **7**, 213-225, doi:10.1023/A:1009208022957 (2000).

67 Williams, W. S. & Cannon, R. E. Alternative Environmental Roles for Cellulose Produced by Acetobacter xylinum. *Appl. Environ. Microbiol.* **55**, 2448-2452 (1989).

68 Esa, F., Tasirin, S. M. & Rahman, N. A. Overview of Bacterial Cellulose Production and Application. *Agriculture and Agricultural Science Procedia* **2**, 113-119, doi:10.1016/j.aaspro.2014.11.017 (2014).

69 Ross, P., Mayer, R. & Benziman, M. Cellulose biosynthesis and function in Bacteria. *Microbiological Reviews* **55**, 35-58 (1991).

70 Lin, S.-P. *et al.* Biosynthesis, production and applications of bacterial cellulose. *Cellulose* **20**, 2191-2219, doi:10.1007/s10570-013-9994-3 (2013).

71 Delmer, D. P. & Amor, Y. Cellulose biosynthesis. *Plant Cell* **7**, 987-1000, doi:10.1105/tpc.7.7.987 (1995).

72 Valla, S. *et al.* Cloning of a gene involved in cellulose biosynthesis in Acetobacter xylinum: Complementation of cellulose-negative mutants by the UDPG pyrophosphorylase structural gene. *Molecular and General Genetics MGG* **217**, 26-30, doi:10.1007/BF00330938 (1989).

73 Cakar, F., Ozer, I., Aytekin, A. O. & Sahin, F. Improvement production of bacterial cellulose by semi-continuous process in molasses medium. *Carbohydr Polym* **106**, 7-13, doi:10.1016/j.carbpol.2014.01.103 (2014).

74 Okiyama, A., Shirae, H., Kano, H. & Yamanaka, S. Bacterial cellulose I. Two-stage fermentation process for cellulose production by Acetobacter aceti. *Food Hydrocolloids* **6**, 471-477, doi:10.1016/s0268-005x(09)80032-5 (1992).

75 Schramm, M. & Hestrin, S. Factors affecting Production of Cellulose at the Air/ Liquid Interface of a Culture of Acetobacter xylinum. *Microbiology* **11**, 123-129, doi:doi:10.1099/00221287-11-1-123 (1954).

76 Kralisch, D., Hessler, N., Klemm, D., Erdmann, R. & Schmidt, W. White biotechnology for cellulose manufacturing--the HoLiR concept. *Biotechnol Bioeng* **105**, 740-747, doi:10.1002/bit.22579 (2010).

77 Hornung, M., Ludwig, M., Gerrard, A. M. & Schmauder, H. P. Optimizing the Production of Bacterial Cellulose in Surface Culture: Evaluation of Substrate Mass Transfer Influences on the Bioreaction (Part 1). *Engineering in Life Sciences* **6**, 537-545, doi:10.1002/elsc.200620162 (2006).

78 Yan, Z., Chen, S., Wang, H., Wang, B. & Jiang, J. Biosynthesis of bacterial cellulose/multi-walled carbon nanotubes in agitated culture. *Carbohydrate Polymers* **74**, 659-665, doi:10.1016/j.carbpol.2008.04.028 (2008).

79 Hwang, J. W., Yang, Y. K., Hwang, J. K., Pyun, Y. R. & Kim, Y. S. Effects of pH and dissolved oxygen on cellulose production by Acetobacter xylinum BRC5 in agitated culture. *Journal of Bioscience and Bioengineering* **88**, 183-188, doi:http://dx.doi.org/10.1016/S1389-1723(99)80199-6 (1999).

80 Toyosaki, H. *et al.* Screening of Bacterial Cellulose-producingAcetobacterStrains Suitable for Agitated Culture. *Bioscience, Biotechnology, and Biochemistry* **59**, 1498-1502, doi:10.1271/bbb.59.1498 (2014).

81 Kouda, T., Yano, H., Yoshinaga, F., Kaminoyama, M. & Kamiwano, M. Characterization of non-newtonian behavior during mixing of bacterial cellulose in a bioreactor. *Journal of Fermentation and Bioengineering* **82**, 382-386, doi:10.1016/0922-338x(96)89155-0 (1996).

82 Kouda, T., Yano, H. & Yoshinaga, F. Effect of agitator configuration on bacterial cellulose productivity in aerated and agitated culture. *Journal of Fermentation and Bioengineering* **83**, 371-376, doi:10.1016/s0922-338x(97)80144-4 (1997).

83 Chisti, M. Y. & Moo-Young, M. Airlift Reactors: Characteristics, Applications and Design Considerations. *Chemical Engineering Communications* **60**, 195-242, doi:10.1080/00986448708912017 (2007).

84 Chao, Y. p., Sugano, Y., Kouda, T., Yoshinaga, F. & Shoda, M. Production of bacterial cellulose by Acetobacter xylinumwith an air-lift reactor. *Biotechnology Techniques* **11**, 829-832, doi:10.1023/a:1018433526709 (1997).

85 Shoda, M. & Sugano, Y. Recent advances in bacterial cellulose production. *Biotechnology and Bioprocess Engineering* **10**, 1-8, doi:10.1007/bf02931175 (2005).

86 Krystynowicz, A. *et al.* Factors affecting the yield and properties of bacterial cellulose. *J Ind Microbiol Biotechnol* **29**, 189-195, doi:10.1038/sj.jim.7000303 (2002).

87 Cheng, K. C., Catchmark, J. M. & Demirci, A. Enhanced production of bacterial cellulose by using a biofilm reactor and its material property analysis. *J Biol Eng* **3**, 12, doi:10.1186/1754-1611-3-12 (2009).

88 Yamanaka, S. *et al.* The structure and mechanical properties of sheets prepared from bacterial cellulose. *Journal of Materials Science* **24**, 3141-3145, doi:10.1007/BF01139032 (1989).

89 Zhou, L. L., Sun, D. P., Hu, L. Y., Li, Y. W. & Yang, J. Z. Effect of addition of sodium alginate on bacterial cellulose production by Acetobacter xylinum. *J Ind Microbiol Biotechnol* **34**, 483-489, doi:10.1007/s10295-007-0218-4 (2007).

90 Son, H.-J. *et al.* Increased production of bacterial cellulose by Acetobacter sp. V6 in synthetic media under shaking culture conditions. *Bioresource Technology* **86**, 215-219, doi:http://dx.doi.org/10.1016/S0960-8524(02)00176-1 (2003).

91 Tarr, H. L. A. & Hibbert, H. Studies on Reactions Relating to Carbohydrates and Polysaccharides. Xxxv. Polysaccharide Synthesis by the Action of Acetobacter Xylinus on Carbohydrates and Related Compounds. *Canadian Journal of Research* **4**, 372-388, doi:10.1139/cjr31-027 (1931).

92 Embuscado, M. E., Marks, J. S. & BeMiller, J. N. Bacterial cellulose. I. Factors affecting the production of cellulose by Acetobacter xylinum. *Food Hydrocolloids* **8**, 407-418, doi:10.1016/s0268-005x(09)80084-2 (1994).

93 Shah, N., Ha, J. H. & Park, J. K. Effect of reactor surface on production of bacterial cellulose and water soluble oligosaccharides by Gluconacetobacter hansenii PJK. *Biotechnology and Bioprocess Engineering* **15**, 110-118, doi:10.1007/s12257-009-3064-6 (2010).

94 Jung, H. I. *et al.* Influence of glycerol on production and structural-physical properties of cellulose from Acetobacter sp. V6 cultured in shake flasks. *Bioresour Technol* **101**, 3602-3608, doi:10.1016/j.biortech.2009.12.111 (2010).

95 Naritomi, T., Kouda, T., Yano, H. & Yoshinaga, F. Effect of ethanol on bacterial cellulose production from fructose in continuous culture. *Journal of Fermentation and Bioengineering* **85**, 598-603, doi:10.1016/s0922-338x(98)80012-3 (1998).

96 Oikawa, T., Morino, T. & Ameyama, M. Production of Cellulose fromD-Arabitol byAcetobacter xylinumKU-1. *Bioscience, Biotechnology, and Biochemistry* **59**, 1564-1565, doi:10.1271/bbb.59.1564 (2014).

97 Chawla, P. R., Bajaj, I. B., Survase, S. A. & Singhal, R. S. Microbial cellulose: Fermentative production and applications. *Food Technology and Biotechnology* **47**, 107-124 (2009).

98 Mikkelsen, D., Flanagan, B. M., Dykes, G. A. & Gidley, M. J. Influence of different carbon sources on bacterial cellulose production by Gluconacetobacter xylinus strain ATCC 53524. *J Appl Microbiol* **107**, 576-583, doi:10.1111/j.1365-2672.2009.04226.x (2009).

99 Pourramezan, G. Z., Roayaei , A. M. & Qezelbash, Q. R. Optimization of culture conditions for bacterial cellulose production by Acetobacter sp. 4B-2. *Biotechnology* **8**, 150-154 (2009).

100 Ishihara, M., Matsunaga, M., Hayashi, N. & Tišler, V. Utilization of d-xylose as carbon source for production of bacterial cellulose. *Enzyme and Microbial Technology* **31**, 986-991, doi:http://dx.doi.org/10.1016/S0141-0229(02)00215-6 (2002).

101 Coban, E. P. & Biyik, H. Effect of various carbon and nitrogen sources on cellulose synthesis by *Acetobacter lovaniensis* HBB5. *African Journal of Biotechnology* **10**, 46, doi:10.5897/AJB10.1693 (2011).

102 Nguyen, V. T., Flanagan, B., Gidley, M. J. & Dykes, G. A. Characterization of cellulose production by a Gluconacetobacter xylinus strain from Kombucha. *Curr Microbiol* **57**, 449-453, doi:10.1007/s00284-008-9228-3 (2008).

103 Basu, A., Vadanan, S. V. & Lim, S. Rational design of a scalable bioprocess platform for bacterial cellulose production. *Carbohydr Polym* **207**, 684-693, doi:10.1016/j.carbpol.2018.10.085 (2019).

104 Hirai, A., Tsuji, M. & Horii, F. Culture conditions producing structure entities composed of Cellulose I and II in bacterial cellulose. *Cellulose* **4**, 239-245, doi:10.1023/a:1018439907396 (1997).

105 Zeng, X. *et al.* Screening of the common culture conditions affecting crystallinity of bacterial cellulose. *J Ind Microbiol Biotechnol* **38**, 1993-1999, doi:10.1007/s10295-011-0989-5 (2011).

106 Hutchens, S. A., Leon, R. V., O'Neill H, M. & Evans, B. R. Statistical analysis of optimal culture conditions for Gluconacetobacter hansenii cellulose production. *Lett Appl Microbiol* **44**, 175-180, doi:10.1111/j.1472-765X.2006.02055.x (2007).

107 Jagannath, A., Kalaiselvan, A., Manjunatha, S. S., Raju, P. S. & Bawa, A. S. The effect of pH, sucrose and ammonium sulphate concentrations on the production of bacterial cellulose (Nata-de-coco) by Acetobacter xylinum. *World Journal of Microbiology and Biotechnology* **24**, 2593-2599, doi:10.1007/s11274-008-9781-8 (2008).

108 Aloni, Y., Delmer, D. P. & Benziman, M. Achievement of high rates of in vitro synthesis of 1,4-beta-D-glucan: activation by cooperative interaction of the Acetobacter xylinum enzyme system with GTP, polyethylene glycol, and a protein factor. *Proc Natl Acad Sci U S A* **79**, 6448-6452, doi:10.1073/pnas.79.21.6448 (1982).

109 Kim, Y. J., Kim, J. N., Wee, Y. J., Park, D. H. & Ryu, H. W. Bacterial cellulose production by Gluconacetobacter sp. PKY5 in a rotary biofilm contactor. *Appl Biochem Biotechnol* **137-140**, 529-537, doi:10.1007/s12010-007-9077-8 (2007).

110 Son, H.-J., Heo, M.-S., Kim, Y.-G. & Lee, S.-J. Optimization of fermentation conditions for the production of bacterial cellulose by a newly isolated Acetobacter. *Biotechnology and Applied Biochemistry* **33**, 1-5, doi:10.1042/BA20000065 (2001).

111 Kongruang, S. Bacterial cellulose production by Acetobacter xylinum strains from agricultural waste products. *Appl Biochem Biotechnol* **148**, 245-256, doi:10.1007/s12010-007-8119-6 (2008).

112 Ha, J. H., Shah, N., Ul-Islam, M., Khan, T. & Park, J. K. Bacterial cellulose production from a single sugar α-linked glucuronic acid-based oligosaccharide. *Process Biochemistry* **46**, 1717-1723, doi:10.1016/j.procbio.2011.05.024 (2011).

113 Song, H.-J., Li, H., Seo, J.-H., Kim, M.-J. & Kim, S.-J. Pilot-scale production of bacterial cellulose by a spherical type bubble column bioreactor using saccharified food wastes. *Korean Journal of Chemical Engineering* **26**, 141-146, doi:10.1007/s11814-009-0022-0 (2009).

114 Li, H. X., Kim, S.-J., Lee, Y.-W., Kee, C. D. & Oh, I. K. Determination of the stoichiometry and critical oxygen tension in the production culture of bacterial cellulose using saccharified food wastes. *Korean Journal of Chemical Engineering* **28**, 2306-2311, doi:10.1007/s11814-011-0111-8 (2011).

115 Saxena, I. M. & Brown, R. M., Jr. Cellulose biosynthesis: current views and evolving concepts. *Ann Bot* **96**, 9-21, doi:10.1093/aob/mci155 (2005).

116 Delmer, D. P. CELLULOSE BIOSYNTHESIS: Exciting Times for A Difficult Field of Study. *Annu Rev Plant Physiol Plant Mol Biol* **50**, 245-276, doi:10.1146/annurev.arplant.50.1.245 (1999).

117 Brown, R. M., Willison, J. H. & Richardson, C. L. Cellulose biosynthesis in Acetobacter xylinum: visualization of the site of synthesis and direct measurement of the in vivo process. *Proceedings of the National Academy of Sciences of the United States of America* **73**, 4565-4569 (1976).

118 Zaar, K. Visualization of pores (export sites) correlated with cellulose production in the envelope of the gram-negative bacterium Acetobacter xylinum. *J Cell Biol* **80**, 773-777, doi:10.1083/jcb.80.3.773 (1979).

119 Vitta, S. & Thiruvengadam, V. Multifunctional bacterial cellulose and nanoparticle-embedded composites. *Current Science* **102**, 1398-1405 (2012).

120 Benziman, M., Haigler, C. H., Brown, R. M., White, A. R. & Cooper, K. M. Cellulose biogenesis: Polymerization and crystallization are coupled processes in Acetobacter xylinum. *Proceedings of the National Academy of Sciences of the United States of America* **77**, 6678-6682 (1980).

121 Haigler, C. H., Brown, R. M., Jr. & Benziman, M. Calcofluor white ST Alters the in vivo assembly of cellulose microfibrils. *Science* **210**, 903-906, doi:10.1126/science.7434003 (1980).

122 Chen, H.-H., Chen, L.-C., Huang, H.-C. & Lin, S.-B. In situ modification of bacterial cellulose nanostructure by adding CMC during the growth of Gluconacetobacter xylinus. *Cellulose* **18**, 1573-1583, doi:10.1007/s10570-011-9594-z (2011).

123 Kuga, S., Takagi, S. & Brown, R. M. Native folded-chain cellulose II. *Polymer* **34**, 3293-3297, doi:10.1016/0032-3861(93)90404-x (1993).

124 Haigler, C. H. & Benziman, M. Biogenesis of Cellulose I Microfibrils Occurs by Cell-Directed Self-Assembly in Acetobacter xylinum. 273-297, doi:10.1007/978-1-4684-1116-4_14 (1982).

125 Gardner, D. J., Oporto, G. S., Mills, R. & Samir, M. A. S. A. Adhesion and Surface Issues in Cellulose and Nanocellulose. *Journal of Adhesion Science and Technology* **22**, 545-567, doi:10.1163/156856108x295509 (2008).

126 O'Sullivan, A. C. Cellulose: the structure slowly unravels. *Cellulose* **4**, 173-207, doi:10.1023/a:1018431705579 (1997).

127 Festucci-Buselli, R. A., Otoni, W. C. & Joshi, C. P. Structure, Organization, and Functions of Cellulose Synthase Complexes in Higher Plants. *Brazillian Journal of Plant Physiology* **19(1)** (2007).

128 Hayashi, J., Sufoka, A., Ohkita, J. & Watanabe, S. The confirmation of existences of cellulose IIII, IIIII, IVI, and IVII by the X-ray method. *Journal of Polymer Science: Polymer Letters Edition* **13**, 23-27, doi:10.1002/pol.1975.130130104 (1975).

129 Festucci-Buselli, R. A., Otoni, W. C. & Joshi, C. P. Structure, organization, and functions of cellulose synthase complexes in higher plants. *Brazilian Journal of Plant Physiology* **19**, 1-13, doi:10.1590/s1677-04202007000100001 (2007).

130 Thompson, N. S., Carlson, J. A., Kaustinen, H. M. & Uhlin, K. I. Tunnel structures in Acetobacter xylinum. *International Journal of Biological Macromolecules* **10**, 126-127, doi:10.1016/0141-8130(88)90021-9 (1988).

131 Pecoraro, E., Manzani, D., Messaddeq, Y. & Ribeiro, S. J. L. Bacterial Cellulose from Glucanacetobacter xylinus-Preparation, properties and applications. *Monomers, Polymers and Composites from Renewable Resources*, 369-383 (2008).

132 Nishi, Y. *et al.* The structure and mechanical properties of sheets prepared from bacterial cellulose. *Journal of Materials Science* **25**, 2997-3001, doi:10.1007/bf00584917 (1990).

133 McKenna, B. A., Mikkelsen, D., Wehr, J. B., Gidley, M. J. & Menzies, N. W. Mechanical and structural properties of native and alkali-treated bacterial cellulose produced by Gluconacetobacter xylinus strain ATCC 53524. *Cellulose* **16**, 1047-1055, doi:10.1007/s10570-009-9340-y (2009).

134 Fang, L. & Catchmark, J. M. Characterization of cellulose and other exopolysaccharides produced from Gluconacetobacter strains. *Carbohydr Polym* **115**, 663-669, doi:10.1016/j.carbpol.2014.09.028 (2015).

135 White, D. C. Prospects for the biosynthesis of microbial cellulose. *Cellulose and wood-chemistry and technol-ogy.*, 573-590 (1989).

136 Tayeb, A. H., Amini, E., Ghasemi, S. & Tajvidi, M. Cellulose Nanomaterials-Binding Properties and Applications: A Review. *Molecules* **23**, doi:10.3390/molecules23102684 (2018).

137 Badel, S., Bernardi, T. & Michaud, P. New perspectives for Lactobacilli exopolysaccharides. *Biotechnol Adv* **29**, 54-66, doi:10.1016/j.biotechadv.2010.08.011 (2011).

138 Shi, Z., Zhang, Y., Phillips, G. O. & Yang, G. Utilization of bacterial cellulose in food. *Food Hydrocolloids* **35**, 539-545, doi:10.1016/j.foodhyd.2013.07.012 (2014).

139 El-Saied, H., Basta, A. H. & Gobran, R. H. Research Progress in Friendly Environmental Technology for the Production of Cellulose Products (Bacterial Cellulose and Its Application). *Polymer-Plastics Technology and Engineering* **43**, 797-820, doi:10.1081/ppt-120038065 (2004).

140 Khan, T., Park, J. K. & Kwon, J.-H. Functional biopolymers produced by biochemical technology considering applications in food engineering. *Korean Journal of Chemical Engineering* **24**, 816-826, doi:10.1007/s11814-007-0047-1 (2007).

141 Park, J. K., Jung, J. Y. & Khan, T. Bacterial cellulose. 724-739, doi:10.1533/9781845695873.724 (2009).

142 Klemm, D., Schumann, D., Udhardt, U. & Marsch, S. Bacterial synthesized cellulose-artifical blood vessels for microsurgery. *Prog. Polym. Sci.* **26**, 1561-1603 (2001).

143 Rajwade, J. M., Paknikar, K. M. & Kumbhar, J. V. Applications of bacterial cellulose and its composites in biomedicine. *Appl Microbiol Biotechnol* **99**, 2491-2511, doi:10.1007/s00253-015-6426-3 (2015).

144 Picheth, G. F. *et al.* Bacterial cellulose in biomedical applications: A review. *Int J Biol Macromol* **104**, 97-106, doi:10.1016/j.ijbiomac.2017.05.171 (2017).

145 Czaja, W., Young, D. J., Kawecki, M. & Brown, R. M., Jr. The Future Prospects of Microbial Cellulose in Biomedical applications. *Biomacromolecules* **8** (2007).

146 Czaja, W., Krystynowicz, A., Bielecki, S. & Brown, R. M., Jr. Microbial cellulose--the natural power to heal wounds. *Biomaterials* **27**, 145-151, doi:10.1016/j.biomaterials.2005.07.035 (2006).

147 Yu, J. *et al.* Production of Hollow Bacterial Cellulose Microspheres Using Microfluidics to Form an Injectable Porous Scaffold for Wound Healing. *Adv Healthc Mater* **5**, 2983-2992, doi:10.1002/adhm.201600898 (2016).

148 Keshk, S. M. A. S. Bacterial Cellulose Production and its Industrial Applications. *Journal of Bioprocessing & Biotechniques* **04**, doi:10.4172/2155-9821.1000150 (2014).

149 Shah, J. & Brown, R. M., Jr. Towards electronic paper displays made from microbial cellulose. *Appl Microbiol Biotechnol* **66**, 352-355, doi:10.1007/s00253-004-1756-6 (2005).

150 Hammock, M. L., Chortos, A., Tee, B. C., Tok, J. B. & Bao, Z. 25th anniversary article: The evolution of electronic skin (e-skin): a brief history, design considerations, and recent progress. *Adv Mater* **25**, 5997-6038, doi:10.1002/adma.201302240 (2013).

151 Takai, M., Nonomura, F., Inukai, T., Fujiwara, M. & Hayashi, J. Filtration and permeation characteristics of bacterial cellulose composite. **47**, 119-129, doi:10.2115/fiber.47.119 (1991).

152 Chen, S., Shen, W., Yu, F. & Wang, H. Kinetic and thermodynamic studies of adsorption of Cu2+ and Pb2+ onto amidoximated bacterial cellulose. *Polymer Bulletin* **63**, 283-297, doi:10.1007/s00289-009-0088-1 (2009).

153 Shibazaki, H., Kuga, S. & Onabe, F. Mechanical properties of papersheet containing bacterial cellulose. *Japan Tappi Journal* **48**, 1621-1630, doi:10.2524/jtappij.48.1621 (1994).

154 Iguchi, M. *et al.* Bacterial cellulose-containing molding material having high dynamic strength. *US patent 4742164* (1988).

155 Tang, X. Z., Kumar, P., Alavi, S. & Sandeep, K. P. Recent advances in biopolymers and biopolymer-based nanocomposites for food packaging materials. *Crit Rev Food Sci Nutr* **52**, 426-442, doi:10.1080/10408398.2010.500508 (2012).

156 Shezad, O., Khan, S., Khan, T. & Park, J. K. Physicochemical and mechanical characterization of bacterial cellulose produced with an excellent productivity in static conditions using a simple fed-batch cultivation strategy. *Carbohydrate Polymers* **82**, 173-180, doi:10.1016/j.carbpol.2010.04.052 (2010).

157 Hu, W., Chen, S., Yang, J., Li, Z. & Wang, H. Functionalized bacterial cellulose derivatives and nanocomposites. *Carbohydr Polym* **101**, 1043-1060, doi:10.1016/j.carbpol.2013.09.102 (2014).

158 Ruka, D. R., Simon, G. P. & Dean, K. M. In situ modifications to bacterial cellulose with the water insoluble polymer poly-3-hydroxybutyrate. *Carbohydrate Polymers* **92**, 1717-1723, doi:http://dx.doi.org/10.1016/j.carbpol.2012.11.007 (2013).

159 Saibuatong, O.-a. & Phisalaphong, M. Novo aloe vera–bacterial cellulose composite film from biosynthesis. *Carbohydrate Polymers* **79**, 455-460, doi:http://dx.doi.org/10.1016/j.carbpol.2009.08.039 (2010).

160 Zhu, W., Li, W., He, Y. & Duan, T. In-situ biopreparation of biocompatible bacterial cellulose/graphene oxide composites pellets. *Applied Surface Science* **338**, 22-26, doi:10.1016/j.apsusc.2015.02.030 (2015).

161 Müller, D., Rambo, C. R., D.O.S.Recouvreux, Porto, L. M. & Barra, G. M. O. Chemical in situ polymerization of polypyrrole on bacterial cellulose nanofibers. *Synthetic Metals* **161**, 106-111, doi:10.1016/j.synthmet.2010.11.005 (2011).

162 Müller, D. *et al.* Electrically conducting nanocomposites: preparation and properties of polyaniline (PAni)-coated bacterial cellulose nanofibers (BC). *Cellulose* **19**, 1645-1654, doi:10.1007/s10570-012-9754-9 (2012).

163 Müller, D. *et al.* Flexible PEDOT-nanocellulose composites produced by in situ oxidative polymerization for passive components in frequency filters. *Journal of Materials Science: Materials in Electronics* **27**, 8062-8067, doi:10.1007/s10854-016-4804-y (2016).

164 Arias, S. L. *et al.* Fabrication of a Functionalized Magnetic Bacterial Nanocellulose with Iron Oxide Nanoparticles. *J Vis Exp*, doi:10.3791/52951 (2016).

165 Ul-Islam, M., Shah, N., Ha, J. H. & Park, J. K. Effect of chitosan penetration on physico-chemical and mechanical properties of bacterial cellulose. *Korean Journal of Chemical Engineering* **28**, 1736-1743, doi:10.1007/s11814-011-0042-4 (2011).

166 Cai, Z. J. & Yang, G. Bacterial Cellulose/Collagen Composite: Characterization and First Evaluation of Cytocompatibility. *Journal of Applied Polymer Science* **120**, 2938-2944, doi:10.1002/app.33318 (2011).

167 Hong, L. *et al.* Hydroxyapatite/bacterial cellulose composites synthesized via a biomimetic route. *Materials Letters* **60**, 1710-1713, doi:10.1016/j.matlet.2005.12.004 (2006).

168 Hutchens, S. A., Benson, R. S., Evans, B. R., O'Neill, H. M. & Rawn, C. J. Biomimetic synthesis of calcium-deficient hydroxyapatite in a natural hydrogel. *Biomaterials* **27**, 4661-4670, doi:10.1016/j.biomaterials.2006.04.032 (2006).

169 Lopes, T. D., Riegel-Vidotti, I. C., Grein, A., Tischer, C. A. & Faria-Tischer, P. C. Bacterial cellulose and hyaluronic acid hybrid membranes: Production and characterization. *Int J Biol Macromol* **67**, 401-408, doi:10.1016/j.ijbiomac.2014.03.047 (2014).

170 Li, Y., Qing, S., Zhou, J. & Yang, G. Evaluation of bacterial cellulose/hyaluronan nanocomposite biomaterials. *Carbohydr Polym* **103**, 496-501, doi:10.1016/j.carbpol.2013.12.059 (2014).

171 Yang, G., Xie, J., Deng, Y., Bian, Y. & Hong, F. Hydrothermal synthesis of bacterial cellulose/AgNPs composite: A "green" route for antibacterial application. *Carbohydrate Polymers* **87**, 2482-2487, doi:10.1016/j.carbpol.2011.11.017 (2012).

172 Barud, H. S. *et al.* Biocellulose-based flexible magnetic paper. *Journal of Applied Physics* **117**, 17B734, doi:10.1063/1.4917261 (2015).

173 Barud, H. S. *et al.* Bacterial cellulose–silica organic–inorganic hybrids. *Journal of Sol-Gel Science and Technology* **46**, 363-367, doi:10.1007/s10971-007-1669-9 (2007).

174 Janpetch, N., Saito, N. & Rujiravanit, R. Fabrication of bacterial cellulose-ZnO composite via solution plasma process for antibacterial applications. *Carbohydr Polym* **148**, 335-344, doi:10.1016/j.carbpol.2016.04.066 (2016).

175 Sun, D., Yang, J. & Wang, X. Bacterial cellulose/TiO2 hybrid nanofibers prepared by the surface hydrolysis method with molecular precision. *Nanoscale* **2**, 287-292, doi:10.1039/b9nr00158a (2010).

176 Wang, W. *et al.* Amperometric hydrogen peroxide biosensor based on the immobilization of heme proteins on gold nanoparticles-bacteria cellulose nanofibers nanocomposite. *Talanta* **84**, 71-77, doi:10.1016/j.talanta.2010.12.015 (2011).

177 Mi, Y. *et al.* Ultra-low mass loading of platinum nanoparticles on bacterial cellulose derived carbon nanofibers for efficient hydrogen evolution. *Catalysis Today* **262**, 141-145, doi:10.1016/j.cattod.2015.08.019 (2016).

178 Pourreza, N., Golmohammadi, H., Naghdi, T. & Yousefi, H. Green in-situ synthesized silver nanoparticles embedded in bacterial cellulose nanopaper as a bionanocomposite plasmonic sensor. *Biosens Bioelectron* **74**, 353-359, doi:10.1016/j.bios.2015.06.041 (2015).

179 Zhang, T. *et al.* Biotemplated Synthesis of Gold Nanoparticle-Bacteria Cellulose Nanofiber Nanocomposites and Their Application in Biosensing. *Advanced Functional Materials* **20**, 1152-1160, doi:10.1002/adfm.200902104 (2010).

180 Shao, W. *et al.* Synthesis and antimicrobial activity of copper nanoparticle loaded regenerated bacterial cellulose membranes. *RSC Advances* **6**, 65879-65884, doi:10.1039/c6ra07984a (2016).

181 Yoon, S. H., Jin, H. J., Kook, M. C. & Pyun, Y. R. Electrically conductive bacterial cellulose by incorporation of carbon nanotubes. *Biomacromolecules* **7**, 1280-1284, doi:10.1021/bm050597g (2006).

182 Kim, Y.-H., Park, S., Won, K., Kim, H. J. & Lee, S. H. Bacterial cellulose-carbon nanotube composite as a biocompatible electrode for the direct electron transfer of glucose oxidase. *Journal of Chemical Technology & Biotechnology* **88**, 1067-1070, doi:10.1002/jctb.3939 (2013).

183 Ul-Islam, M., Khan, T. & Park, J. K. Water holding and release properties of bacterial cellulose obtained by in situ and ex situ modification. *Carbohydrate Polymers* **88**, 596-603, doi:10.1016/j.carbpol.2012.01.006 (2012).

184 Ul-Islam, M., Khan, T. & Park, J. K. Nanoreinforced bacterial cellulose-montmorillonite composites for biomedical applications. *Carbohydr Polym* **89**, 1189-1197, doi:10.1016/j.carbpol.2012.03.093 (2012).

185 Shi, Z. *et al.* In situ nano-assembly of bacterial cellulose–polyaniline composites. *RSC Adv.* **2**, 1040-1046, doi:10.1039/c1ra00719j (2012).

186 Hu, W., Chen, S., Yang, Z., Liu, L. & Wang, H. Flexible electrically conductive nanocomposite membrane based on bacterial cellulose and polyaniline. *J Phys Chem B* **115**, 8453-8457, doi:10.1021/jp204422v (2011).

187 Alonso, E. *et al.* Conductive bacterial cellulose-polyaniline blends: Influence of the matrix and synthesis conditions. *Carbohydr Polym* **183**, 254-262, doi:10.1016/j.carbpol.2017.12.025 (2018).

188 Zhu, H. *et al.* Characterization of bacteriostatic sausage casing: A composite of bacterial cellulose embedded with ε-polylysine. *Food Science and Biotechnology* **19**, 1479-1484, doi:10.1007/s10068-010-0211-y (2010).

189 Azeredo, H. M. C., Barud, H., Farinas, C. S., Vasconcellos, V. M. & Claro, A. M. Bacterial Cellulose as a Raw Material for Food and Food Packaging Applications. *Frontiers in Sustainable Food Systems* **3**, doi:10.3389/fsufs.2019.00007 (2019).

190 Iqbal, H. M., Kyazze, G., Tron, T. & Keshavarz, T. Laccase-assisted grafting of poly(3-hydroxybutyrate) onto the bacterial cellulose as backbone polymer: development and characterisation. *Carbohydr Polym* **113**, 131-137, doi:10.1016/j.carbpol.2014.07.003 (2014).

191 Barud, H. S. *et al.* Bacterial cellulose/poly(3-hydroxybutyrate) composite membranes. *Carbohydrate Polymers* **83**, 1279-1284, doi:10.1016/j.carbpol.2010.09.049 (2011).

192 Wang, B. *et al.* Preparation of Esterified Bacterial Cellulose for Improved Mechanical Properties and the Microstructure of Isotactic Polypropylene/Bacterial Cellulose Composites. *Polymers (Basel)* **8**, doi:10.3390/polym8040129 (2016).

193 Wang, B. *et al.* Mechanical and Rheological Properties of Isotactic Polypropylene/Bacterial Cellulose Composites. *Polymer Korea* **41**, 460-464, doi:10.7317/pk.2017.41.3.460 (2017).

194 Aleshin, A. N. *et al.* Electrical and optical properties of bacterial cellulose films modified with conductive polymer PEDOT/PSS. *Synthetic Metals* **199**, 147-151, doi:10.1016/j.synthmet.2014.11.022 (2015).

195 Khan, S., Ul-Islam, M., Khattak, W. A., Ullah, M. W. & Park, J. K. Bacterial cellulose-poly(3,4-ethylenedioxythiophene)-poly(styrenesulfonate) composites for optoelectronic applications. *Carbohydr Polym* **127**, 86-93, doi:10.1016/j.carbpol.2015.03.055 (2015).

196 Wang, J., Gao, C., Zhang, Y. & Wan, Y. Preparation and in vitro characterization of BC/PVA hydrogel composite for its potential use as artificial cornea biomaterial. *Materials Science and Engineering: C* **30**, 214-218, doi:10.1016/j.msec.2009.10.006 (2010).

197 Parthasarathi, R. *et al.* Theoretical Insights into the Role of Water in the Dissolution of Cellulose Using IL/Water Mixed Solvent Systems. *J Phys Chem B* **119**, 14339-14349, doi:10.1021/acs.jpcb.5b02680 (2015).

198 Suzuki, T., Kono, K., Shimomura, K. & Minami, H. Preparation of cellulose particles using an ionic liquid. *J Colloid Interface Sci* **418**, 126-131, doi:10.1016/j.jcis.2013.12.014 (2014).

199 Lindman, B., Karlström, G. & Stigsson, L. On the mechanism of dissolution of cellulose. *Journal of Molecular Liquids* **156**, 76-81, doi:10.1016/j.molliq.2010.04.016 (2010).

200 Xiong, B., Zhao, P., Hu, K., Zhang, L. & Cheng, G. Dissolution of cellulose in aqueous NaOH/urea solution: role of urea. *Cellulose* **21**, 1183-1192, doi:10.1007/s10570-014-0221-7 (2014).

201 de Carvalho, R. A. *et al.* The potential of TEMPO-oxidized nanofibrillar cellulose beads for cell delivery applications. *Cellulose* **23**, 3399-3405, doi:10.1007/s10570-016-1063-2 (2016).

202 Shanshan, G., Jianqing, W. & Zhengwei, J. Preparation of cellulose films from solution of bacterial cellulose in NMMO. *Carbohydrate Polymers* **87**, 1020-1025, doi:10.1016/j.carbpol.2011.06.040 (2012).

203 Jin, H., Zha, C. & Gu, L. Direct dissolution of cellulose in NaOH/thiourea/urea aqueous solution. *Carbohydr Res* **342**, 851-858, doi:10.1016/j.carres.2006.12.023 (2007).

204 Gao, Q., Shen, X. & Lu, X. Regenerated bacterial cellulose fibers prepared by the NMMO·H2O process. *Carbohydrate Polymers* **83**, 1253-1256, doi:http://dx.doi.org/10.1016/j.carbpol.2010.09.029 (2011).

205 Koga, H. *et al.* Transparent, conductive, and printable composites consisting of TEMPO-oxidized nanocellulose and carbon nanotube. *Biomacromolecules* **14**, 1160-1165, doi:10.1021/bm400075f (2013).

206 Chen, A. Y. *et al.* Synthesis and patterning of tunable multiscale materials with engineered cells. *Nat Mater* **13**, 515-523, doi:10.1038/nmat3912 (2014).

207 Chen, A. Y., Zhong, C. & Lu, T. K. Engineering living functional materials. *ACS Synth Biol* **4**, 8-11, doi:10.1021/sb500113b (2015).

208 Qin, G., Panilaitis, B. J. & Kaplan, Z. S. A cellulosic responsive "living" membrane. *Carbohydr Polym* **100**, 40-45, doi:10.1016/j.carbpol.2013.06.019 (2014).

209 Nguyen, P. Q., Botyanszki, Z., Tay, P. K. & Joshi, N. S. Programmable biofilm-based materials from engineered curli nanofibres. *Nat Commun* **5**, 4945, doi:10.1038/ncomms5945 (2014).

210 Liu, K. & Catchmark, J. M. Enhanced mechanical properties of bacterial cellulose nanocomposites produced by co-culturing Gluconacetobacter hansenii and Escherichia coli under static conditions. *Carbohydr Polym* **219**, 12-20, doi:10.1016/j.carbpol.2019.04.071 (2019).

211 Hulkoti, N. I. & Taranath, T. C. Biosynthesis of nanoparticles using microbes- a review. *Colloids Surf B Biointerfaces* **121**, 474-483, doi:10.1016/j.colsurfb.2014.05.027 (2014).

212 Foresti, M. L., Vazquez, A. & Boury, B. Applications of bacterial cellulose as precursor of carbon and composites with metal oxide, metal sulfide and metal nanoparticles: A review of recent advances. *Carbohydr Polym* **157**, 447-467, doi:10.1016/j.carbpol.2016.09.008 (2017).

213 de Oliveira Barud, H. G. *et al.* A multipurpose natural and renewable polymer in medical applications: Bacterial cellulose. *Carbohydr Polym* **153**, 406-420, doi:10.1016/j.carbpol.2016.07.059 (2016).

214 Kai, A. The Influence of Culture Conditions on the Fibrillation of Cellulose Gel Produced byAcetobacter xylinum. *Bulletin of the Chemical Society of Japan* **57**, 2816-2819, doi:10.1246/bcsj.57.2816 (1984).

215 Wolfe, A. J. & Berg, H. C. Migration of bacteria in semisolid agar. *Proc Natl Acad Sci U S A* **86**, 6973-6977, doi:10.1073/pnas.86.18.6973 (1989).

216 Adler, J. Chemotaxis in bacteria. *Science* **153**, 708-716, doi:10.1126/science.153.3737.708 (1966).

217 Keller, E. F. & Segel, L. A. Traveling bands of chemotactic bacteria: A theoretical analysis. *Journal of Theoretical Biology* **30**, 235-248, doi:10.1016/0022-5193(71)90051-8 (1971).

218 Blair, D. F. How bacteria sense and swim. *Annu Rev Microbiol* **49**, 489-522, doi:10.1146/annurev.mi.49.100195.002421 (1995).

219 Koster, D. A., Mayo, A., Bren, A. & Alon, U. Surface growth of a motile bacterial population resembles growth in a chemostat. *J Mol Biol* **424**, 180-191, doi:10.1016/j.jmb.2012.09.005 (2012).

220 Mishra, B. *et al.* Site specific immobilization of a potent antimicrobial peptide onto silicone catheters: evaluation against urinary tract infection pathogens. *Journal of Materials Chemistry B* **2**, 1706, doi:10.1039/c3tb21300e (2014).

221 Koster, D. A., Mayo, A., Bren, A. & Alon, U. Surface Growth of a Motile Bacterial Population Resembles Growth in a Chemostat. *Journal of Molecular Biology* **424**, 180-191, doi:http://dx.doi.org/10.1016/j.jmb.2012.09.005 (2012).

222 Basu, A. *et al.* Quantitative proteome profiles help reveal efficient xylose utilization mechanisms in solventogenic Clostridium sp. strain BOH3. *Biotechnology and Bioengineering* **114**, 1959-1969, doi:10.1002/bit.26332 (2017).

223 Li, X. *et al.* Antimicrobial functionalization of silicone surfaces with engineered short peptides having broad spectrum antimicrobial and salt-resistant properties. *Acta Biomaterialia* **10**, 258-266, doi:10.1016/j.actbio.2013.09.009 (2014).

224 Mishra, B. *et al.* Lasioglossin-III: antimicrobial characterization and feasibility study for immobilization applications. *RSC Advances* **3**, 9534-9543, doi:10.1039/C3RA40887F (2013).

225 Tomita, Y. & Kondo, T. Influential factors to enhance the moving rate of Acetobacter xylinum due to its nanofiber secretion on oriented templates. *Carbohydrate Polymers* **77**, 754-759, doi:10.1016/j.carbpol.2009.02.022 (2009).

226 Kondo, T. *et al.* Biodirected epitaxial nanodeposition of polymers on oriented macromolecular templates. *Proceedings of the National Academy of Sciences of the United States of America* **99**, 14008-14013, doi:10.1073/pnas.212238399 (2002).

227 Brown, R. M., Jr., Willison, J. H. & Richardson, C. L. Cellulose biosynthesis in Acetobacter xylinum: visualization of the site of synthesis and direct measurement of the in vivo process. *Proceedings of the National Academy of Sciences of the United States of America* **73**, 4565-4569 (1976).

228 van Wyk, J. P. H. & Mohulatsi, M. Biodegradation of wastepaper by cellulase from Trichoderma viride. *Bioresource Technology* **86**, 21-23, doi:http://dx.doi.org/10.1016/S0960-8524(02)00130-X (2003).

229 Lin, S. P. *et al.* Biosynthesis, production and applications of bacterial cellulose. *Cellulose* **20**, 2191-2219, doi:10.1007/s10570-013-9994-3 (2013).

230 Foresti, M. L., Vázquez, A. & Boury, B. Applications of bacterial cellulose as precursor of carbon and composites with metal oxide, metal sulfide and metal nanoparticles: A review of recent advances. *Carbohydrate Polymers* **157**, 447-467, doi:http://dx.doi.org/10.1016/j.carbpol.2016.09.008 (2017).

231 Tindall, M. J., Maini, P. K., Porter, S. L. & Armitage, J. P. Overview of mathematical approaches used to model bacterial chemotaxis II: bacterial populations. *Bulletin of mathematical biology* **70**, 1570-1607, doi:10.1007/s11538-008-9322-5 (2008).

232 Oh, S. Y. *et al.* Crystalline structure analysis of cellulose treated with sodium hydroxide and carbon dioxide by means of X-ray diffraction and FTIR spectroscopy. *Carbohydr Res* **340**, 2376-2391, doi:10.1016/j.carres.2005.08.007 (2005).

233 Kolpak, F. J. & Blackwell, J. Determination of the structure of cellulose II. *Macromolecules* **9**, 273-278, doi:10.1021/ma60050a019 (1976).

234 Lee, J. W. *et al.* Direct incorporation of glucosamine and N-acetylglucosamine into exopolymers by Gluconacetobacter xylinus (=Acetobacter xylinum) ATCC 10245: production of chitosan-cellulose and chitin-cellulose exopolymers. *Appl*

Environ Microbiol **67**, 3970-3975, doi:10.1128/aem.67.9.3970-3975.2001 (2001).

235 Yadav, V. *et al.* Novel in vivo-degradable cellulose-chitin copolymer from metabolically engineered Gluconacetobacter xylinus. *Appl Environ Microbiol* **76**, 6257-6265, doi:10.1128/AEM.00698-10 (2010).

236 Segal, L., Creely, J. J., Martin, A. E. & Conrad, C. M. An Empirical Method for Estimating the Degree of Crystallinity of Native Cellulose Using the X-Ray Diffractometer. *Textile Research Journal* **29**, 786-794, doi:10.1177/004051755902901003 (1959).

237 Barud, H. S. *et al.* Thermal characterization of bacterial cellulose–phosphate composite membranes. *Journal of Thermal Analysis and Calorimetry* **87**, 815-818, doi:10.1007/s10973-006-8170-5 (2007).

238 Kim, S. S., Kim, S. J., Moon, Y. D. & Lee, Y. M. Thermal characteristics of chitin and hydroxypropyl chitin. *Polymer* **35**, 3212-3216, doi:10.1016/0032-3861(94)90124-4 (1994).

239 Kaya, M. *et al.* Differentiations of chitin content and surface morphologies of chitins extracted from male and female grasshopper species. *PLoS One* **10**, e0115531, doi:10.1371/journal.pone.0115531 (2015).

240 Hong, P.-Z. *et al.* Thermogravimetric analysis of chitosan. *Journal of Applied Polymer Science* **105**, 547-551, doi:10.1002/app.25920 (2007).

241 Feng, Y., Zhang, X., Shen, Y., Yoshino, K. & Feng, W. A mechanically strong, flexible and conductive film based on bacterial cellulose/graphene nanocomposite. *Carbohydrate Polymers* **87**, 644-649, doi:10.1016/j.carbpol.2011.08.039 (2012).

242 Yogeswaran, N. *et al.* New materials and advances in making electronic skin for interactive robots. *Advanced Robotics* **29**, 1359-1373, doi:10.1080/01691864.2015.1095653 (2015).

243 Abhang, Y. Review of Different Tactile Sensors Using Piezoresistivity Mechanism. *Journal of Material Science & Engineering* **07**, doi:10.4172/2169-0022.1000432 (2018).

244 Guimard, N. K., Gomez, N. & Schmidt, C. E. Conducting polymers in biomedical engineering. *Progress in Polymer Science* **32**, 876-921, doi:10.1016/j.progpolymsci.2007.05.012 (2007).

245 Humpolicek, P. *et al.* The biocompatibility of polyaniline and polypyrrole: A comparative study of their cytotoxicity, embryotoxicity and impurity profile. *Mater Sci Eng C Mater Biol Appl* **91**, 303-310, doi:10.1016/j.msec.2018.05.037 (2018).

246 Riss, T. L. *et al. Cell Viability Assays*. (Eli Lilly & Company and the National Center for Advancing Translational Sciences, Bethesda (MD), 2004).

247 Chen, C.-h. *et al.* Mechanical characterizations of cast Poly(3,4-ethylenedioxythiophene):Poly(styrenesulfonate)/Polyvinyl Alcohol thin films. *Synthetic Metals* **161**, 2259-2267, doi:10.1016/j.synthmet.2011.08.031 (2011).

248 Kim, S. H., Lee, C. M. & Kafle, K. Characterization of crystalline cellulose in biomass: Basic principles, applications, and limitations of XRD, NMR, IR, Raman, and SFG. *Korean Journal of Chemical Engineering* **30**, 2127-2141, doi:10.1007/s11814-013-0162-0 (2013).

249 Qin, Z. *et al.* Synthesis and characterization of bacterial cellulose sulfates using a SO(3)/pyridine complex in DMAc/LiCl. *Carbohydr Polym* **101**, 947-953, doi:10.1016/j.carbpol.2013.09.068 (2014).

250 Sriprachuabwong, C. *et al.* Inkjet-printed graphene-PEDOT:PSS modified screen printed carbon electrode for biochemical sensing. *Journal of Materials Chemistry* **22**, 5478, doi:10.1039/c2jm14005e (2012).

251 Kvarnström, C. *et al.* In situ spectroelectrochemical characterization of poly(3,4-ethylenedioxythiophene). *Electrochimica Acta* **44**, 2739-2750, doi:10.1016/s0013-4686(98)00405-8 (1999).

252 Chen, C. *et al.* Facile approach to the fabrication of 3D electroconductive nanofibers with controlled size and conductivity templated by bacterial cellulose. *Cellulose* **22**, 3929-3939, doi:10.1007/s10570-015-0770-4 (2015).

253 Pertile, R. A. N., Andrade, F. K., Alves, C. & Gama, M. Surface modification of bacterial cellulose by nitrogen-containing plasma for improved interaction with cells. *Carbohydrate Polymers* **82**, 692-698, doi:10.1016/j.carbpol.2010.05.037 (2010).

254 Flynn, C. N., Byrne, C. P. & Meenan, B. J. Surface modification of cellulose via atmospheric pressure plasma processing in air and ammonia–nitrogen gas. *Surface and Coatings Technology* **233**, 108-118, doi:10.1016/j.surfcoat.2013.04.007 (2013).

255 Castner, D. G., Hinds, K. & Grainger, D. W. X-ray Photoelectron Spectroscopy Sulfur 2p Study of Organic Thiol and Disulfide Binding Interactions with Gold Surfaces. *Langmuir* **12**, 5083-5086, doi:10.1021/la960465w (1996).

256 Wang, G. F., Tao, X. M., Xin, J. H. & Fei, B. Modification of conductive polymer for polymeric anodes of flexible organic light-emitting diodes. *Nanoscale Res Lett* **4**, 613-617, doi:10.1007/s11671-009-9288-8 (2009).

257 Schaarschmidt, A., Farah, A. A., Aby, A. & Helmy, A. S. Influence of nonadiabatic annealing on the morphology and molecular structure of PEDOT-PSS films. *J Phys Chem B* **113**, 9352-9355, doi:10.1021/jp904147v (2009).

258 Greczynski, G. & Hultman, L. X-ray photoelectron spectroscopy: Towards reliable binding energy referencing. *Progress in Materials Science* **107**, 100591, doi:10.1016/j.pmatsci.2019.100591 (2020).

259 Lee, Y.-Y. *et al.* Growth Mechanism of Strain-Dependent Morphological Change in PEDOT:PSS Films. *Scientific Reports* **6**, 25332, doi:10.1038/srep25332 (2016).

260 Elschner, A., Kirchmeyer, S., Lovenich, W., Merker, U. & Reuter, K. PEDOT: Principles and Applications of an Intrinsically Conductive Polymer. doi:10.1201/b10318 (2010).

261 Xu, Y. *et al.* A hybrid material of graphene and poly (3,4-ethyldioxythiophene) with high conductivity, flexibility, and transparency. *Nano Research* **2**, 343-348, doi:10.1007/s12274-009-9032-9 (2009).

262 Zhou, T. *et al.* Electrically conductive bacterial cellulose composite membranes produced by the incorporation of graphite nanoplatelets in pristine bacterial cellulose membranes. *Express Polymer Letters* **7**, 756-766, doi:10.3144/expresspolymlett.2013.73 (2013).

263 Liang, H.-W. *et al.* Highly conductive and stretchable conductors fabricated from bacterial cellulose. *NPG Asia Materials* **4**, e19-e19, doi:10.1038/am.2012.34 (2012).

264 Marins, J. A. *et al.* Structure and properties of conducting bacterial cellulose-polyaniline nanocomposites. *Cellulose* **18**, 1285-1294, doi:10.1007/s10570-011-9565-4 (2011).

265 Lee, B.-H., Kim, H.-J. & Yang, H.-S. Polymerization of aniline on bacterial cellulose and characterization of bacterial cellulose/polyaniline nanocomposite films. *Current Applied Physics* **12**, 75-80, doi:10.1016/j.cap.2011.04.045 (2012).

266 Watanabe, K. *et al.* A new bacterial cellulose substrate for mammalian cell culture. A new bacterial cellulose substrate. *Cytotechnology* **13**, 107-114, doi:10.1007/bf00749937 (1993).

267 Karagkiozaki, V. *et al.* Bioelectronics meets nanomedicine for cardiovascular implants: PEDOT-based nanocoatings for tissue regeneration. *Biochim Biophys Acta* **1830**, 4294-4304, doi:10.1016/j.bbagen.2012.12.019 (2013).

268 Asplund, M. *et al.* Toxicity evaluation of PEDOT/biomolecular composites intended for neural communication electrodes. *Biomed Mater* **4**, 045009, doi:10.1088/1748-6041/4/4/045009 (2009).

269 Khan, S. *et al.* Three-dimensionally microporous and highly biocompatible bacterial cellulose–gelatin composite scaffolds for tissue engineering applications. *RSC Advances* **6**, 110840-110849, doi:10.1039/c6ra18847h (2016).

270 Chen, C. *et al.* Three-Dimensional BC/PEDOT Composite Nanofibers with High Performance for Electrode-Cell Interface. *ACS Appl Mater Interfaces* **7**, 28244-28253, doi:10.1021/acsami.5b07273 (2015).

271 Wu, J. *et al.* Silver nanoparticle/bacterial cellulose gel membranes for antibacterial wound dressing: investigation in vitro and in vivo. *Biomed Mater* **9**, 035005, doi:10.1088/1748-6041/9/3/035005 (2014).

272 Barnhart, M. M. & Chapman, M. R. Curli biogenesis and function. *Annu Rev Microbiol* **60**, 131-147, doi:10.1146/annurev.micro.60.080805.142106 (2006).

273 Dorval Courchesne, N.-M., Duraj-Thatte, A., Tay, P. K. R., Nguyen, P. Q. & Joshi, N. S. Scalable Production of Genetically Engineered Nanofibrous Macroscopic Materials via Filtration. *ACS Biomaterials Science & Engineering* **3**, 733-741, doi:10.1021/acsbiomaterials.6b00437 (2016).

274 Evans, M. L. & Chapman, M. R. Curli biogenesis: order out of disorder. *Biochim Biophys Acta* **1843**, 1551-1558, doi:10.1016/j.bbamcr.2013.09.010 (2014).

275 Andersson, E. K. *et al.* Modulation of curli assembly and pellicle biofilm formation by chemical and protein chaperones. *Chem Biol* **20**, 1245-1254, doi:10.1016/j.chembiol.2013.07.017 (2013).

276 Peigneux, A. *et al.* Learning from magnetotactic bacteria: A review on the synthesis of biomimetic nanoparticles mediated by magnetosome-associated proteins. *J Struct Biol* **196**, 75-84, doi:10.1016/j.jsb.2016.06.026 (2016).

277 Arakaki, A., Masuda, F., Amemiya, Y., Tanaka, T. & Matsunaga, T. Control of the morphology and size of magnetite particles with peptides mimicking the Mms6 protein from magnetotactic bacteria. *J Colloid Interface Sci* **343**, 65-70, doi:10.1016/j.jcis.2009.11.043 (2010).

278 Narayanan, K. B. & Sakthivel, N. Biological synthesis of metal nanoparticles by microbes. *Adv Colloid Interface Sci* **156**, 1-13, doi:10.1016/j.cis.2010.02.001 (2010).

279 Lenders, J. J. M. *et al.* A Bioinspired Coprecipitation Method for the Controlled Synthesis of Magnetite Nanoparticles. *Crystal Growth & Design* **14**, 5561-5568, doi:10.1021/cg500816z (2014).

280 Wu, W., He, Q. & Jiang, C. Magnetic iron oxide nanoparticles: synthesis and surface functionalization strategies. *Nanoscale Res Lett* **3**, 397-415, doi:10.1007/s11671-008-9174-9 (2008).

281 Sun, S. & Zeng, H. Size-controlled synthesis of magnetite nanoparticles. *J Am Chem Soc* **124**, 8204-8205, doi:10.1021/ja026501x (2002).

282 Petrova, T. M., Fachikov, L. & Hristov, J. The magnetite as adsorbent for some hazardous species from aqueous solutions: A review. *arXiv e-prints* (2011).

283 Zhang, L., He, R. & Gu, H.-C. Oleic acid coating on the monodisperse magnetite nanoparticles. *Applied Surface Science* **253**, 2611-2617, doi:10.1016/j.apsusc.2006.05.023 (2006).

284 Ma, M. *et al.* Preparation and characterization of magnetite nanoparticles coated by amino silane. *Colloids and Surfaces A: Physicochemical and Engineering Aspects* **212**, 219-226, doi:10.1016/s0927-7757(02)00305-9 (2003).

285 Sriplai, N., Mongkolthanaruk, W., Eichhorn, S. J. & Pinitsoontorn, S. Magnetically responsive and flexible bacterial cellulose membranes. *Carbohydr Polym* **192**, 251-262, doi:10.1016/j.carbpol.2018.03.072 (2018).

286 Liang, C.-C., Park, A. Y. & Guan, J.-L. In vitro scratch assay: a convenient and inexpensive method for analysis of cell migration in vitro. *Nature Protocols* **2**, 329-333, doi:10.1038/nprot.2007.30 (2007).

287 Galland, S. *et al.* Cellulose nanofibers decorated with magnetic nanoparticles – synthesis, structure and use in magnetized high toughness membranes for a prototype loudspeaker. *Journal of Materials Chemistry C* **1**, 7963, doi:10.1039/c3tc31748j (2013).

288 Zeng, M., Laromaine, A., Feng, W., Levkin, P. A. & Roig, A. Origami magnetic cellulose: controlled magnetic fraction and patterning of flexible bacterial cellulose. *J. Mater. Chem. C* **2**, 6312-6318, doi:10.1039/c4tc00787e (2014).

289 Fischer, A., Schmitz, M., Aichmayer, B., Fratzl, P. & Faivre, D. Structural purity of magnetite nanoparticles in magnetotactic bacteria. *J R Soc Interface* **8**, 1011-1018, doi:10.1098/rsif.2010.0576 (2011).

290 Jacob, J. J. & Suthindhiran, K. Magnetotactic bacteria and magnetosomes - Scope and challenges. *Mater Sci Eng C Mater Biol Appl* **68**, 919-928, doi:10.1016/j.msec.2016.07.049 (2016).

291 Baumgartner, J., Carillo, M. A., Eckes, K. M., Werner, P. & Faivre, D. Biomimetic magnetite formation: from biocombinatorial approaches to mineralization effects. *Langmuir* **30**, 2129-2136, doi:10.1021/la404290c (2014).

292 Larsen, E. K. *et al.* Accumulation of magnetic iron oxide nanoparticles coated with variably sized polyethylene glycol in murine tumors. *Nanoscale* **4**, 2352-2361, doi:10.1039/c2nr11554a (2012).

293 Katepetch, C. & Rujiravanit, R. Synthesis of magnetic nanoparticle into bacterial cellulose matrix by ammonia gas-enhancing in situ co-precipitation method. *Carbohydrate Polymers* **86**, 162-170, doi:10.1016/j.carbpol.2011.04.024 (2011).

294 Persson, K. Materials Data on Fe3O4 (SG:227) by Materials Project. *United States.*, doi:10.17188/1194194 (2015).

295 Marins, J. A., Soares, B. G., Barud, H. S. & Ribeiro, S. J. Flexible magnetic membranes based on bacterial cellulose and its evaluation as electromagnetic interference shielding material. *Mater Sci Eng C Mater Biol Appl* **33**, 3994-4001, doi:10.1016/j.msec.2013.05.035 (2013).

296 Zheng, Y. *et al.* Synthesis of flexible magnetic nanohybrid based on bacterial cellulose under ultrasonic irradiation. *Mater Sci Eng C Mater Biol Appl* **33**, 2407-2412, doi:10.1016/j.msec.2013.02.007 (2013).

297 Zhang, W. *et al.* Facile fabrication of flexible magnetic nanohybrid membrane with amphiphobic surface based on bacterial cellulose. *Carbohydrate Polymers* **86**, 1760-1767, doi:10.1016/j.carbpol.2011.07.015 (2011).

298 Nata, I. F., Sureshkumar, M. & Lee, C.-K. One-pot preparation of amine-rich magnetite/bacterial cellulose nanocomposite and its application for arsenate removal. *RSC Advances* **1**, 625, doi:10.1039/c1ra00153a (2011).

299 Taylor, R. M. & Schwertmann, U. Maghemite in soils and its origin: I. Properties and observations on soil maghemites. *Clay Minerals* **10**, 289-298, doi:10.1180/claymin.1974.010.4.07 (1974).

300 Yamashita, T. & Hayes, P. Analysis of XPS spectra of Fe2+ and Fe3+ ions in oxide materials. *Applied Surface Science* **254**, 2441-2449, doi:10.1016/j.apsusc.2007.09.063 (2008).

301 García-Jimeno, S. & Estelrich, J. Ferrofluid based on polyethylene glycol-coated iron oxide nanoparticles: Characterization and properties. *Colloids and Surfaces*

A: Physicochemical and Engineering Aspects **420**, 74-81, doi:10.1016/j.colsurfa.2012.12.022 (2013).

302 Park, M., Cheng, J., Choi, J., Kim, J. & Hyun, J. Electromagnetic nanocomposite of bacterial cellulose using magnetite nanoclusters and polyaniline. *Colloids Surf B Biointerfaces* **102**, 238-242, doi:10.1016/j.colsurfb.2012.07.046 (2013).

303 Sureshkumar, M., Siswanto, D. Y. & Lee, C.-K. Magnetic antimicrobial nanocomposite based on bacterial cellulose and silver nanoparticles. *Journal of Materials Chemistry* **20**, 6948, doi:10.1039/c0jm00565g (2010).

304 Gil, S. & Mano, J. F. Magnetic composite biomaterials for tissue engineering. *Biomater. Sci.* **2**, 812-818, doi:10.1039/c4bm00041b (2014).

305 Mohammed, L., Gomaa, H. G., Ragab, D. & Zhu, J. Magnetic nanoparticles for environmental and biomedical applications: A review. *Particuology* **30**, 1-14, doi:10.1016/j.partic.2016.06.001 (2017).

306 Inukai, A. *et al.* Synthesis and hyperthermia property of hydroxyapatite–ferrite hybrid particles by ultrasonic spray pyrolysis. *Journal of Magnetism and Magnetic Materials* **323**, 965-969, doi:10.1016/j.jmmm.2010.11.080 (2011).

307 Ghaemy, M. & Naseri, M. Synthesis of chitosan networks: Swelling, drug release, and magnetically assisted BSA separation using Fe3O4 nanoparticles. *Carbohydr Polym* **90**, 1265-1272, doi:10.1016/j.carbpol.2012.06.069 (2012).

308 Ajeesh, M., Francis, B. F., Annie, J. & Harikrishna Varma, P. R. Nano iron oxide-hydroxyapatite composite ceramics with enhanced radiopacity. *J Mater Sci Mater Med* **21**, 1427-1434, doi:10.1007/s10856-010-4005-9 (2010).

309 Kuda, O. *et al.* Effect of Fe3O4, Fe and Cu doping on magnetic properties and behaviour in physiological solution of biological hydroxyapatite/glass composites. *Journal of Materials Processing Technology* **209**, 1960-1964, doi:10.1016/j.jmatprotec.2008.04.061 (2009).

310 Galateanu, B. *et al.* In Vitro Studies of Bacterial Cellulose and Magnetic Nanoparticles Smart Nanocomposites for Efficient Chronic Wounds Healing. *Stem Cells Int* **2015**, 195096, doi:10.1155/2015/195096 (2015).

311 Klemm, D. *et al.* Nanocellulose as a natural source for groundbreaking applications in materials science: Today's state. *Materials Today* **21**, 720-748, doi:10.1016/j.mattod.2018.02.001 (2018).

312 Prabha, G. & Raj, V. Preparation and characterization of chitosan-Polyethylene glycol-polyvinylpyrrolidone-coated superparamagnetic iron oxide nanoparticles as carrier system: Drug loading and in vitro drug release study. *J Biomed Mater Res B Appl Biomater* **104**, 808-816, doi:10.1002/jbm.b.33637 (2016).

313 Lecomte, A. *et al.* Silk and PEG as means to stiffen a parylene probe for insertion in the brain: toward a double time-scale tool for local drug delivery. *Journal of Micromechanics and Microengineering* **25**, 125003, doi:10.1088/0960-1317/25/12/125003 (2015).

314 Muhammad, A. A., Pauzi, N. A., Arulselvan, P., Abas, F. & Fakurazi, S. In vitro wound healing potential and identification of bioactive compounds from

Moringa oleifera Lam. *Biomed Res Int* **2013**, 974580, doi:10.1155/2013/974580 (2013).

315 Sapir, Y., Cohen, S., Friedman, G. & Polyak, B. The promotion of in vitro vessel-like organization of endothelial cells in magnetically responsive alginate scaffolds. *Biomaterials* **33**, 4100-4109, doi:10.1016/j.biomaterials.2012.02.037 (2012).

316 Hughes, S., El Haj, A. J. & Dobson, J. Magnetic micro- and nanoparticle mediated activation of mechanosensitive ion channels. *Med Eng Phys* **27**, 754-762, doi:10.1016/j.medengphy.2005.04.006 (2005).

317 Gupta, A. K. & Gupta, M. Synthesis and surface engineering of iron oxide nanoparticles for biomedical applications. *Biomaterials* **26**, 3995-4021, doi:10.1016/j.biomaterials.2004.10.012 (2005).

318 Hola, K., Markova, Z., Zoppellaro, G., Tucek, J. & Zboril, R. Tailored functionalization of iron oxide nanoparticles for MRI, drug delivery, magnetic separation and immobilization of biosubstances. *Biotechnol Adv* **33**, 1162-1176, doi:10.1016/j.biotechadv.2015.02.003 (2015).

319 Moniri, M. *et al.* In vitro molecular study of wound healing using biosynthesized bacteria nanocellulose/silver nanocomposite assisted by bioinformatics databases. *Int J Nanomedicine* **13**, 5097-5112, doi:10.2147/IJN.S164573 (2018).

320 Khamrai, M., Banerjee, S. L. & Kundu, P. P. Modified bacterial cellulose based self-healable polyeloctrolyte film for wound dressing application. *Carbohydr Polym* **174**, 580-590, doi:10.1016/j.carbpol.2017.06.094 (2017).

321 Dobson, J. Magnetic nanoparticles for drug delivery. *Drug Development Research* **67**, 55-60, doi:10.1002/ddr.20067 (2006).

322 Du, J., Vepachedu, V., Cho, S. H., Kumar, M. & Nixon, B. T. Structure of the Cellulose Synthase Complex of Gluconacetobacter hansenii at 23.4 A Resolution. *PLoS One* **11**, e0155886, doi:10.1371/journal.pone.0155886 (2016).

323 Greanya, V. Bioinspired Photonics. *Boca Raton: CRC Press*, doi:10.1201/b18516 (2016).

324 Tadepalli, S., Slocik, J. M., Gupta, M. K., Naik, R. R. & Singamaneni, S. Bio-Optics and Bio-Inspired Optical Materials. *Chem Rev* **117**, 12705-12763, doi:10.1021/acs.chemrev.7b00153 (2017).

325 Processes., N. R. C. U. C. o. B. M. a. Inspired by Biology: From Molecules to Materials to Machines. *Washington (DC): National Academies Press (US)*, doi:10.17226/12159 (2008).

326 Wu, L. *et al.* Optical Functional Materials Inspired by Biology. *Advanced Optical Materials* **4**, 195-224, doi:10.1002/adom.201500428 (2016).

327 Retegi, A. *et al.* Sustainable optically transparent composites based on epoxidized soy-bean oil (ESO) matrix and high contents of bacterial cellulose (BC). *Cellulose* **19**, 103-109, doi:10.1007/s10570-011-9598-8 (2011).

328 Nevo, Y. *et al.* Nano bio optically tunable composite nanocrystalline cellulose films. *RSC Advances* **5**, 7713-7719, doi:10.1039/c4ra11840e (2015).

329 Tamerler, C. & Sarikaya, M. Molecular biomimetics: nanotechnology and bionanotechnology using genetically engineered peptides. *Philos Trans A Math Phys Eng Sci* **367**, 1705-1726, doi:10.1098/rsta.2009.0018 (2009).

330 Xia, Y. *et al.* Printable Fluorescent Hydrogels Based on Self-Assembling Peptides. *Sci Rep* **7**, 9691, doi:10.1038/s41598-017-10162-y (2017).